IDENTIFICATION OF RECEPTOR TRANSPORTING PROTEINS

AS CONSERVED ANTIVIRAL EFFECTORS

IN VERTEBRATES

APPROVED BY SUPERVISORY COMMITTEE

John Schoggins, Ph.D., Supervising Professor

Michael Shiloh, M.D., Ph.D., Chair

Neal Alto, Ph.D.

Dustin Hancks, Ph.D.

Nan Yan, Ph.D.

DEDICATION

I dedicate this dissertation to my friends, my family, my mentors, and my cats.

I thank John for his mentorship, critical eye, and support. This, alongside the freedom he gave me, has been in the core of my development as a scientist, experimentalist, and thinker.

I thank all the members of the Schoggins lab for their constant support.

I thank my committee members for their critiques that made this project what it became.

I thank my long-term baymate and mentor Katrina for challenging me as a scientist and as a person; it has been a privilege to work and learn alongside you.

I thank my family for their support and understanding over the past few years. I have dropped off the map a few times, and I am grateful that you have been there when I have reached back out. It has been such a blessing to be separated by only a short drive up I-75.

I thank my Allen friends for reconnecting during the pandemic. I don't know what the last chapter of grad school would have been like without you all; I am beyond thankful that I have such good friends from childhood. Maddie, I especially thank you for taking the initiative.

Finally, I thank Chelsea for her support, understanding, and occasional statistical consulting over the years. Grad school is tough and doing it together has made it so much better.

IDENTIFICATION OF RECEPTOR TRANSPORTING PROTEINS AS CONSERVED ANTIVIRAL EFFECTORS IN VERTEBRATES

by

IAN NICHOLAS BOYS

DISSERTATION

Presented to the Faculty of the Graduate School of Biomedical Sciences

The University of Texas Southwestern Medical Center at Dallas

In Partial Fulfillment of the Requirements

For the Degree of

DOCTOR OF PHILOSOPHY

The University of Texas Southwestern Medical Center at Dallas

Dallas, Texas

Degree Conferral August, 2021

IDENTIFICATION OF RECEPTOR TRANSPORTING PROTEINS

AS CONSERVED ANTIVIRAL EFFECTORS

IN VERTEBRATES

Publication No. _____

Ian Nicholas Boys, Ph.D.

The University of Texas Southwestern Medical Center at Dallas, 2021

Supervising Professor: John Schoggins, Ph.D.

PREFACE

Viruses and their hosts are engaged in "genetic arms races" in which each side attempts to gain the advantage over evolutionary time. Results of these conflicts are wide-ranging: viruses diversify, hosts establish species-specific barriers to some viruses while remaining susceptible to others, and the lines for future genetic conflicts are drawn. In mammals, many antiviral effectors – proteins that directly inhibit viral infection – show species- or lineage-specific properties which are believed to be the result of past or ongoing conflicts. Bats harbor a greater diversity of

viruses than any other mammalian order, and a growing body of research has described unique adaptations in bats that are in part responsible for, and perhaps a response to, this unique status. We hypothesized that the frequent encounters between bats and viruses would drive unique adaptations in the antiviral effectors that serve on the front lines of virus-host genetic conflicts. We identified RTP4 from the bat *Pteropus alecto* as a potent inhibitor of flavivirus infection. Mechanistic studies determined that RTP4 is an RNA-binding protein that associates with flavivirus replication machinery, binds replicating viral RNA, and suppresses viral genome amplification. Phylogenomic analysis revealed that RTP4 has evolved under positive selection in several mammalian lineages, consistent with a model in which host-virus conflicts have shaped its evolution as a restriction factor not only in bats but across mammals. We assessed the antiviral efficacy of diverse mammalian RTP4 orthologs and found that orthologs exhibit striking patterns of antiviral specificity. Further highlighting the specificity of the host-virus arms race, experimental evolution demonstrated that a flavivirus can mutate to escape RTP4-imposed restriction in a species-specific manner. In follow-up work, we identified signatures of positive selection in several non-mammalian RTP homologs, indicative of a putative role in innate immunity. We screened a collection of vertebrate RTPs against a panel of viruses and identified antiviral RTPs in the African clawed frog, *Xenopus laevis*. These antiviral *Xenopus* RTPs exhibit mosaic phenotypes that resemble those of mammalian RTP4 orthologs. Within the context of our findings with mammalian RTP4, these data suggest that Receptor Transporter Proteins are involved in host-virus genetic conflicts outside of Mammalia.

TABLE OF CONTENTS

PRIOR PUBLICATIONS

Boys, I.N., Mar, K.B., Schoggins., J.W. Functional-genomic analysis reveals intraspecies diversification of antiviral receptor transporter proteins in Xenopus laevis. *PLOS Genetics* (2021) PMID: 34014925

Boys, I.N., Xu, E., Mar, K.B., *et al.* RTP4 is a Potent IFN-Inducible Anti-flavivirus Effector Engaged in a Host-Virus Arms Race in Bats and Other Mammals. *Cell Host & Microbe* (2020) PMID: 33113352

Pfaender, S., Mar, K.B., Michailidis, E., Kratzel, A., **Boys, I.N.**, *et al*. LY6E impairs coronavirus fusion and confers immune control of viral disease. *Nat Microbiol* (2020) PMID: 32511345

Farag, A.*, Wang, P.*, **Boys, I.N.***, *et al.*, Identification of Atovaquone, Ouabain and Mebendazole as FDA Approved Drugs Targeting SARS-CoV-2. *ChemRxiv* (2020) (*equal contribution)

Mar, K.B., Rinkenberger, N.R**., Boys, I.N.** *et al.* LY6E mediates an evolutionarily conserved enhancement of virus infection by targeting a late entry step. *Nat Commun* 9**,** 3603 (2018) PMID: 30190477

Richardson, B., Ohlson, M.B., Eitson, J.L., Kumar, Ashwani., McDougal, M.B., **Boys, I.N.**, *et al* A CRISPR screen identifies IFI6 as an ER-resident interferon effector that blocks flavivirus replication. *Nat Microbiol* 3**,** 1214–1223 (2018) PMID: 30224801

LIST OF FIGURES

LIST OF TABLES

LIST OF APPENDICES

LIST OF DEFINITIONS

AAV – adeno-associated virus

aBSREL – adaptive branch-site REL test for episodic diversification

ADAR – Adenosine Deaminase RNA Specific

AGM – African green monkey

APOBEC – apolipoprotein B mRNA editing enzyme, catalytic polypeptide-like

ASR – ancestral sequence reconstruction

bp – base pair

BUSTED – Branch-Site Unrestricted Statistical Test for Episodic Diversification (software)

cGAS – Cyclic GMP-AMP synthase

CLIP – cross-linking immunoprecipitation

CPE – cytopathic effect

CRISPR – clustered regularly interspaced short palindromic repeats

Ctrl – Control

CVB – coxsackievirus b

DENV –dengue virus

DMV – double-membrane vesicle

dN/dS – ration of nonsynonymous to synonymous amino acid substitutions

dsRNA – double-stranded RNA

DTN – Digitonin

E11 – echovirus 11

EAV – equine arteritis virus

ENTV – Entebbe bat virus

ER – endoplasmic reticulum

FC – fold-change

FL – full-length

FLuc – firefly luciferase

FUBAR – fast unconstrained Bayesian approximation for inferring selection (software)

GARD – genetic algorithm for recombination detection (software)

GLuc – Gaussia luciferase

HA – hemagglutinin tag

HCoV-OC43 – human coronavirus strain OC43

HCV – hepatitis C virus

HIV – human immunodeficiency virus

HSV1 – herpes simplex virus 1

HyPhy – hypothesis testing using phylogenies (software)

IAV – influenza A virus

IFN – interferon

IKK – IkB kinase

IP – immunoprecipitation

IRES – internal ribosomal entry site

IRF – interferon regulatory factor

ISG – interferon stimulated gene

ISGF3 – interferon stimulated gene factor 3

ISRE – interferon sensitive response element

JAK – Janus kinase

KDEL – ER-target sequence

KO – knockout

LGP2 – RIG-I-like receptor protein 3

MAVS – mitochondrial anti-viral signaling protein

MDA5 – myeloma differentiation-associated protein 5

MenV – mengovirus

MOI – multiplicity of infection

MX1 – MX dynamin like GTPase 1

NS3 – nonstructural protein 3 (flavivirus protease/helicase)

NS5 – nonstructural protein 5 (flavivirus polymerase/methyltransferase)

NWM – new world monkey

ONNV – o'nyong'nyong virus

ORF – open reading frame

OWM – old world monkey

PAML – Phylogenetic Analysis by Maximum Likelihood

PAMP – pathogen-associated molecular pattern

PIV3 – human parainfluenza virus 3

poly(I:C) – polyinosinic:polycytidylic acid

PV – polio virus

RBV – Rio Bravo virus

RdRP – RNA-dependent RNA polymerase

RIG-I – retinoic acid-inducible gene I

RLR – RIG-I-like-receptor

RLuc – Renilla luciferase

RTP – receptor transporting protein (also receptor transporter protein)

SPRY – SPla and the RYanodine Receptor domain

STAT – signal transducer and activator of transcription

STING – stimulator of interferon genes

TBK1 – TANK-binding kinase I

THOV – thogotovirus

TM – transmembrane

TRAF – TNF receptor (TNFR) associated factor protein family

TRIM – tripartite motif-containing protein

UTR – untranslated region

VEEV – Venezuelan equine encephalitis virus

VSV – vesicular stomatitis virus

WGA – wheat germ agglutinin

WNV – West Nile virus

WT – wild-type

YFV – yellow fever virus

ZFD – zinc finger domain

ZIKV – Zika virus

CHAPTER ONE
Review of the Literature

CELL-INTRINSIC ANTIVIRAL IMMUNITY

Origins and Necessity of Antiviral Immunity

Viruses infect all known cellular life. Viral infection is often detrimental to host cells, as viruses rely on host resources to replicate and reproduce. This virus-mediated fitness cost has driven the evolution of diverse antiviral defenses in all known species (tenOever, 2016). A common component of cellular antiviral defenses is the discrimination of self from non-self (Schlee and Hartmann, 2016). Such distinction is crucial both in immune sensing, where pattern recognition receptors (PRRs) detect and initiate transcriptional responses to viral infection, and at the stage of effector function, where antiviral proteins must specifically target viral nucleic acids or protein. Mechanisms of recognition and antagonism of viral infection at the cellular level constitute cell-intrinsic antiviral systems. Some antiviral systems are ancient: restriction enzyme and CRISPR-Cas defenses are conserved across most bacteria and archaea (Westra et al., 2019) and RNA interference is critical in plants and invertebrates (tenOever, 2016). However, a more recent evolutionary innovation, the type I interferon (IFN) response, is the dominant antiviral system in vertebrates. This coordinated antiviral transcriptional response is reviewed below in further detail (Schneider et al., 2014).

In conjunction with these systems, antiviral effectors, a broad set of proteins which directly inhibit viral infection, are important components of antiviral immunity from bacteria to vertebrates. Some antiviral effectors are conserved across billions of years. Viperin, a mammalian effector that produces a chain terminator which poisons RNA virus replication (Gizzi et al., 2018),

has functional homologs with similar, yet distinct, antiviral properties in prokaryotes (Bernheim et al., 2021). Other effectors represent more recent innovations. For example, antiviral cytidine (APOBEC) and adenosine (ADAR) deaminases are vertebrate-specific antiviral effectors, though they share common features and a probable evolutionary history with metabolic deaminases that are found in all domains of life (Christofi and Zaravinos, 2019; Conticello, 2008). The same is true for several antiviral TRIM proteins, such as TRIM5-alpha (TRIM5α) and TRIM22, which likely originated in the common ancestor of eutherian mammals (Sawyer et al., 2007). In vertebrates, many antiviral effectors are induced by IFN as part of the IFN response, a coordinated antiviral system (Schneider et al., 2014). The IFN response is critical in mammals. For example, in humans, loss-of-function mutations in STAT1, a key component in the IFN signaling cascade (reviewed below), lead to virus-associated mortality (Dupuis et al., 2003).

The Type I Interferon Response

The type I IFN response is conserved across jawed vertebrates, placing its evolutionary origin roughly 465 million years ago (Secombes and Zou, 2017). The interferon response is comprised of two broad phases: the induction of IFN, a small cytokine, and the recognition of IFN by cognate receptors, which leads to a subsequent transcriptional response (Platanias, 2005).

The primary pathogen-associated molecular pattern (PAMP) for viruses is viral nucleic acid (Schlee and Hartmann, 2016). Viral DNA is primarily recognized by the cGAS-STING signaling axis (Chen et al., 2016). Viral RNA is recognized by endosomal toll like receptors (dsRNA: TLR3, viral ssRNA: TLR7/8 in mammals), as well as the cytosolic RIG-I-like receptors (RLR) RIG-I, which recognizes RNA moieties with 5’ triphosphates, and MDA5, which recognizes long dsRNA,

in some cases with its cofactor LGP2 (Reikine et al., 2014). Following engagement with RNA, CARD-CARD interactions between RLRs and mitochondrial antiviral signaling protein (MAVS) nucleate MAVS polymers on the mitochondrial membrane, leading to activation of interferon response factors (IRFs) via a TRAF-TBK1/IKKε signaling cascade (Hou et al., 2011). The cGAS-STING and RLR-MAVS pathways both converge on TBK1, which phosphorylates IRF3 and IRF7. Once phosphorylated, IRFs dimerize, translocate to the nucleus as active transcription factors, and induce Type I IFNs and a subset of interferon-stimulated genes (ISGs).

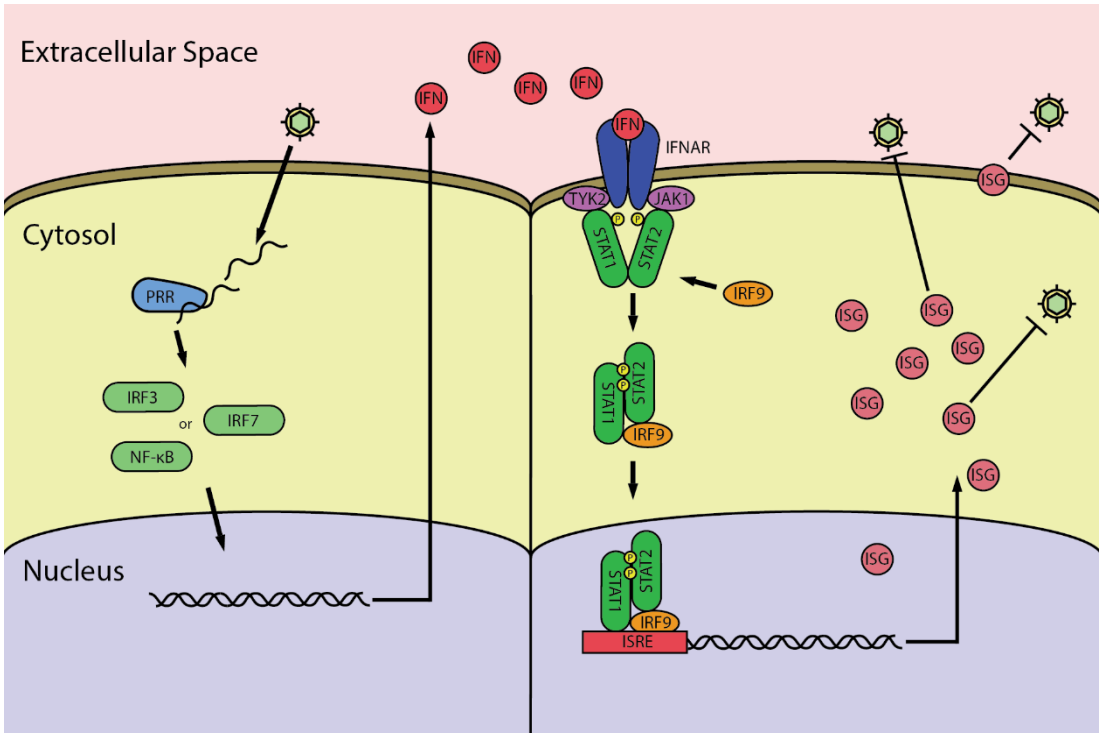

Figure 1. Simplified schematic of the type I IFN response. Left: PRRs recognize PAMPs associated with viral infection, leading to the production of IFN. Right: IFN signals in a paracrine or autocrine manner through cognate IFNAR receptors and the JAK-STAT signaling pathway, resulting in the induction of ISGs.

Type I IFNs signal in an autocrine or paracrine manner. Mammals have several classes of type I IFNs, of which the most conserved, widely expressed, and well-studied IFNs are IFNα and IFNβ (Riera Romo et al., 2016). Type I IFNs in other vertebrates such as amphibians and fish are not considered to be direct orthologs of mammalian IFNα or IFNβ but serve a similar function (Zou et al., 2007). In mammals, type I IFNs bind to IFNAR1/2 heterodimeric receptors, recruiting TYK2 and JAK1 kinases, which phosphorylate and activate STAT1 and STAT2. Activated STAT1 and STAT2 form heterodimers, which recruit IRF9 to form the transcription factor complex ISGF3. ISGF3 translocates to the nucleus and binds to interferon sensitive response elements (ISREs), inducing the transcription of ISGs (Platanias, 2005). Additionally, there exists in mammals an orthogonal and complementary IFN system, the type III IFN system, in which members of the cytokine family IFN-λ induce ISGs via the JAK-STAT signaling cascade, albeit with different physiological functions (Lazear et al., 2019). Many ISGs encode antiviral effector proteins (Schoggins et al., 2011). These effectors antagonize viruses and in doing so exert selective pressure, giving rise to so-called "genetic arms races" between hosts and viruses (Daugherty and Malik, 2012).

HOST-VIRUS GENETIC CONFLICTS

Underlying Forces of Host-virus Genetic Conflicts

Leigh Van Valen's "Red Queen hypothesis" posits that co-existing organisms must continually adapt to pressures imposed by one another to survive (Van Valen, 1973). Such conflicts between viruses and their hosts play out at the molecular level over an evolutionary timescale. Mutation rates within viruses are exponentially higher than those in their hosts

(Sniegowski et al., 2000). RNA viruses in particular exist as "quasispecies", since few viruses within a particular viral population are genetically identical (Domingo, 1992). This diversity, coupled with the relatively short generation time of viruses compared to their hosts, allows viral variants to arise which can evade selective pressure (Domingo et al., 2012). Viruses that evade host immunity have a selective advantage, as observed for HIV (Kamp et al., 2000; Venkatesan et al., 2018). Increased viral fitness in turn places increased selective pressure on components of host immune systems, driving host evolution over time (Enard et al., 2016). Such evolutionary "tit-for-tat" conflicts are a hallmark of host-pathogen co-evolution and have profound implications for viral host range and host immune function.

Methodology and Theories in the Study of Host-virus Genetic Conflicts

Gene and residue-level signatures of positive selection can be inferred by comparing sequence data from related species. Most statistical models that detect positive selection rely on the calculation of ω, the ratio of nonsynonymous (dN) to synonymous (dS) codon substitutions at any given site (Anisimova et al., 2001). Sites with $\omega > 1$ are considered to be undergoing positive selection, as dN outweighs dS. Sites with $\omega < 1$ are undergoing purifying selection, whereas sites with $\omega = 0$ are considered to be undergoing genetic drift. Importantly, elevated dN/dS across a phylogeny is indicative of continued, or pervasive, positive selection, whereas fixed adaptations are more often the result of episodic positive selection. Pervasive positive selection is most consistent with the concept of a host-pathogen "molecular arms race" where adaptations are met by counter-adaptations over time.

Regions or residues within antiviral effectors which display an elevated ω are theorized to be hotspots of host-pathogen molecular arms races (Daugherty and Malik, 2012). Indeed, empirical studies have demonstrated that adaptations at such sites can be critical for effector function, as is the case for MX1 (Mitchell et al., 2012) and TRIM5α (Sawyer et al., 2005). Evidence of continued selection at such sites implies that viruses have likewise evolved to escape host adaptations. Indeed, similar methodologies have been applied to identify evolutionary hotspots in host-interacting viral proteins, such as residues in nucleoprotein (NP) of pandemic influenza viruses which confer resistance to targeting by host MX1 (Manz et al., 2013).

In addition to pervasive positive selection, gene family expansion is another common form of genomic innovation in host-pathogen arms races (Duggal and Emerman, 2012). For example, the restriction factor APOBEC3 has expanded in multiple mammalian lineages (Conticello et al., 2005), placing increased and varied pressure on retroviruses. Similarly, the antiviral IFITM family has expanded in mammals, with consequences for antiviral immunity (Siegrist et al., 2011). Domain shuffling can also augment host defenses, as evidenced by an alternate gene fusion of the restriction factor TRIM5α and Cyclophylin A, TRIMCyp, which complements TRIM5α by targeting different sets of viruses in some primates (Sayah et al., 2004).

Examples of Species-specific Effector Function

Virus-imposed evolutionary pressures drive the diversification of antiviral effectors among species. Empirical evidence of this phenomenon has been established most prominently by comparative studies in primates. A well-studied example of species specificity of antiviral effectors is the primate retroviral restriction factor tripartite motif-containing protein 5 (TRIM5α).

Prior to the discovery of TRIM5α, it was appreciated that rhesus macaque cells were refractory to infection with lentiviruses such as HIV-1. To determine whether macaques possess a unique HIV-1 restriction factor, cDNA libraries generated from macaque cells were screened by ectopic expression for genes that that protected human cells from HIV-1 infection (Stremlau et al., 2004). Using this functional screening approach, Stremlau et al identified the rhesus macaque ortholog of TRIM5α as a potent restriction factor of HIV-1 infection that blocks viral infection at a post-entry step, prior to reverse transcription. Subsequent studies uncovered profound variability in the antiviral activity of primate TRIM5α orthologs (Johnson and Sawyer, 2009). Hominid TRIM5α orthologs effectively restrict the gammaretrovirus murine leukemia virus (MLV) and endogenous retroviruses, but do not inhibit lentiviruses such as HIV-1. Orthologs of TRIM5α from old world monkeys (OWMs) generally inhibit HIV-1 infection yet show differential activity against different strains of simian immunodeficiency virus (SIV), a closely-related lentivirus. Orthologs of TRIM5α from new world monkeys (NWMs), however, show more diverse patterns of retroviral restriction. The c-terminal SPRY domain of TRIM5α has been implicated as the source of much of this variability. Evolutionary analysis identified a positively-selected patch of 11 amino acids that is responsible for much of the phenotypic variation between rhesus and human TRIM5α (Sawyer et al., 2005). When this region was reciprocally swapped between the rhesus and human proteins, the resultant chimeric proteins nearly recapitulated the antiviral activity of the parental protein that was the source of the positively-selected patch. Human TRIM5α bearing the positively-selected macaque residues exhibited markedly enhanced anti-lentiviral activity, whereas rhesus TRIM5α with the human residues exhibited a marked loss of function. This observation underscores the importance of genetic variation in host-pathogen interactions, as positive selective pressures

exerted by viruses over evolutionary time have driven genetic changes with functional consequences for the antiviral potential of ISGs, even among closely-related species.

In a more extreme example, a single amino acid difference between the African green monkey (AGM) and human orthologs of the orthomyxovirus restriction factor MX1 was identified as the sole residue that underlies the ability of human MX1 to inhibit Thogoto virus (THOV) and an MX1-susceptible strain of influenza A virus (IAV) while AGM MX1 cannot (Mitchell et al., 2012). In a case that is analogous to the SPRY domain of TRIM5α, a hotspot of positive selection in primate MX1, loop L4, was identified and probed for its role in antiviral restriction. The genetic determinant of this differential phenotype was pinpointed to residue 561, a component of loop L4 that in humans is a phenylalanine and in AGM is a valine. A F561V mutation on human MX1 yields a complete loss of functional inhibition of THOV, whereas a V561F mutation of AGM MX1 yields a protein that suppresses THOV infection as efficiently as human MX1.

Species-specific restriction factors outside of primates have not been as extensively studied. Recent studies in bats, which are important reservoirs of zoonotic viruses, have provided insight into species-specific adaptations that are reminiscent of those found in primates for the restriction factors IFITM3 (Benfield et al., 2020) and Mx family GTPases (Fuchs et al., 2017). Further, genome-scale phylogenetic analyses have identified immune effectors in bats that are evolving under positive selection, suggestive of host-pathogen arms races(Hawkins et al., 2019). The most parsimonious conclusion would be that such virus-driven species-specific host effector adaptations are as ubiquitous as viral infection itself.

POSITIVE-SENSE RNA VIRUS EVOLUTION AND REPLICATION

Overview of RNA Viruses

Many viruses that cause human disease have RNA genomes (ME et al., 2013). Despite being less numerous than DNA viruses, RNA viruses contain an enormous amount of genetic diversity and are particularly expanded in eukaryotes (Koonin and Dolja, 2013; Koonin et al., 2015). Indeed, a single recent metagenomic study of the virome of 10 liters of seawater doubled the total number of known RNA viruses, highlighting their diversity and ubiquity (Wolf et al., 2020). The only unifying feature of RNA viruses is the RNA-dependent RNA polymerase (RdRP), which is critical for their ability to replicate. Phylogenetic and structural analyses suggest that all viral RdRPs share a common origin, enabling comparison of the evolutionary history of all RNA viruses based on their RdRPs (Pflug et al., 2014; Wolf et al., 2018).

Broadly, RNA viruses have either positive-sense single-stranded (+ssRNA), negative-sense single-stranded (-ssRNA), or double-stranded (dsRNA) genomes. Reconstructions of their evolutionary history suggest that +ssRNA viruses represent the most prototypical RNA viruses, which is perhaps intuitive since their genomes directly encode protein (Wolf et al., 2018). Positive-sense RNA viruses contain many viral families that are of particular relevance to human health, such as *Picornaviridae, Flaviviridae,* and *Coronaviridae* (Simmonds et al., 2017). These and other positive-sense RNA viruses have similar steps in their viral replication cycles – namely entry, translation of genomic RNA, genome amplification, assembly, and egress. An overview of +ssRNA virus replication, with a focus on the *Flaviviridae* is included below.

Positive-sense RNA Virus Replication

The *Flaviviridae* is a medically relevant family of viruses that contains emergent and re-emergent members, including West Nile (WNV), Zika (ZIKV), dengue (DENV), and yellow fever (UFV) viruses, which place a substantial burden on global health, infecting over 400 million people annually (Pierson and Diamond, 2020). Many flaviviruses are arboviruses, meaning that their transmission requires an arthropod vector, though some members of the family, including the hepacivirus Hepatitis C virus (HCV), are transmitted by direct contact with bodily fluids.

Flaviviruses enter cells via receptor-mediated endocytosis (Perera-Lecoin et al., 2013). Endosomal acidification triggers fusion of viral and host membranes, promoting the release of the viral genome into the cytosol (White and Whittaker, 2016). As with other +ssRNA viruses, the genome is immediately available for translation by host translation machinery. Within the *Flaviviridae*, translation of HCV and other hepaciviruses depends on an internal ribosomal entry site (IRES) in the 5' UTR of the genome (Johnson et al., 2017) while flavivirus translation is cap-dependent (Garcia-Blanco et al., 2016). Like many +ssRNA viruses, the genomic RNA is translated as a single polyprotein which is subsequently cleaved by host and viral proteases to produce functional viral proteins (Barrows et al., 2018). Flaviviruses and hepaciviruses both rearrange host membranes to form replication organelles that serve as the site of viral genome amplification and are thought to help sequester viral PAMP from innate sensing pathways (Paul and Bartenschlager, 2015). While both genuses use the host ER to form these replication organelles, hepaciviruses form outward-budding double-membrane vesicles (DMVs) while flaviviruses form inward-budding invaginations.

Within the replication complex, genome amplification is conducted by the coordinated activity of NS3, a helicase, and the NS5 (or NS5B in the case of hepaciviruses) polymerase (Brand et al., 2017). Several factors including genome circularization (Romero-Lopez et al., 2014) and NS5 occupancy (Fajardo et al., 2020) are thought to regulate the balance between translation of viral protein and genome amplification during this stage. At this point, an exponential increase in viral protein and RNA is observed, allowing for the assembly of viral progeny.

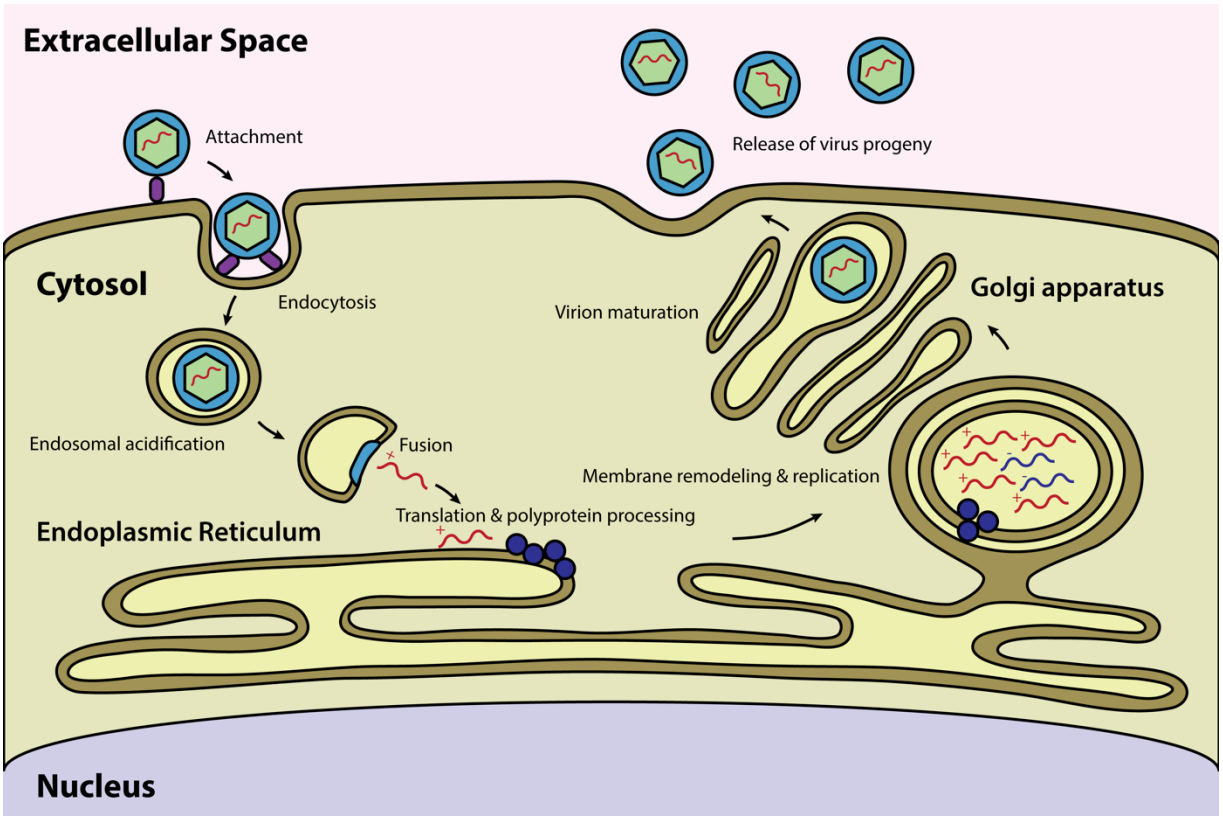

Figure 2. Simplified schematic of hepacivirus replication. Key stages of the viral replication cycle, discussed in further detail in the text, are indicated.

While there are many commonalities between replication of other +ssRNA viruses and the *Flaviviridae*, there are some key differences that are noteworthy. In addition to producing full-length polyproteins, some +ssRNA viruses such as coronaviruses produce subgenomic ORFs that

encode additional proteins (Sawicki et al., 2007). While all of these viruses utilize host membranes to form their replication organelles, the origin and location of these membranes differ widely. For example, alphaviruses replicate on ER, plasma membrane, and endosome-derived compartments, and picornaviruses replicate in ER and golgi-derived organelles (den Boon et al., 2010). Coronaviruses replicate in outward-budding DMVs at the ER, similar to hepaciviruses. Notably, coronaviruses also contain the only known proofreading RdRPs, a feature which is thought to underlie their relatively large genome size among RNA viruses (Robson et al., 2020).

ZOONOTIC VIRUSES

Zoonotic Viruses in Human Health and Disease

The majority of disease-causing RNA viruses in humans are the results of zoonoses (ME et al., 2013). Zoonotic viruses are those which "jump" from a natural reservoir to another species, such as humans. The cadence of zoonotic events has increased over time, and research has demonstrated that many factors such as urbanization, human encroachment on wilderness, factory farming, and increased global travel are contributing to this trend (Daszak et al., 2001; Olival et al., 2017). There are many biological barriers that prevent viral zoonoses; of the predicted hundreds of thousands of animal viruses, only several hundred have been documented to infect humans (Warren and Sawyer, 2019). It is generally accepted that the most common biological barriers are incompatibility of viral receptors, the presence of restriction factors, and differences in required host factors for viral replication.

Since the turn of the century, several emergent and re-emergent zoonotic RNA viruses, such as the flaviviruses WNV and ZIKV, the coronaviruses SARS-CoV, MERS-CoV, and SARS-CoV-

2, and Ebola virus (EBOV) have caused widespread morbidity and mortality in humans. There are several factors that make zoonotic disease of particular concern for global health. Perhaps most critically, a lack of pre-existing immunity within the human population can facilitate the spread of disease among humans, as has been the case for the COVID-19 pandemic (Sette and Crotty, 2020).

Bats as Reservoirs of Zoonotic Viruses

Many zoonotic viruses, including SARS-CoV (Shi and Hu, 2008), SARS-CoV-2 (Zhou et al., 2020) and EBOV (Olival and Hayman, 2014), have been linked to bats. The study of bats as a reservoir of zoonotic viruses has thus been an area of focused research (Luis et al., 2013). Studies have demonstrated both that bats contain more viral species per taxa than other mammals and that these viruses often have characteristics associated with enhanced zoonotic potential (Olival et al., 2017).

In nature, certain bat species can be productively yet asymptomatically infected with viruses that cause overt disease in other species (Calisher et al., 2006). There is a growing consensus that a combination of decreased immunopathology and enhanced innate control of infection underly this phenomenon. For example, unique adaptations in immunoregulatory factors that result in decreased inflammation and presumably increased tolerance of viral infection have been described. These include natural killer cell receptors (Pavlovich et al., 2018), components of the inflammasome (Ahn et al., 2019; Zhang et al., 2013), and signaling molecules such as STING (Xie et al., 2018), IRF3 (Banerjee et al., 2020), IRF1, and IRF7 (Irving et al., 2020). Further, studies have revealed both expansion and contraction of IFNs in different bat species, indicative of potential regulatory differences from other mammals (Pavlovich et al., 2018; Zhou et al., 2016).

Indeed, studies have identified differences in the kinetics of the IFN response in bats, with possible functional implications (De La Cruz-Rivera et al., 2018). As mentioned in the above section "Examples of Species-Specific Effector Function", studies have begun to characterize consequences of host-virus arms races in bats on effector function.

RECEPTOR TRANSPORTING PROTEINS

Discovery of Receptor Transporting Proteins

Receptor transporting proteins (RTPs, also referred to as receptor transporter proteins) were first functionally characterized in a landmark paper in which Saito et al screened highly expressed cDNAs from olfactory neurons with predicted transmembrane domains for their ability to stabilize odorant receptors (Saito et al., 2004). Saito et al found that two members of the family, RTP1 and RTP2, interacted with and enhanced the expression of odorant receptors and thus predicted that they acted as chaperones. Further studies have demonstrated that RTP1 and RTP2 can interact with each other and in some cases have divergent roles in regulating receptor expression (Yu et al., 2017). Indeed, RTP1 was found in another study to form homodimers and heterodimers with RTP2, and RTP2 can, to a lesser degree, form heterodimers with RTP4 (Fukutani et al., 2019). Importantly, a recent study by Sharma et al found a physiological role for RTP1 and RTP2 (Sharma et al., 2017). Mice genetically deficient for both *Rtp1* and *Rtp2* demonstrate reduced olfactory receptor trafficking and an overabundance of receptors that are typically rare, demonstrating a developmental role for RTPs.

RTP3 and RTP4 were not found by Saito et al to have receptor transporting activity, though later studies demonstrated roles for RTP3 and RTP4 in modulating bitter taste receptor (Behrens et al., 2006) levels, and specifically for RTP4 in regulating opioid receptor levels (Decaillot et al.,

2008). Mechanisms of RTP4-mediated receptor stabilization remain somewhat unclear; it was suggested that for bitter taste receptors, RTP4 modulates the ER versus Golgi-localization of receptors, allowing their trafficking to the cell surface (Behrens et al., 2006), though in the case of opioid receptors it seems that expression of RTP4 reduces degradation of opioid receptors, permitting their trafficking to the cell surface – an observation that is consistent with the hypothesis that RTP4 acts as a chaperone (Decaillot et al., 2008).

Localization and Expression of Receptor Transporting Proteins

RTPs have been described as predominantly having Golgi (Behrens et al., 2006) and, in the case of RTP1 when co-expressed with odorant receptors (Wu et al., 2012), plasma membrane localization. These studies have largely relied upon ectopic expression of RTPs by plasmid transfection; only a recent study of endogenous murine RTP4 in N2A neuroblastoma cells interrogated localization of endogenous protein and described RTP4 as exhibiting both ER and Golgi localization, albeit without any co-stains for ER or Golgi markers (Fujita et al., 2019). The precise subcellular localization of endogenous RTPs thus remains a gap in the field's knowledge.

RTPs exhibit differential tissue expression profiles. *Rtp1* and *Rtp2* are highly expressed in olfactory neurons within the olfactory bulb in mice (Saito et al., 2004). A recent study demonstrated that RTP4 is predominantly expressed in the hippocampus and that it is upregulated following morphine administration (Fujita et al., 2019). RTP4 is conserved as an ISG in several mammals (Shaw et al., 2017) and has also been shown to be highly expressed in several immune cell populations (Tabula Muris et al., 2018). RTP4 is also highly expressed (alongside other ISGs)

during pregnancy in ungulates though the functional consequences – if any – of this expression pattern have not been explored (Gifford et al., 2008).

Receptor Transporting Proteins in Immunity

Unique among mammalian RTPs, RTP4 has an emerging role in immunity. In a comprehensive overexpression-based screen of ISGs (Schoggins et al., 2011), human RTP4 was identified as having modest antiviral properties towards yellow fever virus when ectopically expressed. Ectopically-expressed RTP4 was also found to modestly inhibit a human norovirus (HNoV) replicon, though this phenotype was not confirmed with live virus (Dang et al., 2018). Intriguingly, a homolog of RTPs was found to be highly IFN-induced in the Asian seabass (Liu et al., 2016), and a variant allele associated with disease phenotypes in experimental infection with nervous necrosis virus (NNV), a nodavirus, was later identified (Liu et al., 2017). Of note, YFV, HNoV, and NNV are all positive-sense RNA viruses, perhaps indicative of antiviral specificity of RTP4.

Outside of potential antiviral roles as an ISG, RTP4 was identified in a loss-of-function screen (Wroblewska et al., 2018) as a regulator of cytotoxic T cell mediated killing. Ablation of RTP4 in target cells resulted in defective killing by T cells in multiple models, though the mechanism by which this occurs remains undefined. More recently, an immunoregulatory role for RTP4 in both mice and humans was uncovered (He et al., 2020). Investigators found that RTP4 associates with TBK1, interfering with both its expression and its phosphorylation. Murine models of both malaria parasitemia and West Nile virus infection demonstrated an *in vivo* role of Rtp4 in modulating IFN signaling. Namely, disease severity was reduced in *Rtp4*-deficient mice, with

particular apparent protection in the brain. This is consistent with a model in which RTP4, perhaps in a tissue-specific manner, acts as a negative regulator of IFN signaling. RTP4 thus appears to be a multifunctional protein with antiviral, immunoregulatory, and neurodevelopmental roles.

CHAPTER TWO
Methodology

Cell culture

Huh7.5 (Male), HEK-293T (Female), U2OS (Female), and MDCK (Female) cells were maintained in DMEM supplemented with 10% FBS. *STAT1*$^{-/-}$ fibroblasts (Female) were maintained in RPMI supplemented in 10% FBS. BHK-21J (Male) cells were maintained in MEM supplemented with 10% FBS. PaKi (Male) and RO6E (sex unknown) cells were maintained in DMEM/F12 supplemented with 10% or 5% FBS, respectively. HCT-8 (Male) cells were maintained in RPMI supplemented with 10% horse serum. PK15 (Male) and Tb 1 Lu (Female) cells were maintained in MEM supplemented with sodium pyruvate and 10% FBS. All cells were cultured at 37°C in 5% CO2. A6 cells (ATCC CCL-102) were maintained in NCTC 109 media supplemented with 1x L-Glutamine, 15% ddH2O, and 10% FBS. A6 cells were maintained at 28°C in 5% CO2. Stable cell lines were maintained by passaging in the presence of 4μg/mL puromycin (Huh7.5, *STAT1*$^{-/-}$ fibroblasts, PaKi) or 15μg/mL blasticidin (Huh7.5).

Viruses

The generation and propagation of the following viruses have been previously described: EAV-GFP, ONNV-GFP, PIV3-GFP, YFV17D-Venus, HCV genotype 2a intragenotypic chimera expressing Ypet GFP (HCV-Ypet), CVB-GFP, WNV-GFP, and ZIKV strain PRVABC59 (Schoggins et al., 2011) (Schoggins et al., 2014) (Hanners et al., 2016). Infectious HCV-GLuc was generated from the infectious clone Jc1FLAG(p7-nsGluc2A) as previously described (Marukian

et al., 2008). VSV-GFP was produced by passaging in BHK cells. IAV (A/WSN/33) was produced by inoculation of sub-confluent MDCK cells as previously described (Szretter et al., 2006). An infectious clone of non-reporter WNV (strain TX02) was kindly provided by I. Frolov (University of Alabama Birmingham) and the virus was propagated as described for WNV-GFP. A ZIKV MR766-GFP infectious clone (kindly provided by M. Evans, Icahn School of Medicine at Mount Sinai) was used to generate the virus as described (Schwarz et al., 2016). The infectious clone pACNR-FLYF-17Dx (kindly provided by C. Rice) was used to generate non-reporter YFV-17D as previously described (Richardson et al., 2018). VEEV-GFP (strain TC83, a kind gift of I. Frolov) was generated by passaging in BHK-21J cells. Mengovirus (a kind gift of Julie Pfeiffer), echovirus E11 (a kind gift of Carolyn Coyne), and poliovirus (a kind gift of Julie Pfeiffer) were propagated on HeLa cells. VSV (kindly provided by Jack Rose) was generated by passaging in BHK-21J cells. ENTV (ATCC VR-378) was produced by passaging in BHK-21J cells. DENV (serotype 2 strain 16681, bearing a L52F mutation in NS4B) was propagated as previously described (Schoggins et al., 2012). HSV-1: (a kind gift of David Leib) was produced by passaging in VeroE6 cells. Human coronavirus OC43 (ATCC strain VR-1558) was propagated in HCT-8 cells as specified by the ATCC. Viral titers were determined by antibody staining (MAB9012, Millipore) and flow cytometry. All viral stocks were clarified by centrifugation, aliquotted, and stored at -80°C until use.

Lentiviral pseudoparticle production and transductions

All lentiviral pseudoparticles were generated by co-transfecting sub-confluent 293T cells with expression plasmids [pTRIP.CMV.IVSb.ISG.ires.TagRFP (Schoggins et al., 2011), pSCRPSY

(Kane et al., 2016), pSCRBBL (Richardson et al., 2018), or pLentiCRISPRv2 (Sanjana et al., 2014)], HIV-1 *gag-pol*, and VSV-glycoprotein at a ratio of 5:4:1 (TRIP), 25:5:1 (SCRPSY, SCRBBL), or 10:5:7 (LentiCRISPR) using XtremeGene 9 (Roche). Two to six hours post-transfection, media was replaced with DMEM containing 3% FBS. Supernatants were collected at 48h and 72h, pooled, filtered with a 0.45μM filter, supplemented with 20mM HEPES, aliquotted, and stored at -80°C until use.

Cells were either transduced by passive infection or by spinoculation. Briefly, lentivirus was added to a minimum volume of transduction media (3% FBS, appropriate base media for each cell line, 4μg/mL polybrene, 20mM HEPES) and added to cells. For passive transductions, cells were allowed to rest with pseudoparticle-containing media for 1-2 hours before addition of complete medium. For spinoculations, cells were centrifuged at 800xg at 37°C for 40 minutes, after which media was replaced with standard growth media.

AAV production

AAV-DJ was produced with the helper-free AAV-DJ system (CellBioLabs). Briefly, pHelper, pAAV-DJ, and pAAV-Gateway expression cassettes were transfected with XtremeGene9 into subconfluent 293T cells at a ratio of 1:1:1. 48h post-transfection, supernatant and lifted cells were combined, freeze-thawed four times in a dry ice/ethanol bath, centrifuged to clear debris, aliquotted, and stored at -80C until use. The pAAV-Gateway cassette, a kind gift from Matthew Nolan (Addgene# 32671) (White et al., 2011), was packaged for gene expression. AAV titers were determined by qPCR with ITR-specific primers.

CRISPR editing

RTP4 KO clonal PaKi cell lines: PaKi cells were seeded at 250,000 c/w on a 6w plate. Cells were transfected the following day with LentiCRISPRv2 plasmid containing guide specific to *RTP4* using lipofectamine. 48h post-transfection cells were replated into puromycin (4µg/mL) selective media. After two days, selective media was replaced with complete non-selective media. Cells were plated in limiting dilutions and single-cell clones were expanded and targeted clones were identified by Sanger sequencing.

STAT1 KO cells: PaKi cells were seeded at 250,000 c/w on a 6w plate. Cells were transduced with lentiviral pseudoparticles containing a CRISPR guide specific to *STAT1*. 48h post-transduction cells were replated into puromycin (4µg/mL) selective media. Following selection, cells were plated in limiting dilutions and single-cell clones were expanded and targeted clones were identified by western blotting.

Dual-guide U2OS cells: U2OS cells were co-transduced with lentiviral pseudoparticles containing two separate guides specific to human *RTP4* from the Brunello library (Broad Institute) under either a puromycin or a blasticidin selection cassette. The bulk population of cells was passaged in selective media (1µg/mL puromycin and 10µg/mL blasticidin) for one week and then maintained in lower-concentration selective media (0.5µg/mL puromycin and 5µg/mL blasticidin).

Dual-guide PK15 cells: PK15 cells were co-transduced with lentiviral pseudoparticles containing two separate guides specific to pig *RTP4* under either a puromycin or a blasticidin selection cassette. The bulk population of cells was passaged in selective media.

Genomically Tagged HA-RTP4 cells: PaKi cells were seeded at 250,000 c/w on a 6w plate. Cells were transfected the next day with a 2:1 ratio of an HA-tagged homology arm (Related Data:

Supplementary File 4) and LentiCRISPRv2 plasmid containing a guide specific to RTP4 using Lipofectamine 3000 (Invitrogen) in the presence of 0.1µm SCR-7, a DNA ligase IV inhibitor (Tocris). 72h post-transfection cells were replated into puromycin (4µg/mL) selective media. After three days, selective media was replaced with complete non-selective media. Cells were plated in limiting dilutions and single-cell clones were expanded. Targeted cells were identified by PCR and validated by Sanger sequencing and western blotting.

Transfection of PaKi cells

PaKi cells were transfected with Lipofectamine 3000 (ThermoFisher) per manufacturer protocols. For cells seeded on a 24w plate, cells 500ng of plasmid was mixed with 25µl of Optimem and 1µl of p3000 reagent. This mixture was added to premixed Lipofectamine (1.5µl) and Optimem (25µl). After ten minutes, 50µl of the transfection complex was added to each well. Mixes were scaled linearly with well size for transfections on other formats, and master mixes were made when appropriate.

Viral infections

Cells were seeded at 50,000-100,000 (24w plate),150,000-200,000 (12w plate), 4,000,000 (10cm dish), or 12,000,000 (15cm dish) cells per well, depending upon experiment endpoint, the day prior to infection. Virus was added to cells in a minimal volume and incubated for one hour (all viruses besides DENV) or two hours (DENV). After incubation, complete media was added to maintain cells until harvest. Unless specifically stated, all infections were performed at an MOI $\leq$ 1 infectious units per cell to ensure that most cells were infected by only one viral particle. All

infected cells were incubated at 37C with the exception of HCoV-OC43, which was incubated at 33C. For infections to assess viral production by plaque assay, inoculum was aspirated and cells were washed four times with PBS prior to addition of complete media. Unless specifically mentioned in the figure legend, infectivity for experiments is quantified by flow cytometry. All WNV infections were performed in a Biosafety Level 3 (BSL3) facility according to institutional guidelines provided by the UT Southwestern Office of Business and Safety Continuity.

Plaque assays

For WNV, ENTV, and YFV plaque assays, BHK-21J cells were seeded at 400,000 cells per well on 6 well plates one day prior to infection. Supernatants were serially diluted in MEM supplemented with 1% FBS and 200ul of relevant dilutions were applied to BHKs. Cells were incubated with intermittent rocking for one hour, after which wells were overlaid with overlay media (1% Avicel, DMEM, 4% FBS, 100U/mL penicillin/100µg/mL streptomycin, 10mM HEPES, 0.1%$NaHCO_3$). After three days, wells were fixed with formaldehyde and plaques were visualized by staining with crystal violet.

Crystal violet stains

To assess cell survival, cells were fixed by direct addition of formaldehyde to culture media to a final concentration of 2% and subsequently stained with crystal violet. Images of crystal violet stains were captured using a Google Pixel 2 smartphone.

Intracellular antibody staining for flow cytometry

Intracellular staining was performed using the CytoFix/Cytoperm Solution Kit (BD). Briefly, cells were fixed/permeabilized for 30 minutes, washed once, incubated in primary antibody (4G2: 1:2500, 0G5: 1:2000, 542-7D: 1:500, MAB8251: 1:1000) for 30 minutes, washed once, incubated with secondary antibody for 30 minutes, washed once, and resuspended in FACS buffer (PBS plus 3%FBS). Viral proteins used for assessing viral infection: E protein (4G2 (BioXCell): DENV, ZIKV, WNV, ENTV; 0G5 (Novus): YFV), N protein (542-7D (Millipore-Sigma): HCoV-OC43), NP (MAB8251 (Millipore-Sigma): IAV), dsRNA (J2 (Scicons: PV, E11, MenV).

Flow cytometry

Samples were run in a Stratedigm S1000 flow cytometer with a A600 96-well plate reader. When necessary, compensation was performed at the time of collection in CellCapture (Stratedigm). FlowJo (BD) was used to quantify data.

Digitonin membrane association assays

For immunofluorescence: cells were washed once with PBS, washed once with HCN buffer (50mM HEPES, 150mM $NaCl_2$, 2mM $CaCl_2$), then either mock treated or permeabilized with 20µM digitonin in 250µl HCN for 15 minutes at RT, washed once with PBS, and fixed with PFA. Standard immunofluorescence was used to detect protein.

For western blotting: 100,000 cells were washed once with PBS, and once with HCN. Cells were resuspended in 100µl of HCN supplemented with 20µM digitonin (or mock) and incubated for 20 minutes at 4C with end-over-end rotation. Cells were pelleted, supernatant was removed and

combined with 2X SDS loading buffer, and pellets were washed once with 500µl of HCN buffer. Pellets were resuspended in SDS loading buffer.

CLIP-qPCR

CLIP experiments were performed as previously described with slight modification (Conrad, 2008). Briefly, cells were washed with PBS and cross-linked with 150mJ/cm^2 in a Spectrolinker XL1000 or XL1500 (Spectroline). Cells were scraped, pelleted, and snap-frozen. Cells were thawed and lysed in SDS lysis buffer (0.5% SDS, 50mM Tris-Cl pH 6.8, 1mM EDTA, 0.125mg/mL heparin, 2.5mg/mL torula yeast RNA (Sigma), and 1x protease inhibitors (Roche)). Samples were boiled at 65C for 5 minutes and returned to ice. Buffer was adjusted to RIPA by addition of a correction buffer (1.25%NP-40, 0.625% sodium deoxycholate, 62.5mM Tris-HCl pH 8.0, 2.25mM EDTA, 187.5mM NaCl). Lysate was passed through a QIAshredder (Qiagen) twice (10cm plates) or three times (15cm plates). Lysates were cleared by three high-speed spins with tube transfers. Cleared lysates were supplemented with 5mM $CaCl_2$ and treated with 30U of DNase (NEB) for 15 minutes. When performed, nuclease digestion was completed by addition of 50 gel units of micrococcal nuclease for ten minutes, which was then quenched by addition of EGTA to a final concentration of 20mM. RIPA buffer (1%NP-40, 0.5% sodium deoxycholate, 0.1% SDS, 150mM NaCl, 50mM Tris-Cl pH 8.0, 2mM EDTA). Antibody conjugated beads (preconjugated HA or 10ug of antibody/protein A-conjugated beads) were added to samples (Pierce). Samples were rotated end over end at 4C for 2h. Samples were placed on a magnetic separator and washed three times with RIPA, once with RIPA supplemented with 1M Urea, and twice with RIPA. RNA was eluted from beads by addition of Proteinase K buffer (0.5mg/mL Proteinase K (Ambion),

0.5% SDS, 20mM Tris-Cl pH 7.5, 5mM EDTA, 16.7ng/µl GlycoBlue (Invitrogen), 0.1mg/mL torula yeast RNA) and incubation for 1-2h with shaking at 37C. Following elution, RNA was extracted with phenol-chloroform-isoamyl alcohol, extracted with chloroform, precipitated, DNase-treated, re-purified, and cDNA was generated using Superscript IV and random hexamers. cDNA was treated with RNase H and RNase A, precipitated, and resuspended in a low volume of water for storage at -20C. cDNA was diluted prior to qPCR.

Polysome profiling

Cycloheximide was added to culture media to a final concentration of 100ug/mL and cells were incubated on ice for five minutes to fix ribosomes to RNA. Media was aspirated and cells were resuspended in 500µl of Polysome extraction buffer (140mM KCl, 5mM $MgCl_2$, 20mM Tris-HCl pH 8.0, 1mM DTT, 100ug/mL cycloheximide). Cells were pelleted and resuspended in 200µl of PEB + 1% Triton-X100. Cells were incubated on ice for 20 minutes with intermittent tipping. Lysates were cleared by centrifugation (10,000xg, 10m, 4C) and transferred to a fresh tube. 10 OD 260 of lysate was resolved on a 5mL gradient (50% w/v to 12.5% w/v sucrose in PEB) by centrifugation for 150,000xg for 1.5h in an SW40ti rotor. Following centrifugation, the bottom of the tube was pierced and 500µl fractions were collected. Polysome-containing fractions were identified by spectroscopy, and both polysome-associated and input RNA were isolated with TRIzol (Invitrogen) and cDNA was synthesized using Mu-MLV RT (NEB).

Quantitative RT-PCR

For most experiments, RNA was isolated using TRIzol (Invitrogen) and cDNA was reverse-transcribed using MμLV reverse transcriptase (NEB). RT-qPCR reactions were performed using iTaq Universal SYBR Green Supermix (Bio-Rad). For some gene expression assays and the viral cold-bind experiment, one-step reverse transcriptase pPCR was performed using the QuantiFast SYBR Green RT-PCR kit (Qiagen).

Immunofluorescence

Cells were fixed with 4% PFA in PBS. Cells were washed with PBS, then permeabilized with 0.2% Triton-X 100. Cells were blocked with 10%BSA/5%Goat Serum/PBS for at least 30 minutes. Primary antibody was added in blocking solution and incubated for 1-2 hours. Cells were washed 3x with PBS, after which secondary antibody was added in 3% BSA and incubated for 30 minutes. When included, wheat germ agglutinin was added to the secondary antibody dilution. Cells were washed 3x with PBS, and then mounted using ProLong Diamond (ThermoFisher). Imaging was performed either on an Olympus FV10i-LIV or a Zeiss Observer Z.1. Images were processed in ImageJ or Fluoview Viewer (Olympus).

Tyramide signal amplification

The Tyramide SuperBoost system (ThermoFisher) was used per manufacturer specifications with a labeling time of five minutes. Cells were subsequently counterstained by standard immunofluorescence.

Proximity ligation assay

The DuoLink proximity ligation assay system (Sigma) was used per manufacturer protocol. Briefly, cells were fixed with 4% PFA, washed, and blocked. Primary antibodies were incubated for two hours, after which cells were washed twice and incubated with anti-mouse and anti-rabbit probes for one hour. After two washes, adapters were ligated and rolling circle amplification was performed. Following final washes, slides were mounted with DuoLink mounting media with DAPI and immediately imaged. Single primary and no primary controls were included with every replicate.

Immunoprecipitations

Cells were harvested with Accumax, pelleted, and resuspended in RSB150T (50mM TRIS-HCl 7.5, 150mM $NaCl_2$, 2.5mM MgCl2, 1mM CaCl2, 1% Triton-X100). Lysates were treated with DNase (NEB) at 20U/mL for 10 minutes, after which lysates were cleared by centrifugation at 16,000xg for 10 minutes at 4C. Lysates were subsequently incubated with equilibrated beads for one hour, after which beads were captured on a magnetic separator and washed seven times in RSB150T, including one wash with 0.1% SDS. Protein was eluted by boiling in 1x SDS buffer.

cDNA library construction

PaKi cells were seeded at 2E6 cells in two 10cm dishes. The following day, cells were treated with universal Type I interferon at 100U/mL. After 6 hours, RNA was isolated with TRIol. mRNA was purified with an mRNA purification kit (Miltenyi). The CloneMiner II cDNA library construction kit (ThermoFisher) was used to generate the Gateway-compatible cDNA library from 2ug of

mRNA. Library size was calculated by plating dilutions on agarose plates. The library was qualified by restriction digest to ensure appropriate average insert size (Supplemental Figure 5A). The cDNA library was transferred into an expression library (pSCRPSY) by several pooled LR reactions. Libraries were amplified using SeaPrep soft agar (Lonza) per manufacturer recommendations. Briefly, 2X LB/SeaPrep agar was autoclaved and chilled to 25°C in a water bath, after which antibiotics and library-transformed bacteria were added. Inoculated LB was aliquotted into 50mL conical vials and submerged in wet ice for one hour, after which conicals were incubated at 37°C for 48h. Conicals were centrifuged, agar was decanted, and pellets were pooled and maxiprepped (Qiagen). Library statistics are included in Table 1.

Screen for antiviral bat cDNAs

Huh7.5 cells were transduced at an MOI of 0.5 with lentiviral pseudoparticles containing the black flying fox cDNA library (estimated transcriptome coverage: 20x) to limit the number of cells with multiple lentiviral inserts. The library was introduced at roughly 10x coverage and cells were expanded prior to infection. Library-transduced Huh7.5 cells were infected with DENV (library coverage 20x) or ZIKV (library coverage 100x) at an MOI of 0.01. RNA was harvested from cells at 14 days (ZIKV) and 31 days (DENV) post-infection. RNA from surviving cells was compared to RNA from uninfected, library-transduced cells (10x coverage) to identify enriched cDNAs.

Plasmids and cloning

RTP4 orthologs were cloned from oligo(dT)-primed cDNA from IFN-treated cells as follows: Egyptian fruit bat, RO6E cells; dog, MDCK cells; Mexican free-tailed bat, Tb 1 Lu cells; pig, PK15 cells, using gene-specific primers. Black flying fox *RTP4* was cloned from the black flying fox cDNA library generated in this work using gene-specific primers. Human *RTP4* and *IRF1* were previously cloned (Schoggins et al., 2011). Rhesus macaque *RTP4* was previously cloned (Kane et al., 2016). Mouse *RTP4* was synthesized as a gBlock (IDT). Cow *RTP4* was cloned from the Mammalian Gene Collection clone ID 8120985 (Dharmacon) using gene-specific PCR primers. Reconstructed ancestral mammalian *RTP4* was synthesized (IDT). Black flying fox *IFI6* was synthesized (Genewiz). Black flying fox *SHFL* was cloned from the black flying fox cDNA library generated in this work using gene-specific primers.

The following orthologs were HA-tagged by restriction digest and ligation of annealed HA oligos: cow, black flying fox, rhesus macaque, human, Egyptian fruit bat. HA tags were integrated into the cloning primers for mouse, Mexican free-tailed bat, pig, dog, and ancestral reconstructed *RTP4*.

Serial truncations of black flying fox *RTP4* were cloned by PCR using primers listed in Supplemental Table 3. Black flying fox *RTP4* ZFD point mutations were cloned by restriction digest using synthesized gBlocks (IDT). Human *RTP4* ZFD point mutation was introduced using QuickChange mutagenesis.

Other RTP homologs were synthesized as gBlocks (IDT). Loss-of-function point mutations were introduced via QuickChange mutagenesis using Herculase II (Agilent).

A doxycycline-inducible RTP4 expression construct was generated by directional ligation of PCR-amplified HA-tagged paRTP4 using primers with flanking AgeI and MluI cut sites into pTRIPZ (Dharmacon).

The freetail bat RTP4 escape mutant infectious clone was generated by overlap extension PCR. Briefly, primers containing the identified point mutation (YFV17DE2057K-F, YFV17DE2057K-R) were used along with primers (10F and 11R) that flanked upstream (NheI) and downstream (NgoMIV) cut sites to amplify fragments of the YFV genome with the desired point mutation. These fragments were purified and stitched together, and the resulting product was ligated into the parental pACNR-FLYF-17Dx plasmid.

CRISPRdirect (Naito et al., 2015) was used to design CRISPR guides for black flying fox *RTP4,* black flying fox *STAT1*, and pig *RTP4*. Human *RTP4* guides were generated based on on the Brunello Library (Broad). CRISPR guides were cloned into LentiCrisprV2 as previously described (Sanjana et al., 2014). pUC57-KAN-HApaRTP4locus (the donor vector that was used for genomic tagging) was synthesized by Genewiz.

All expression constructs were cloned into the Gateway expression vectors pSCRPSY (Kane et al., 2016), pSCRBBL (Richardson et al., 2018), pTRIP (Schoggins et al., 2011), or pAAV-Gateway by LR recombinase reactions. All relevant primers are included in Appendix A.

In vitro transcription of viral and replicon RNA

Viral infectious clone (see: Cell Culture and Viruses) and replicon (YFV-R.luc2A-RP) (Jones et al., 2005) RNA was transcribed using the mMessage mMachine SP6 kit (Ambion). RNA was purified using either RNeasy mini kit (Qiagen) or MEGAClear (ThermoFisher).

Electroporation of viral RNA

Electroporations were performed as previously described (Lindenbach and Rice, 1997). Briefly, BHK-21J or *STAT1*$^{-/-}$ human fibroblasts were trypsinized, washed in ice-cold PBS, and 8E6 cells in 400ul of PBS were aliquotted into cuvettes along with 5µg of viral RNA. Cells were electroporated at 860V with five pulses and re-seeded into flasks or dishes for production.

Western blotting

Unless otherwise noted, cells were lysed directly in 1x SDS loading buffer (10% glycerol, 5% BME, 62.5mM TRIS-HCl pH 6.8, 2% SDS, and BPB), boiled, and sonicated (Sonics Vibra-Cell CV188). Samples were run on 12% TGX FastCast acrylamide gels (Bio-Rad) and transferred to nitrocellulose or PVDF membranes using a TransBlot Turbo system (Bio-Rad). Blots were blocked in 5% dry milk/TBS-T for 30 minutes to an hour at RT or overnight at 4C. Primary antibodies were diluted in 5%BSA/TBS-T and added for 1 to 2 hours at RT or overnight at 4C. Blots were washed four times in TBS-T before addition of HRP-conjugated secondary antibody in 5% milk for thirty minutes. Blots were washed four times in TBS-T prior to detection with either Pierce ECL (ThermoFisher) or Clarity ECL (Bio-Rad) substrate and exposure to radiography film. For quantitative blotting, LI-COR IRDye secondary antibodies were used and signal was detected using a LI-COR Odyssey Fc detection system.

Replicon assay

Cells were seeded at 35,000 cells per well in 48 well plates the day before transfection. 100ng YFRluc-2A RNA was transfected into each well using TransIT-mRNA (Mirus). Cells were

washed once with PBS and lysed in Renilla lysis buffer and assayed using the Renilla Luciferase Assay System (Promega).

HCV-GLuc assay

Cells were seeded at 35,000 cells per well in 48 well plates the day before infection. Cells were infected with HCV-GLuc at an MOI of 0.5. Supernatants were collected and replaced with fresh media at the indicated time points. Supernatants were stored at -80C for the duration of the time course, after which they were quantified by luciferase assay using the Renilla Luciferase Assay System (Promega).

Viral cold bind-qPCR assay

PaKi cells were plated at 7E5 cells per well on a 24-well plate. The next day, cells were equilibrated to 4 °C for 30 min in growth medium. Media was then aspirated and YFV-17D diluted in cold 1% FBS/RPMI was added and incubated for 1 h at 4 °C. Cells were then washed 2 x with ice-cold PBS and harvested for RNA by RNeasy Mini Kit (Qiagen). Viral concentration was quantified by qRT-PCR. A standard curve was generated by spiking in vitro transcribed YFV-17D RNA into a background of 40 ng uninfected cellular RNA and used to back-calculate fg YFV RNA for each sample based on C_T value.

Doxycycline induction for viral infections

One day after plating, media was replaced with doxycycline-containing media at indicated concentrations. 24 hours post-treatment, cells were infected as per standard protocol. After one

hour, inoculum was aspirated and freshly-diluted doxycycline-containing media was added back for the duration of the infection. 50mg/mL doxycycline stocks were stored in DMSO at -20C and diluted into sterile water at a 1000x concentration, which was then added to growth media.

Serial passaging and viral sequencing

Huh7.5 cells expressing RTP4 orthologs were infected with YFV-17D, ENTV, or WNV at an MOI of 5 (ENTV, YFV) or 30 (WNV). After one (ENTV) or two (YFV and WNV) days, one-third of the supernatant was transferred to naive cells and allowed to infect for two days. Serial passaging proceeded for seven (ENTV, YFV) or 15 (WNV) passages. After validation of the YFV escape mutant, BHKs were infected with limiting dilutions of viral stocks and clonal YFV populations were derived from a dilution at which roughly 40% of challenged wells exhibited CPE. BHK-21J cells were infected with clonal YFV escape mutant viral stocks for 48h, after which RNA was extracted with TRIzol. cDNA synthesis was primed with random hexamers and RT was performed using SuperScript IV (Invitrogen). Tiling PCR was used to amplify the viral genome in roughly 1kb fragments. Sanger sequencing was used to identify mutations relative to wild-type YFV-17D.

Poly(I:C) transfection of A6 cells

One day prior to transfection, A6 cells were seeded at 400,000 cells per well on a 6-well plate in 2mL of media. Cells were transfected with 2µg/well of pPoly(I:C) (HMW, InvivoGen) using Lipofectamine 3000. Briefly, a master mix containing 2µg of poly(I:C), 4µl of p3000 reagent, and 100µL of OptiMEM was mixed with a master mix containing 100µl of OptiMEM and 6µl of

Lipofectamine 3000, incubated for 10 minutes, and added directly to each well. For mock treatments, the same protocol was used with the omission of poly(I:C).

RNA isolations and sequencing (A6 cells)

RNA was isolated using Direct-zol (Zymo). Samples were treated with DNase, per manufacturer recommendation. RNA Sequencing was performed by Novagene (NovaSeq 6000 PE150 configuration). As input, 1µg RNA per sample was polyA-enriched and sequencing libraries were generated using NEBNext® UltraTM RNA. Library Prep Kit for Illumina® (NEB, USA) was used according to manufacturer's recommendations.

Analysis of RNA-seq data

Reads were mapped to the NCBI Xenopus_Laevis_V2 assembly (GCF_001663975.1) using HISAT2. DESeq2 (Love et al., 2014) was used to identify differentially-expressed genes. Adjusted P values were calculated using Benjamini and Hochberg's approach for controlling the False Discovery Rate (FDR). For temporal clustering analysis, DESeq2 was used to filter low-count transcripts (final count: 22,208) and perform pairwise comparisons of treated conditions and mock. Log_2Fold-Change values were subsequently scaled and per-transcript induction profiles were clustered using Ward's method (Ward, 1963) as implemented in R.

Annotation of Xenopus laevis transcripts

BLAST was used to confirm transcript identity by homology. To identify ISGs, homologs were assessed for induction on either the Orthologous Clusters of Interferon-Stimulated Genes database (http://isg.data.cvr.ac.uk/) or the Interferome (interferome.org/).

Phylogenetic analysis

Multiple sequence alignments were generated using MUSCLE as implemented in MEGA X (Kumar et al., 2018). Alignments were trimmed using Gblocks (Castresana, 2000). When required, file formats were converted using ALTER (Glez-Pena et al., 2010). PAML was used to assess signatures of evolutionary pressure present in nucleic acid alignments. Briefly, CodeML was used with the F3x4 codon frequency table and default settings (Yang, 2007). Likelihood ratio tests were used to compare Model 8 (beta and omega - allowing for positive selection) and Model 7 (beta - no positive selection), as well as Model 8 and Model 8a (beta and omega, constrained to no positive selection). Sites that passed a stringent test (Bayes empirical bayes) test were considered to be undergoing positive selection. To perform a free-ratio analysis, PAML was run with Model 1 (branch) and NSsites = 0 to obtain a dN/dS value for each branch. HyPhy analyses (FUBAR, BUSTED, aBSREL, GARD) were either run on a local system or performed as implemented on DataMonkey (Weaver et al., 2018).

Ancestral sequence reconstruction

An alignment of 35 mammalian *RTP4* sequences was input into FastML (Ashkenazy et al., 2012) using default parameters. The resulting sequence was synthesized (IDT).

Clustering and correlation analysis of phylogenetic, expression, and infectivity data

Hierarchical clustering was used to generate dendrograms for infectivity data (normalized to vector control) and protein expression (normalized to actin) in R. The package dendextend (Galili, 2015) was used to compare clusters to a phylogenetic tree of all orthologs using the Baker's gamma statistic, a measure of the similarity of two tree topologies. R code is available upon request.

Colocalization analysis

Colocalization analysis was performed using coloc2 in ImageJ. When possible, individual cells or small clusters of cells were independently analyzed by defining ROIs based on bright field images.

RNA sequencing and analysis (ISG screen)

RNA Sequencing was performed by Genewiz (NextSeq 500 2x150PE configuration). Fastq files were subjected to quality check using fastqc and fastq_screen. Reads from each sample were mapped to the *Pteropus alecto* (assembly ASM32557v1) using STAR (V2.5.3) (Dobin et al., 2013). Read counts mapping uniquely to *Pteropus alecto* genes were generated using STAR and differential expression analysis was performed using edgeR (Robinson et al., 2010).

Synteny analysis

NCBI and EMSEMBL genome viewers were used to manually assess the location of RTPs relative to proximal genomic elements. NCBI BLAST was used to probe for pseudogenes or un-annotated RTPs.

ISG length analysis

ISG ortholog lengths were downloaded from the NCBI on 2/10/2020. Outliers were removed using the ROUT test with Q = 1. N = 72 (Mx1), 101 (Viperin), 85 (IFI6), 145 (SHFL), and 118 (RTP4).

Quantification and statistical analysis

Statistical analyses were performed using GraphPad Prism unless otherwise noted. Unless otherwise indicated, all comparisons are relative to control (Ctrl), as labeled. For data with two groups, two-tailed t-tests were used. For data with more than two groups, ANOVA tests were used and appropriate adjustments were made for multiple hypothesis testing. Additional details are available in all figure legends where any statistical tests were performed. Unless otherwise specified, P values are denoted as follows: n.s. not significant, *P<0.05, **P<0.01, ***P<0.001, ****P<0.0001.

CHAPTER THREE
Results

RTP4 IS A POTENT IFN-INDUCIBLE ANTI-FLAVIVIRUS EFFECTOR ENGAGED IN A HOST-VIRUS ARMS RACE IN BATS AND OTHER MAMMALS

Introduction

Host-virus conflicts drive the evolution of antiviral restriction factors, many of which exhibit divergent properties among related species (Daugherty and Malik, 2012). In mammals, a class of antiviral effectors – interferon-stimulated genes (ISGs) – are induced as part of the interferon (IFN) response. The combined activities of ISGs restrict viral infection, but our understanding of the mechanism of action and species specificities of many ISGs is limited. For example, we know the identity, and in some cases the mechanisms, of several human ISGs targeting mosquito-borne flaviviruses (e.g. dengue virus (DENV), yellow fever virus (YFV), West Nile virus (WNV), and Zika virus (ZIKV)) (Li et al., 2013; Richardson et al., 2018; Schoggins et al., 2014; Schoggins et al., 2011; Suzuki et al., 2016). However, flaviviruses are zoonotic pathogens; they can be transmitted to humans from animals such as birds or other mammals, frequently via an arthropod vector. We know little about antiviral mechanisms targeting flaviviruses in non-human hosts.

Among mammals, bats are particularly rich in zoonotic viruses, including flaviviruses (Olival et al., 2017). In nature, certain bat species can be productively yet asymptomatically infected with viruses that cause overt disease in other species (Calisher et al., 2006). Of the 1200+ extant bat species, one of the most studied species from the standpoint of viral zoonoses is the black flying fox, *Pteropus alecto*. It is best known as a reservoir host of henipaviruses (Halpin et

al., 2000), though flaviviruses can infect the black flying fox in experimental settings (van den Hurk 2009) and may also naturally circulate in this species (Irving et al., 2019). Experimental studies have demonstrated the ability of the black flying fox to transmit the flavivirus Japanese encephalitis virus (JEV) to mosquitos, highlighting the species' potential as a reservoir for zoonotic flaviviruses (van den Hurk et al., 2009). Studies of bat immunity suggest that bats have adapted to either tolerate or control viral infection. For example, unique adaptations in immunoregulatory factors that result in decreased inflammation and presumably increased tolerance of viral infection have been described. These include natural killer cell receptors (Pavlovich et al., 2018), components of the inflammasome (Ahn et al., 2019; Zhang et al., 2013), and signaling molecules such as STING (Xie et al., 2018) and IRF3 (Banerjee et al., 2020). Further, studies have revealed both expansion and contraction of IFNs in different bat species (Pavlovich et al., 2018; Zhou et al., 2016). However, efforts to characterize antiviral effector mechanisms in bats are relatively limited. Targeted studies of individual effectors, such as IFITM3 (Benfield et al., 2020) and Mx family GTPases (Fuchs et al., 2017), have yielded insight into unique adaptations in bats. Genome-scale phylogenetic analyses have identified many immune factors (including effectors) that exhibit a signature of positive selection in bats (Hawkins et al., 2019). Otherwise, little is known about the antiviral effector repertoire in bats relative to other mammals.

Here, we screen black flying fox ISGs for their ability to restrict flavivirus infection. We identify and characterize black flying fox Receptor Transporting Protein 4 (RTP4) as a potent IFN-inducible effector that suppresses genome amplification. We further assess the antiviral properties of RTP4 from nine diverse mammals and find that each exhibits a striking level of functional specialization across mammalian species. Moreover, experimental evolution of a flavivirus yielded

an adaptation that promotes the escape of inhibition by one RTP4 ortholog but not others, underscoring the specificity of the host-virus molecular arms race.

Results

A gain of function screen identifies black flying fox RTP4 as an inhibitor of flavivirus infection

IFN induces ISGs and protects black flying fox cells from viral infection (De La Cruz-Rivera et al., 2018) (Zhou et al., 2016). To establish a screening platform to identify these protective genes, we treated kidney-derived black flying fox cells (PaKi cells) (Crameri et al., 2009) with IFN to generate a cDNA library enriched for antiviral ISGs (Figure 3A) (Table 1). We expressed the cDNA library in Huh7.5 cells and infected them with dengue (DENV) and Zika (ZIKV) viruses. Virus-induced cell death eliminated cells that expressed non-protective cDNAs. Cells that resisted infection, presumably via antiviral gene expression, were expanded, and the enriched bat cDNAs were identified by RNA-sequencing (Figure 4A). Three black flying fox ISGs were enriched in cells that survived either DENV (RTP4 and SHFL) or ZIKV (RTP4, SHFL, and IFI6) infection (Figure 4B). We and others have characterized human IFI6 as a flavivirus restriction factor (Dukhovny et al., 2019; Richardson et al., 2018), and human SHFL is a known effector with broad antiviral activity (Balinsky et al., 2017; Suzuki et al., 2016; Wang et al., 2019). Human RTP4, however, had only modest antiviral activity in our previous ISG screens (Schoggins et al., 2011) and was therefore not studied in detail.

RTP4 belongs to a family of proteins (RTP1s, RTP2, RTP3, and RTP4 in humans) that regulate the expression of cell-surface G-coupled protein receptors (Saito et al., 2004). Previous literature has implicated RTP4 as a regulator of opioid and taste receptors (Behrens et al., 2006;

Decaillot et al., 2008), but its antiviral role has not been explored. RTP4 is the only known IFN-inducible member of the RTP protein family in humans and is conserved as an ISG across mammals (Shaw et al., 2017). We confirmed by RT-qPCR that *RTP4* is an ISG in black flying fox cells (Figure 3B). To validate our screen, we assessed the ability of ectopically-expressed black flying fox RTP4, SHFL, and IFI6 to inhibit the flaviviruses ZIKV, DENV, and YFV and found that all three inhibited each virus tested (Figure 4C).

Humans and bats diverged roughly 96 million years ago (Kumar et al., 2017). At the amino acid level, human and black flying fox orthologs of SHFL, IFI6, and RTP4 share 95.1%, 67.7%, and 58.4% identity, respectively, suggesting that RTP4 may be a relatively divergent effector. We thus compared the ability of RTP4 from the black flying fox (*Pteropus alecto*, paRTP4) and humans (*Homo sapiens*, hsRTP4) to inhibit YFV when ectopically expressed in either human or black flying fox cells. In either species, paRTP4 exhibited greater antiviral activity than hsRTP4, suggesting that paRTP4 is functionally divergent and that this phenotype is not a result of expression in a heterologous cellular background (Figures 4D-F). Importantly, however, ectopically-expressed paRTP4 expresses at much higher levels than hsRTP4 (Figure 3C) and therefore expression may contribute to differences in antiviral potency. To assess whether endogenous paRTP4 is antiviral, we used CRISPR-Cas9 to genetically ablate RTP4 in PaKi cells. Two clonal RTP4-knockout cell lines (Figure 3D) were challenged with YFV (Figure 4G). Loss of RTP4 led to enhanced infectivity relative to nontargeting control cell lines, albeit to a lesser degree than a STAT1 knockout cell line (Figure 3E-F). We observed no difference in binding of virus to RTP4 KO cells relative to control cells (Figure 3G), suggesting that RTP4 ablation does

not influence flavivirus receptor levels, as may have been expected given the role of RTP4 in chemosensory receptor trafficking (Decaillot et al., 2008).

RTP4 restricts the replication of viruses that replicate at the ER

We next sought to determine the antiviral specificity of paRTP4 and hsRTP4. We compared the ability of ectopically-expressed paRTP4 and hsRTP4 to restrict viruses from several families (Figures 5A and 6A). RTP4 orthologs exhibited strong (paRTP4) or modest (hsRTP4) antiviral activity against the flaviviruses (ZIKV, YFV, and DENV). paRTP4, but not hsRTP4, restricted the closely-related *Flaviviridae* member, the hepacivirus hepatitis C virus (HCV), and to a lesser degree the nidoviruses equine arteritis virus (EAV) and human coronavirus OC43 (HCoV-OC43). Neither ortholog inhibited the picornavirus coxsackievirus B3 (CVB), the alphaviruses Venezuelan equine encephalitis virus (VEEV) and o'nyong'nyong virus (ONNV), the rhabdovirus vesicular stomatitis virus (VSV), the paramyxovirus human parainfluenza virus type 3 (PIV3), the orthomyxovirus influenza A virus (IAV), or the herpesvirus herpes simplex virus 1 (HSV-1). Of note, the viruses inhibited by both RTP4 orthologs are unified in their use of the host ER as a site for viral replication (Gillespie et al., 2010; Knoops et al., 2008). As a control, human IRF1 inhibited most viruses tested, as previously shown (Schoggins et al., 2014; Schoggins et al., 2011).

Since RTP4 potently inhibits flaviviruses, we next examined which step of the flavivirus lifecycle it targets. We infected cells expressing paRTP4, hsRTP4, or a vector control with a reporter HCV that expresses Gaussia luciferase (GLuc), which is secreted into culture supernatant when viral protein is translated (Figure 5B). This tool distinguishes early (entry and primary translation of incoming viral RNA) and late (genome replication) phases of infection. paRTP4 had

no effect on GLuc production during primary translation but markedly reduced GLuc levels during viral replication. hsRTP4 did not reduce GLuc production at any time point, consistent with its lack of activity towards HCV observed when testing multiple viruses (Figure 5A). We next used a minimal, replication-competent, Renilla luciferase (RLuc)-expressing YFV RNA referred to as a 'subgenomic replicon' to confirm that RTP4 targets the replication phase of viral infection. When transfected into cells, this naked viral RNA bypasses canonical viral entry routes and, like HCV-GLuc, distinguishes primary viral translation from genome amplification. Compared to human IRF1, which inhibits primary translation and replication (Schoggins et al., 2011), neither ortholog inhibited primary translation, and both inhibited replication, with paRTP4 exhibiting stronger antiviral activity than hsRTP4 (Figure 5C).

The 3CXXC zinc finger domain of black flying fox RTP4 is necessary and sufficient for antiviral activity

Previous literature has suggested that murine and human RTP4 are localized to the Golgi apparatus and the ER (Fujita et al., 2019). Since RTP4 inhibits ER-replicating viruses, we tested whether black flying fox RTP4 exhibits ER localization. Antibodies for bat RTP4 are not available, so we used CRISPR-mediated 'gene-tagging' to fuse an HA epitope tag to the N terminus of endogenous RTP4 in PaKi cells (Figure 7A). Subcellular localization was assessed by immunofluorescence, using anti-KDEL antibody and wheat germ agglutinin (WGA) as counterstains for the ER and the trans-Golgi network, respectively (Figure 8A). HA-tagged paRTP4 displayed overlap with KDEL and only minimally overlapped with WGA signal, suggesting that endogenous paRTP4 is predominantly ER-localized. Indeed, colocalization

analysis revealed higher overlap between paRTP4 and KDEL than between either paRTP4 and WGA or KDEL and WGA (Figure 7B).

All RTP4 orthologs have three domains: an N-terminal 3CXXC zinc finger domain (ZFD), an intrinsically-disordered variable region, and a transmembrane (TM) anchor (Figure 8B). We generated a 22 amino acid C-terminal truncation (paRTP4ΔTM) to determine whether the hydrophobic TM domain is required for localization and antiviral function. To confirm that paRTP4ΔTM was deficient for membrane association, we permeabilized cells expressing HA-tagged paRTP4 and paRTP4ΔTM with digitonin to release free cytosolic contents. Immunofluorescence microscopy and western blotting demonstrated that the membrane association of paRTP4ΔTM was lost, as permeabilization promoted the release of paRTP4ΔTM (Figures 8C and 7C-D). In the absence of digitonin treatment, paRTP4ΔTM significantly overlapped with KDEL (Figures 8C and 7C), suggesting that RTP4 localization does not solely depend upon its membrane anchor. Indeed, loss of membrane association did not abrogate the ability of paRTP4 to restrict YFV (Figure 8D). We next generated serial C-terminal truncations of paRTP4 (Figure 8E) and found that all truncations expressed to similar or greater levels as full-length paRTP4 (Figure 8F). None of the truncations, including an additional truncation (Δ246: C5) which deletes 57.5% of the protein, exhibited a substantial loss of antiviral activity (Figures 8G and 7E). These data suggest that the N terminal 3CXXC zinc finger domain of paRTP4 is sufficient for robust antiviral activity and that the disordered variable region is largely dispensable for inhibition of YFV, HCV, and HCoV-OC43.

We next mutated one cysteine in each conserved CXXC motif and a conserved histidine within the N-terminal ZFD (Figure 8H). C63A and C101A mutations resulted in decreased protein

expression levels (Figure 8I), whereas proteins with H157A and C162A mutations expressed to higher levels than wild-type paRTP4. All mutant proteins had a near-complete loss of antiviral activity in human cells (Figure 8J), suggesting that the CXXC motifs are critical for antiviral function. We next assessed the antiviral phenotype of a severe truncation (C4) and a well-expressed ZFD point mutant (C162A) in black flying fox cells to validate our findings in an autologous background. Truncated paRTP4 retained most of its antiviral activity, whereas perturbation of the ZFD completely disrupted its function (Figure 8K). Finally, to eliminate endogenous paRTP4 as a potential confounding factor, we reconstituted RTP4 KO cells with several paRTP4 constructs. Full-length and truncated (C5) paRTP4 were both antiviral, whereas paRTP4-H157A was not (Figure 7F). Together, these results suggest that the zinc-finger domain of paRTP4 is minimally required for antiviral function.

Black flying fox RTP4 binds replicating viral RNA and suppresses viral genome amplification

We next sought to gain insight into the molecular mechanism underlying the antiviral function of RTP4. Since paRTP4 nearly completely abrogates YFV replication, we used the related flavivirus West Nile virus (WNV), which replicates at low levels in paRTP4-expressing cells when infected at high, but not low, multiplicity of infection (Figures 9A and 10A). We first assessed whether RTP4 binds viral and/or host RNA, since the 3CXXC ZFD of RTP4 is similar to that of the known RNA-binding proteins Zar1 and Zar2 (Charlesworth et al., 2012). Using cross-linking immunoprecipitation (CLIP) paired with qPCR, we found that RTP4 robustly binds sense and antisense viral RNA, as well as host RNAs, with no apparent bias towards any region of the viral genome (Figures 9B and 10B). The 3CXXC zinc finger domain was sufficient for RNA binding, implicating it as the RNA binding domain of RTP4 (Figure 10C). Similar results were found with

YFV and endogenous paRTP4 in genomically-tagged cells, suggesting that this interaction is not specific to WNV and that it occurs natively in black flying fox cells (Figure 9C).

Since RTP4 suppresses viral replication (Figures 5B-C), we investigated RNA-dependent processes upstream of viral assembly and egress. We used polysome profiling to determine whether paRTP4 affects the ribosome association of viral RNA, a critical step in translation. paRTP4 did not alter the association of WNV RNA with polysomes during infection (Figure 9D). However, polysome association of *ACTB* mRNA differed between control and paRTP4-expressing cells during infection (Figure 9D). This is consistent with decreased overall translation in highly-infected vector control cells as indicated by a reduction in high-molecular weight polysomes (Figure 10D). Together with our HCV reporter virus (Figure 5B) and YFV replicon data (Figure 5C), this suggests that paRTP4 does not suppress the translation of viral protein.

Flavivirus RNA is amplified by two components of the viral replicase: NS5 (a multifunction enzyme that contains an RNA-dependent RNA polymerase) and NS3 (a multifunction enzyme that has helicase activity) (Lindenbach and Rice, 2003) (Saeedi and Geiss, 2013). To determine whether paRTP4 inhibits genome amplification, we used flow cytometry and immunofluorescence to compare levels of NS5 and the intermediate replication product double-stranded RNA (dsRNA) in WNV-infected cells expressing either paRTP4 or a vector control. Surprisingly, while NS5 was present at similar levels, dsRNA was drastically reduced in paRTP4-expressing cells relative to control cells (Figures 9E-F). This confirms that paRTP4 does not block the production of viral protein but instead targets genome amplification. Since paRTP4 binds both sense and antisense viral RNA, we predicted that paRTP4 would associate with the site of viral replication. Indeed, a

proximity ligation assay revealed apposition of paRTP5 with NS5 and paRTP4 with dsRNA, thereby localizing paRTP4 to active replication machinery (Figures 9G and 10E).

The coordinated activity of flavivirus NS3 and NS5 is required for viral replication. Since paRTP4 associates with replicating viral RNA, we hypothesized that paRTP4-mediated restriction of genome amplification may alter interactions between NS3 and NS5. Co-immunoprecipitation and quantitative western blotting revealed that the association of WNV NS5 and NS3 is roughly six-fold lower in paRTP4-expressing cells relative to control cells (Figures 9I-J). Further, WNV NS3-NS5 association correlates (R-squared 0.859) with viral production in the presence of paRTP4 constructs that exhibit reduced antiviral activity (C5, H157A) relative to full-length paRTP4 when infected at a high MOI (Figures 9H and 10F-G). We additionally used CLIP with limited nuclease digestion and found that the binding profile of NS5 across the WNV genome is skewed in paRTP4-expressing cells relative to control cells (Figure 9K). This skewed binding is consistent with a model where RTP4, perhaps by binding replicating viral RNA, perturbs events that occur during genome amplification, likely resulting in the dramatic reduction in dsRNA production observed in (Figures 9E-F).

RTP4 is a species-specific mammalian restriction factor

While hsRTP4 and paRTP4 express at different levels (Figure 3C), we suspected that expression alone could not explain drastic differences in antiviral potential such as the ability of paRTP4 to inhibit HCV while hsRTP4 does not (Figures 5A-B). We noted that hsRTP4 and paRTP4 differ substantially in length (246 and 428 amino acids, respectively), and a comparison of protein lengths in therian (live-bearing) mammals revealed that while other antiviral effectors exhibit a unimodal distribution of protein lengths, RTP4 lengths are trimodal, ranging from just

under 200 to over 600 residues (Figure 11A). This suggested that neither hsRTP4 nor paRTP4 is uniquely representative of mammalian RTP4s, and we thus expanded our studies to include RTP4 orthologs from multiple mammalian lineages.

Antiviral effectors often exhibit signatures of pervasive positive selection, as they are hotspots in the "molecular arms race" between viruses and their hosts (Daugherty and Malik, 2012). Using Phylogenetic Analysis by Maximum Likelihood (PAML) (Yang, 1993), we found that RTP4 displays a signature of rapid evolution in several mammalian lineages (bats, ungulates, carnivores, rodents, and primates) (Table 2, Figure 11B). Notably, bats comprise the only lineage that displays a gene-wide dN/dS (the ratio of nonsynonymous over synonymous codon changes at a given site) of greater than 1, indicative of robust positive selection. All lineages display a dN/dS > 1 for their C-terminal variable region, and no lineage has a dN/dS > 1 for its ZFD alone. Further, a free-ratio analysis of bat RTP4 in PAML produced dN/dS ratios > 1 on several branches in both bat suborders (Yinpterochiroptera and Yangochiroptera), indicative of widespread episodic positive selection (Figure 11C). These data are consistent with a model in which RTP4 and the viruses that it inhibits are locked in a classic "Red Queen conflict" (Van Valen, 1973), where RTP4 in diverse species has adapted over evolutionary time to the selective pressures imposed by constantly-evolving viruses.

To explore functional consequences of this genetic conflict, we compared the ability of RTP4 orthologs from three bat species (two megabats, the black flying fox and the Egyptian fruit bat, and one microbat, the Mexican free-tailed bat), two ungulates (cow and pig), one carnivore (dog), two primates (human and rhesus macaque), and one rodent (house mouse) to restrict a panel of flaviviruses (DENV, ZIKV, WNV, YFV, and Entebbe bat virus (ENTV)), the hepacivirus HCV,

and the nidoviruses EAV and HCoV-OC43. We found that different RTP4 orthologs exhibit striking species- and lineage-specific properties (Figure 12A). While protein expression levels varied among the orthologs, a hierarchical clustering approach (Baker, 1974) suggests that phylogeny is closely correlated with antiviral phenotype (Baker's Gamma Index: phenotype/expression 0.03; phenotype/phylogeny 0.79; phylogeny/expression -0.17) (Figures 13A-B). There are however instances where expression levels trend with differences in antiviral potency. Among bats, black flying fox RTP4 expressed at the highest levels and most-potently restricted all viruses. Among ungulates, cow RTP4 expressed at roughly twice the levels of pig RTP4 and was typically more antiviral. However, there are instances where expression does not predict potency. For example, mouse RTP4, despite expressing at roughly the same level as the broadly-inhibitory cow RTP4, is the weakest effector against most viruses, only potently restricting HCV. To further address the relationship between protein expression and viral inhibition, we used a doxycycline-inducible HA-tagged paRTP4 construct to titrate paRTP4 expression levels prior to YFV infection and found that paRTP4 inhibited YFV in a dose-dependent manner (Figure 13C).

If evolutionary pressure has driven the specialization of different RTP4 orthologs, we would predict that 1) an ancestral RTP4 would be antiviral and 2) it would perhaps exhibit less specialization than the evolutionarily-honed mammalian RTP4 orthologs that exist in nature. We used maximum-likelihood modeling to infer an ancestral RTP4 sequence (asrRTP4) based on data from 35 mammalian genomes representative of 96 million years of evolution. We synthesized asrRTP4 and assessed its ability to inhibit infection by YFV, ZIKV, HCV, and HCoV-OC43. We found that asrRTP4, which expresses at roughly 65% the level of paRTP4 (Figure 13D), inhibited

each virus, albeit with limited potency relative to paRTP4 for ZIKV, YFV, and HCV (Figure 12B). As with less-inhibitory orthologs, relative expression levels may explain some of its decreased potency, though its weak phenotype towards HCV and relative strength against HCoV are unique among RTP4 proteins. This supports a model in which RTP4 has been selected for enhanced activity towards certain, but not all, viruses in different mammalian lineages, and is consistent with research on other antiviral effectors such as the plant Rx protein and mammalian MX1, which exhibit a tradeoff between potency and specificity (Farnham and Baulcombe, 2006) (Colon-Thillet et al., 2019).

We noted that RTP4 from two bats, the Egyptian fruit bat (raRTP4) and the Mexican free-tailed bat (tbRTP4), and two primates, humans and the rhesus macaque (mmulRTP4), exhibited opposite antiviral phenotypes during ENTV and YFV infection (Figure 12A). ENTV is a bat-specific, non-vectored flavivirus that belongs to the YFV group, and is the closest relative to YFV within our screen (Figure 12C) (Simmonds et al., 2017). We validated by plaque assay that ectopically-expressed mmulRTP4 and hsRTP4 potently restrict ENTV, but not YFV, while tbRTP4 and raRTP4 potently restrict YFV, but not ENTV (Figure 12D).

ENTV is the only virus that is potently inhibited by hsRTP4 among all viruses screened in the present work (Figures 5A, 12A) and in our previous publications (Schoggins et al., 2014; Schoggins et al., 2011). To assess the significance of RTP4 as a human antiviral effector, we explored whether our mechanistic findings for paRTP4 could be recapitulated with hsRTP4 in the context of ENTV. CLIP-qPCR showed that hsRTP4 binds ENTV RNA during infection (Figure 12E), and a ZFD-targeted point mutation disrupts its antiviral function (Figures 12F and 13E). Importantly, we found that CRISPR-based silencing of RTP4 in human U2OS osteosarcoma cells

resulted in increased ENTV infection relative to nontargeting control cells, suggesting that endogenous hsRTP4 is antiviral (Figure 12G). This result is similar to those obtained in gene silencing studies of broadly-inhibitory black flying fox (Figure 4G) and pig (Figure 13F) RTP4 orthologs in the context of YFV infection. These data suggest that human RTP4 is not a "weak" RTP4 ortholog – instead, it is best adapted to inhibit certain viruses, such as ENTV, and is poorly adapted to inhibit others, such as YFV.

The error prone nature of RNA virus replication often allows the emergence of viral variants that can overcome selective pressure, such as that imposed by a restriction factor (Domingo et al., 2012). We observed that some viruses resisted inhibition by certain RTP4 orthologs (Figure 12A), suggesting that adaptive evolution may have enabled escape from RTP4-mediated restriction in a species-specific manner. To model this experimentally, we serially passaged YFV and ENTV in cells expressing tbRTP4 or mmulRTP4 to determine if either virus could overcome the antiviral effects of an RTP4 ortholog that inhibits it. After six passages, we obtained a YFV escape mutant (YFV-17Dres$_p$) that was able to replicate in the presence of tbRTP4 (Figure 12H). We did not obtain an mmulRTP4 ENTV escape mutant (Figure 12H) or paRTP4 WNV escape mutant (Figure 13G). YFV-17Dres$_p$ exhibits roughly ten-fold enhanced replication in tbRTP4-expressing cells as compared to YFV-17D (Figure 12I). Sequencing of clonal escape mutants identified a single point mutation (G6287A) that results in a missense E573K mutation in NS3 (Figures 12J and 13H, Table 3). An engineered virus (YFV-17Dres$_c$) containing this mutation phenocopied YFV-17Dres$_p$ (Figure 13I). We compared the replicative capacity of YFV-17Dres$_c$ in the presence of RTP4 from other bats (black flying fox and Egyptian fruit bat), cow, or humans to determine 1) if this escape was specific to freetail bat RTP4 and 2) if the mutation attenuates the virus. Indeed, we found that

while this mutation confers enhanced replication in the presence of tbRTP4, YFV-17Dres$_c$ was attenuated relative to wild type virus in cells expressing other mammalian RTP4s (Figures 12K and 13J-K). This complements our phylogenetic analysis (Table 2) and the specificity observed in our ortholog screen (Figure 12A), providing evidence that RTP4 may be involved in a classic Red Queen conflict with flaviviruses, in which diversification of both hosts and viruses has yielded a complex pattern of antiviral specificity of mammalian RTP4 orthologs.

Discussion

In the present study, we identify black flying fox (*Pteropus alecto*) RTP4 as a potent anti-flavivirus effector that binds viral RNA and restricts viral genome amplification. We find that RTP4-mediated restriction is associated with alterations in the flavivirus replicase (Figures 9I-K) and that a virus can escape RTP4-mediated restriction through a mutation in NS3, a component of its replicase (Figures 12H-K). Uncovering the precise molecular mechanism of RTP4-mediated inhibition may provide insight into novel therapeutic targets, as well as further our understanding of flavivirus genome replication. Our observation that black flying fox and human RTP4 exhibit differential phenotypes (Figure 5) led us to test the inhibitory potential of RTP4 orthologs from several species, and we uncovered an intricate pattern of antiviral specificity across Mammalia (Figure 12A). Our study is only representative of the approximately 70 known flaviviruses, half of which are considered potential human pathogens (Simmonds et al., 2017). Screening more diverse mammalian RTP4s against other flaviviruses may reveal additional layers of specificity underlying this virus-host conflict.

Often, studies of immune effectors with species-specific antiviral activity have focused on the careful comparison of orthologs from closely-related species to identify genetic signatures of recurrent, or pervasive, positive selection. Pervasive positive selection is a hallmark of the molecular application of Leigh Van Valen's "Red Queen hypothesis", which posits that co-existing organisms must continually adapt to pressures imposed by one another in order to survive (Van Valen, 1973). Notable examples of host-virus molecular arms races include TRIM5α, where a positively-selected patch of residues underlies differences in antiretroviral potency of rhesus and human orthologs, (Sawyer et al., 2005) and MX1, where a single positively-selected residue confers the ability of human MX1 to inhibit certain orthomyxoviruses (Mitchell et al., 2012). Our functional comparative study of representative RTP4 orthologs from diverse mammalian clades complements such approaches and highlights the value of looking beyond closely-related species when investigating host-virus conflicts. Indeed, while there is evidence of positive selection in RTP4 in multiple lineages, we do not find positively-selected patches of residues that are common among lineages (Table 2, Figure 11B). This could suggest that the Red Queen conflicts between RTP4 orthologs and the viruses that they inhibit have led to unique innovations both in viruses and their mammalian hosts. Importantly, this model is supported experimentally by the emergence of a viral variant that escapes inhibition by one RTP4 ortholog but not by others (Figure 12K). We suspect that evolutionary pressure imposed by inhibitory RTP4s may have driven viral adaptation, with a possible fitness cost being impairment of replication due to mutation in NS3. Conversely, over long evolutionary time scales, mammals may have incurred flavivirus-driven fitness costs that drove complex RTP4 adaptations, including single amino acid changes and modifications to the intrinsically-disordered C-terminal domain. Fascinatingly, a recent study (He et al., 2020) has

found that RTP4 in humans and mice is a negative regulator of interferon signaling. It is tempting to speculate that RTP4 may have evolved unique regulatory functions across Mammalia in addition to its pathogen-driven evolution as an antiviral effector.

Table 1: cDNA Library Statistics

	# Clones	Avg. Insert	Coverage
Entry Library	$1.03x10^7$	1.55kb	442x
Expression Library	$4.75x10^5$		20x

Estimated coverage is calculated using the estimated total number of transcripts in the *P. alecto* transcriptome (release 100: 23,328).

Table 2: PAML analysis of mammalian *RTP4*

Clade	# Sequences	*P* (M7 vs M8)	*P* (M8a vs M8)	# Positively-Selected Sites	dN/dS - Full	dN/dS - ZFD	dN/dS - CTD
Bats	9	6.19E-12	1.36E-12	16	1.11435	0.54532	1.69034
Ungulates	9	0.0007	0.0002	2	0.88649	0.57696	1.15441
Carnivores	11	0.1490	0.0765	3	0.66288	0.27508	1.21071
Rodents	10	0.0119	0.0041	11	0.66831	0.54678	1.03903
Primates	11	0.0167	0.0043	1	0.69046	0.52927	1.30167

Positively-selected sites are those with an M8 BEB >95%. Both M7 vs M8 and M8a vs M8 tests compare site models which allow positive selection (M8) and those that do not (M7, M8a).

Table 3: Escape Mutant ORF Sequencing

		Escape Mutants			Control	WT
Mutation	Type	Clone A	Clone B	Clone D	Clone C	Parental
C979T	Silent	T	C	C	C	C
A1275G	Silent	A	A	G	A	A
G6287A	E/K	A	A	A	G	G

Results of Sanger sequencing of PCR amplicons for escape mutant, control, and parental viruses. The entire ORF of clone A was sequenced and corresponding positions for any mismatches were sequenced in all other clones. A1275G mutation in clone D was uncovered due to is proximity to C979T in clone A.

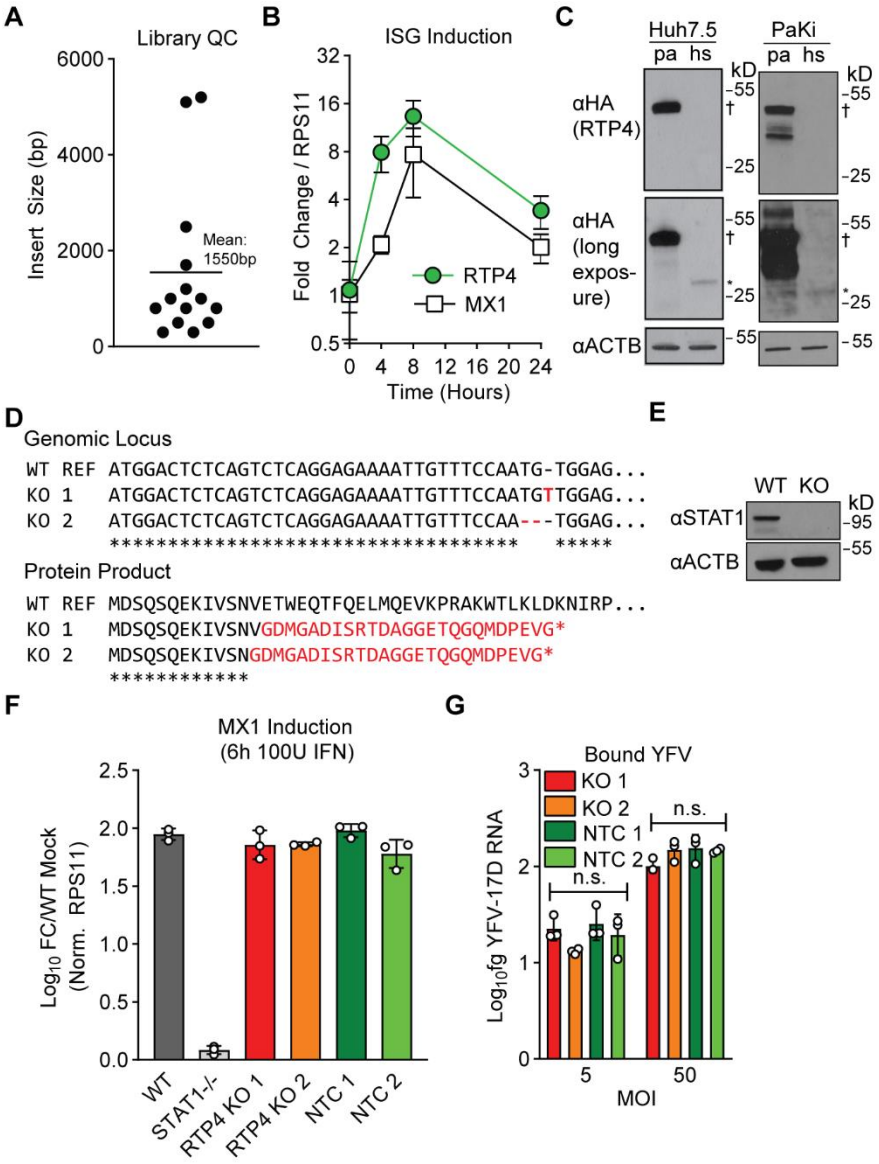

Figure 3. Supporting data for figure 4

a) Library quality control. Individual library clones were miniprepped and digested with BsrGI to release cDNA inserts. Insert length was estimated by agarose gel electrophoresis. b) PaKi cells were treated with 100U/mL of universal type I IFN. At the indicated time points, RNA was harvested with TRIzol and one-step RT-qPCR was performed to quantify gene expression. Points indicate the mean ±SD of N = 3 biological replicates. c)Western blot of Huh7.5 or PaKi cells stably

expressing HA-tagged paRTP4 (†) and hsRTP4 (*). Representative of at least three independent experiments showing similar results. Cell lines were independent of those used in Figure 1D-F. d) Western blot validating STAT1 KO PaKi clone. e) Results of Sanger sequencing of genomic DNA amplified from RTP4 KO clones. KO 1 includes an insertion of a T at position 38. KO 2 includes a two-base deletion at position 38. Both mutations result in frameshifts and a truncated protein product. f) PaKi cells were treated with 100U/mL of universal type I IFN for six hours, after which RNA was harvested with TRIzol and one-step RT-qPCR was performed to quantify gene expression. STAT1 KO cells are totally deficient for Mx1 induction, whereas Mx1 induction is retained in RTP4 KO cells. Bars indicate the mean ±SD of N = 3 biological replicates. g) PaKi cells were incubated at 4°C with YFV-17D at the indicated MOI for 1 hour to allow virus to bind. Following binding, cells were extensively washed to remove unbound virus and bound viral RNA was quantified by qPCR. Data generated by Katrina B. Mar. Bars indicate the mean ±SD of N = 3 biological replicates.

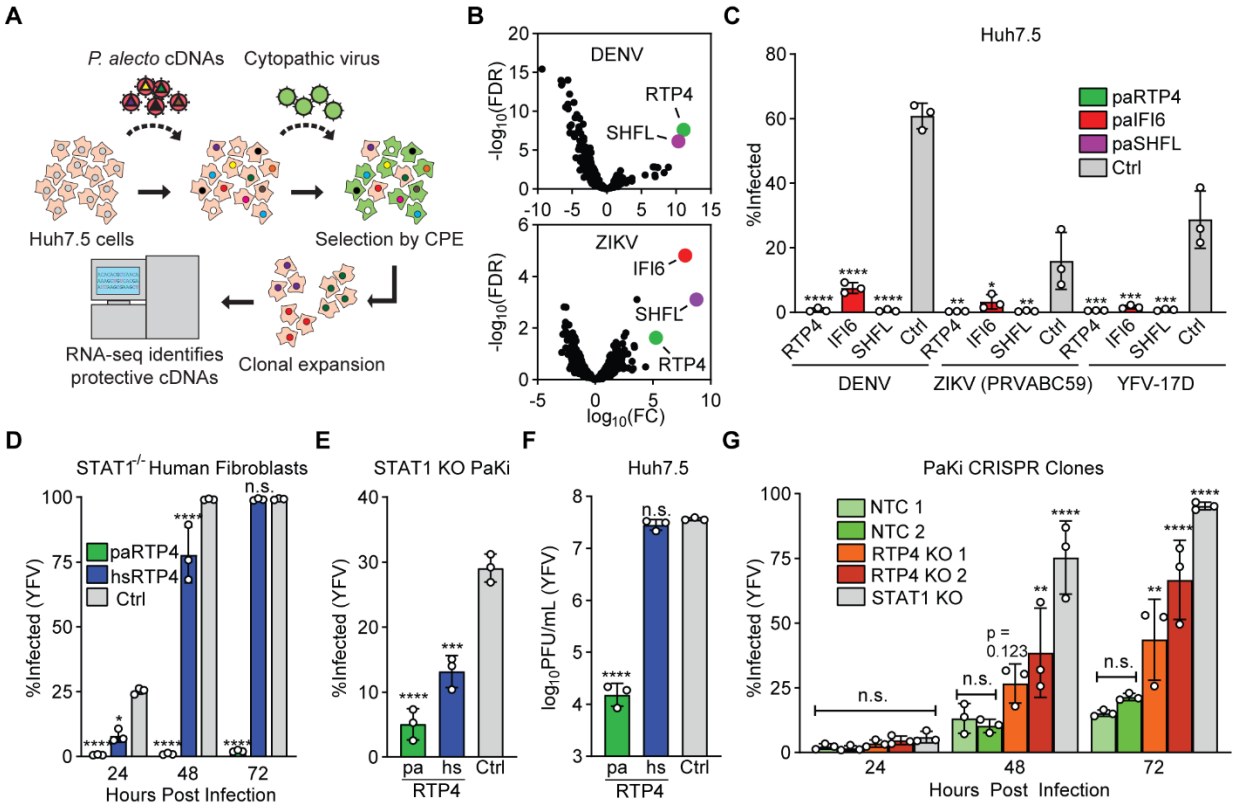

Figure 4. Black flying fox RTP4 restricts flavivirus infection

a) cDNA library screening pipeline. Related data: Supplemental Table 1, Supplemental Figure 1A. b) Results of triplicate DENV and ZIKV screens. c) Huh7.5 cells expressing black flying fox RTP4, IFI6, or SHFL were infected with DENV, ZIKV (PRVABC59), and YFV-17D-Venus (YFV-Venus) for 24 (YFV, ZIKV) or 48 (DENV) hours. Bars: mean ± SD of N = 3 biological replicates. One-way ANOVA with Dunnett's test. d) *STAT1*$^{-/-}$ human fibroblasts transduced with lentiviral pseudoparticles encoding paRTP4, hsRTP4, or firefly luciferase (Fluc) were infected with YFV-Venus for 24, 48, and 72h. Bars: mean ± SD of N = 3 biological replicates. Two-way ANOVA with Holm-Sidak test. e) AAV-transduced *STAT1* KO PaKi cells were infected with YFV-Venus for 24h. Bars: mean ± SD of N = 3 biological replicates. One-way ANOVA with Dunnett's test. f) Huh7.5 cells expressing paRTP4, hsRTP4, or a vector control were infected with

YFV-17D (MOI of 10) for 24h. Quantification by plaque assay. Bars: mean ± SD of N = 3 biological replicates. One-way ANOVA on log-transformed data with Dunnett's test. g) CRISPR *RTP4* KO PaKi clones were infected with YFV-Venus (MOI of 0.05). Bars: mean ± SD of N = 3 biological replicates. All statistics relative to NT.1. Two-way ANOVA with Holm-Sidak test.

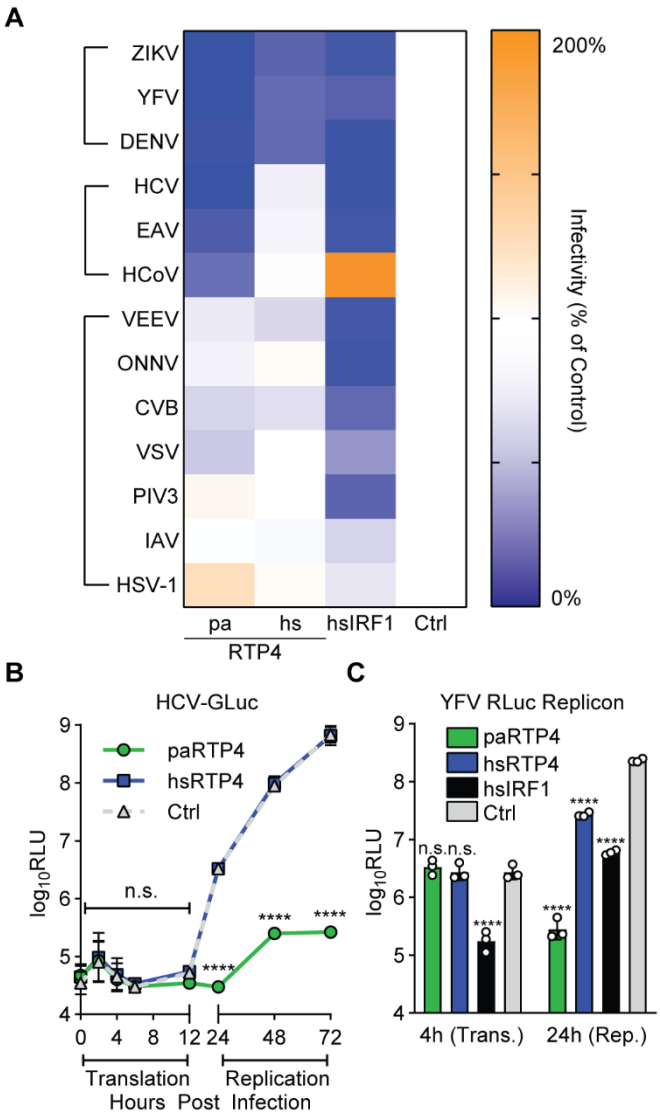

Figure 5. RTP4 restricts the replication of viruses that replicate at the ER

a) Relative infectivity of cells expressing paRTP4, hsRTP4, hsIRF1, or an empty vector. Heatmap cells represent the mean of N = 3 biological replicates, normalized to control. Raw infectivity and experimental details: Supplemental Figure 2. b) HCV-GLuc infection of Huh7.5 cells expressing paRTP4, hsRTP4, or a vector control. Points indicate the mean ± SD Relative Light Units (RLU) of N = 3 biological replicates. RM ANOVA on log-transformed data with Holm-Sidak test. c)

Huh7.5 cells expressing paRTP4, hsRTP4, hsIRF1, or vector control were transfected with YFRluc2a replicon RNA. Bars: mean ± SD RLU of N = 3 biological replicates. Two-way ANOVA on log-transformed data with Holm-Sidak test.

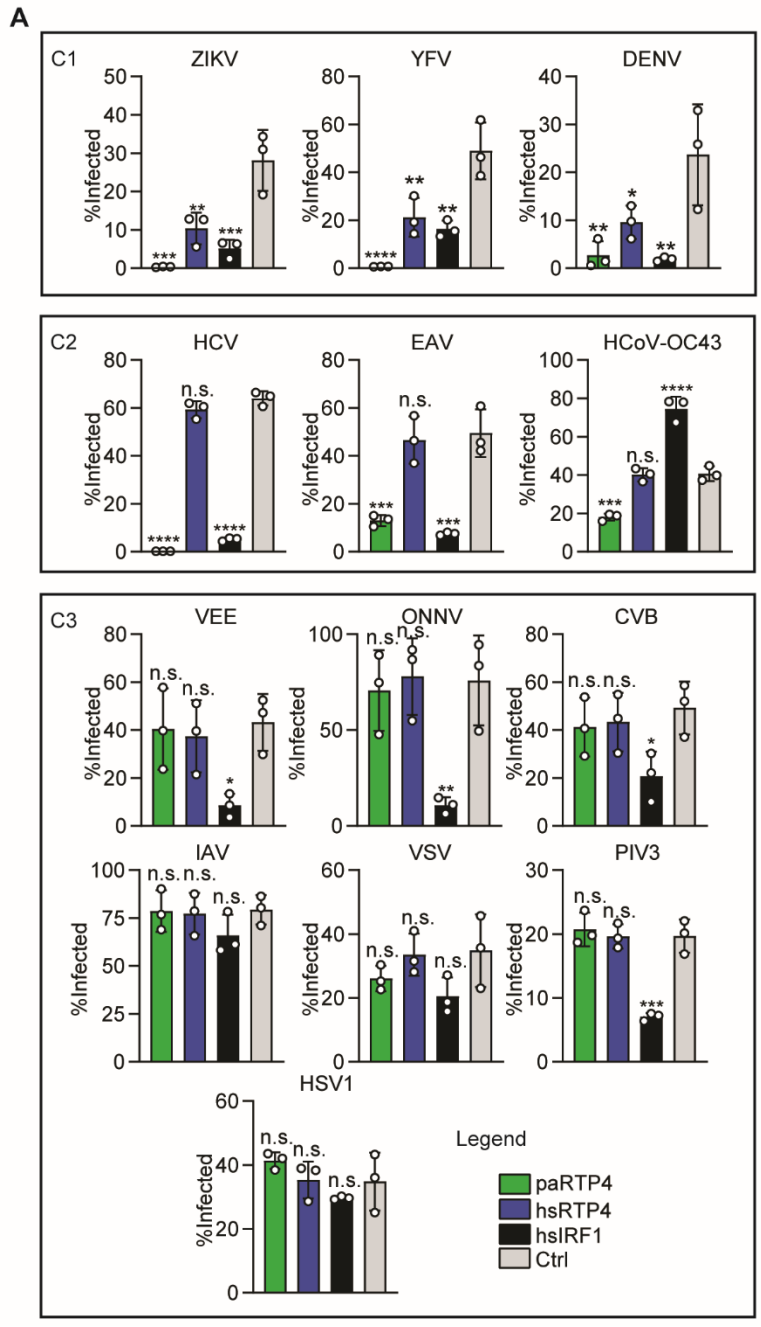

Figure 6. Supporting data for figure 5

a) Raw data from (Figure 2A). Infectivity of STAT1-deficient fibroblasts (EAV: 16h, PIV3: 16h, VEEV: 5.5h, VSV:4h , ONNV:16h, IAV:8h, HSV-1:18h) or Huh7.5 cells (YFV:24h, DENV:48h, ZIKV-MR766:24h, CVB:5.5h, HCV:48h, HCoV-OC43:24h) stably expressing paRTP4, hsRTP4, hsIRF1 as a positive control, or an empty vector. Cells were infected at an MOI of 0.25 to 1. Infection was quantified by flow cytometry. Cells represent the mean of n = 3 biological replicates. One-way ANOVA with Dunnett's test for multiple comparisons. (* $P < 0.05$, ** $P < 0.01$, *** $P < 0.001$, **** $P < 0.0001$).

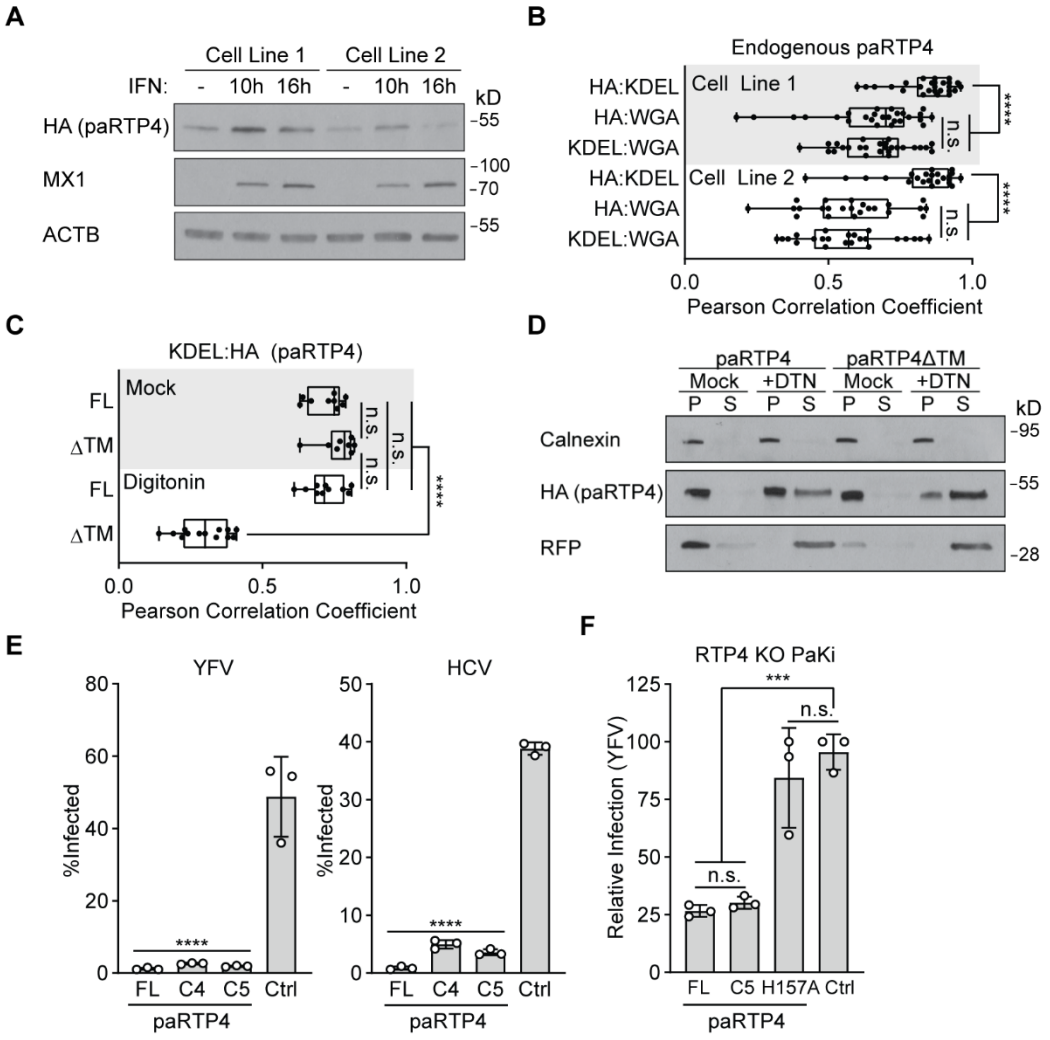

Figure 7. Supporting data for figure 8

a) Genomically tagged PaKi cells were treated with universal type I IFN at 100U/mL for the indicated times. Western blot of N = 1 replicate for both cell lines. MX1 and ACTB were probed on a separate membrane from HA. b) Colocalization analysis of endogenous paRTP4 (related to Figure 8A). Pearson coefficients for N = 26 (cell line 1) or N = 23 (cell line 2) individual cells across N = 3 biological replicates are indicated. One-way ANOVA with Tukey's test for multiple comparisons (**** $P < 0.0001$). c) Colocalization analysis of overexpressed HA.paRTP4 or HA.paRTP4ΔTM in Huh7.5 cells (related to Figure 8C).

Pearson coefficients for N = 9 (FL/Mock), 8 (ΔTM/Mock), 10 (FL/digitonin), and 13 (ΔTM/digitonin) individual cells across N = 3 biological replicates are indicated. One-way ANOVA with Tukey's test for multiple comparisons (**** $P < 0.0001$). d) Cells stably expressing HA.paRTP4 or HA.paRTP4ΔTM were treated with digitonin (DTN) to promote the release of cytosolic contents. Following treatment, membrane-associated components were pelleted by centrifugation and separated from supernatant. Western blotting for Calnexin (membrane-bound control), HA (RTP4), or RFP (unbound control) was performed on the supernatant (S) and pellet (P). Representative blot of N = 3 biological replicates. e) Huh7.5 cells stably expressing paRTP4, paRTP4-C4, paRTP4-C5 (ΔC246), or a vector control were infected with YFV or HCV and infectivity was quantified by flow cytometry. Bars indicate the mean ± SD of N = 3 biological replicates. One-way ANOVA with Dunnett's test for multiple comparisons. (* $P < 0.05$, ** $P < 0.01$, *** $P < 0.001$, **** $P < 0.0001$). f) PaKi RTP4 KO cells (clone 1) were transfected with 500ng of plasmid containing either full-length paRTP4 (FL), paRTP4-C5, paRTP4-H157A, or a vector control. 24 hours post-transfection, cells were infected with YFV-17D-Venus. Flow cytometry was used to quantify the percent of transfected (RFP+) cells that were infected (GFP+). Bars indicate the mean ± SD of N = 3 biological replicates. One-way ANOVA with Sidak correction performed on raw data. (***P=0.0002).

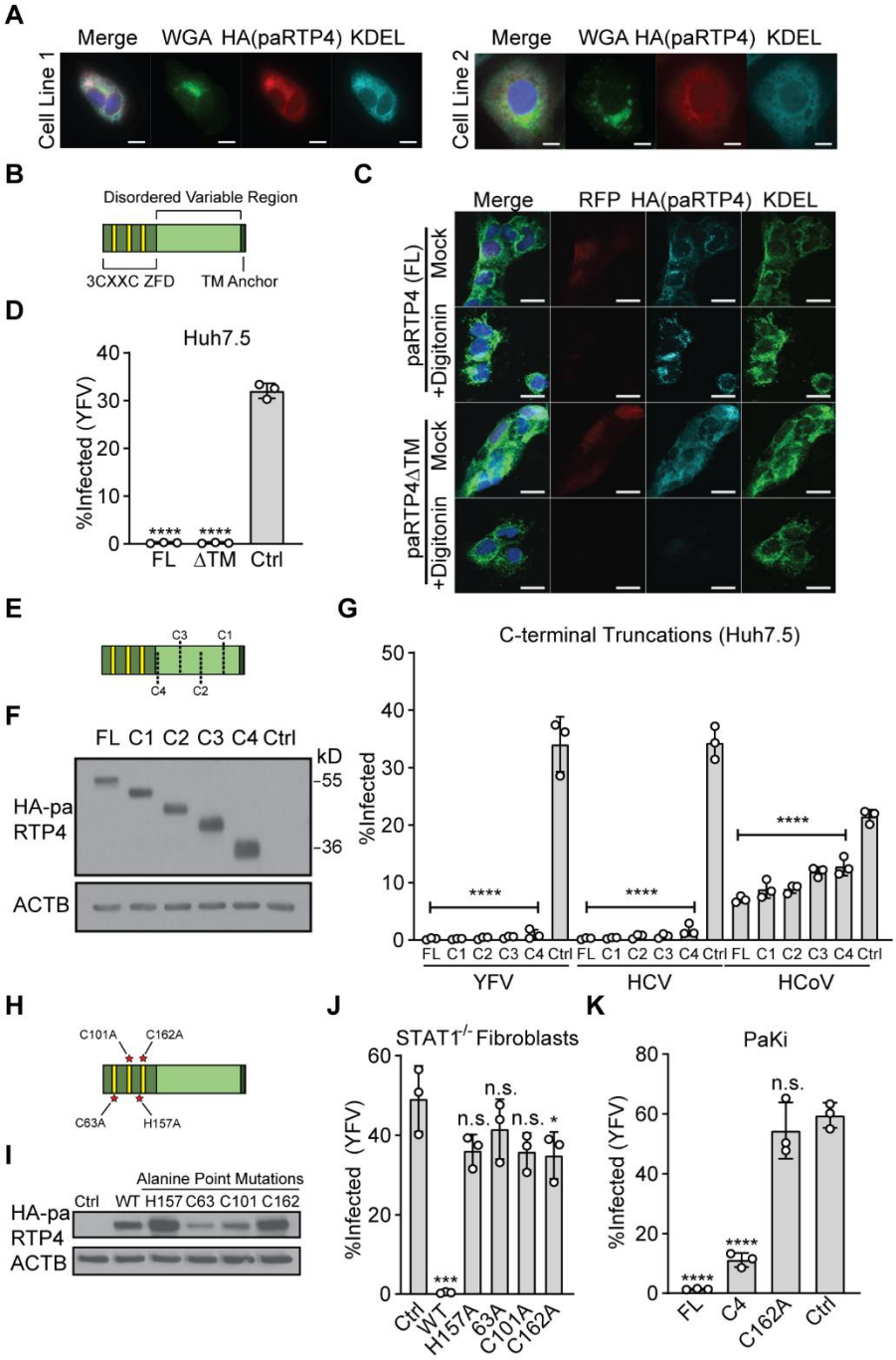

Figure 8. The 3CXXC zinc finger domain of black flying fox RTP4 is necessary and sufficient for antiviral activity

a) Endogenous RTP4 bearing a gene-edited HA epitope tag was detected in PaKi cells by tyramide signal amplification following treatment with 100U/mL IFN for 8h. Representative images of N =

3 biological replicates for two clonal cell lines. Linear adjustments were made to all channels separately. Scale bar: 10μm. b) Cartoon depicting the 3CXXC zinc finger domain (ZFD), disordered variable region, and transmembrane (TM) anchor of paRTP4. c) Huh7.5 cells expressing HA.paRTP4 or HA.paRTP4ΔTM were treated with digitonin prior to fixation. Cells were stained with antibodies against HA or KDEL. Co-expressed RFP serves as a control for untethered cytosolic contents and KDEL serves as a control for membrane-bound proteins. Scale bar: 20μm. d) Huh7.5 cells expressing HA.paRTP4ΔTM, full-length HA.paRTP4, or a vector control were infected with YFV-Venus for 24h. Bars: mean ± SD of N = 3 biological replicates. One-way ANOVA with Dunnett's test. e) Cartoon depicting serial C-terminal truncations of RTP4. C1:Δ56; C2:Δ106; C3:Δ156; C4:Δ206. f) Representative western blot (N = 3) of Huh7.5 cells expressing HA-tagged C-terminal truncations or full-length (FL) paRTP4. g) Huh7.5 cells expressing the indicated constructs were infected with YFV-Venus (24h), HCV (48h), or HCoV-OC43 (24h). Bars: mean ± SD of N = 3 biological replicates. One-way ANOVA with Dunnett's test. h) Cartoon depicting ZFD-directed point mutations of RTP4. i) Western blot (N = 1) of *STAT1*$^{-/-}$ fibroblasts transduced with the indicated HA-tagged constructs. j) *STAT1*$^{-/-}$ fibroblasts transduced with the indicated constructs were infected with YFV-Venus. Bars: mean ± SD of N = 3 biological replicates. One-way ANOVA with Dunnett's test. k) PaKi cells expressing the indicated constructs were infected with YFV-Venus. Bars: mean ± SD of N = 3 biological replicates. One-way ANOVA with Dunnett's test.

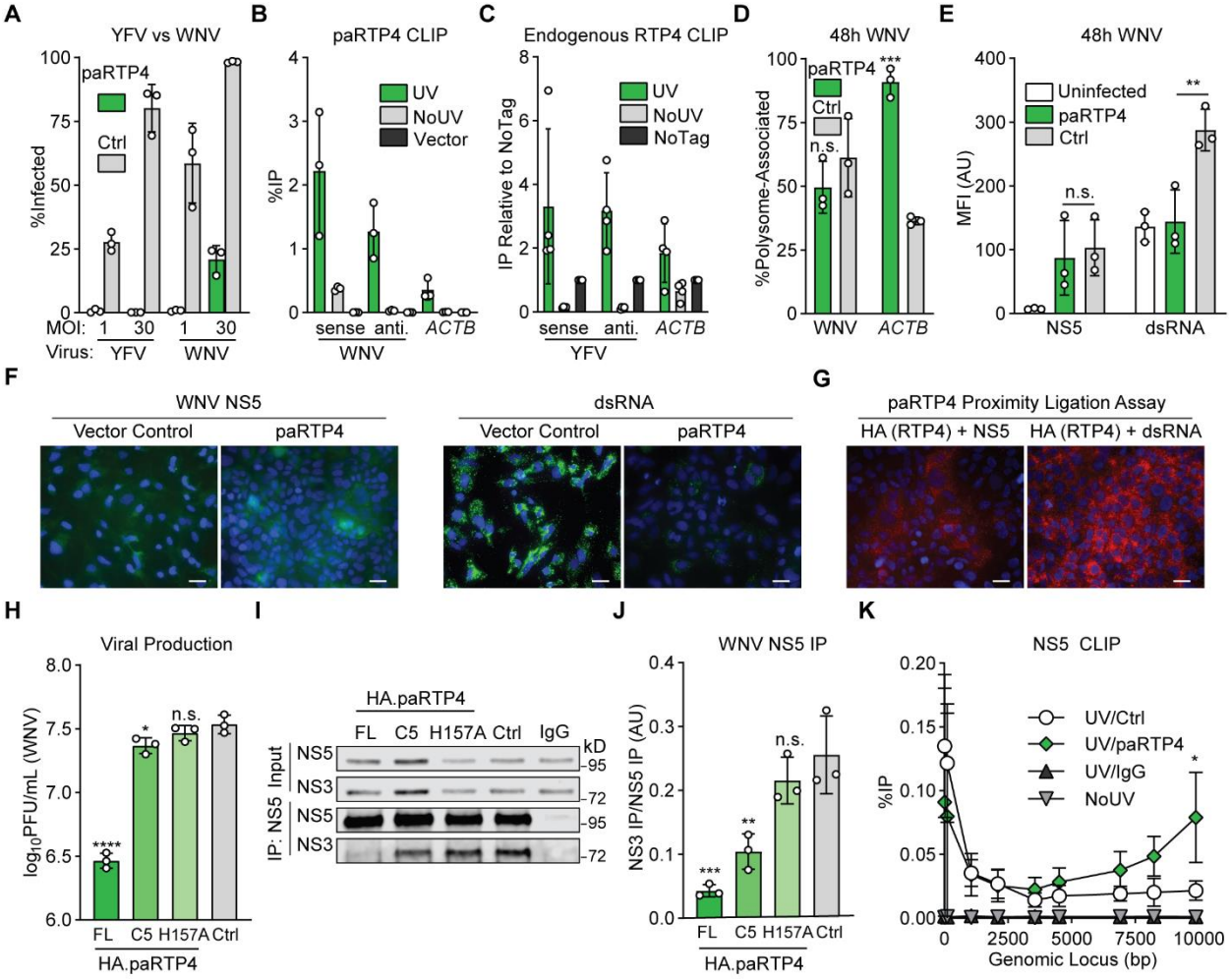

Figure 9. Black flying fox RTP4 binds replicating viral RNA and suppresses viral genome amplification

a) Huh7.5 cells expressing HA.paRTP4 or a vector control were infected with WNV or YFV-17D (MOI of 1 or 30) and harvested at 24h. Bars: mean ± SD of N = 3 biological replicates. Related data: Figure 10A b) Huh7.5 cells expressing HA.paRTP4 or a vector control were infected with WNV (MOI of 30) for 48h. CLIP-qPCR identified RNA bound by RTP4. UV: UV crosslinked HA.paRTP4 cells. NoUV: non-crosslinked HA.paRTP4 cells. Vector: UV crosslinked vector control cells. Bars: mean ± SD of N = 3 biological replicates. Related data: Figure 10B-C c) PaKi

cells were infected with YFV-17D (MOI of 5) for 48h. CLIP-qPCR identified RNA bound by HA.paRTP4. UV: crosslinked endogenously-tagged cells. NoUV: non-crosslinked endogenously-tagged cells. NoTag: crosslinked wild-type cells. Bars: mean ± SD of N = 4 biological replicates. d) Polysome association of WNV vRNA and *ACTB* in Huh7.5 cells expressing HA.paRTP4 or a vector control infected with WNV (MOI of 30) for 48h. Bars: mean ± SD of N = 3 biological replicates. Two-way ANOVA with Holm-Sidak test. Related data: Figure 10D e) Huh7.5 cells expressing HA.paRTP4 or FLuc as a negative control were infected with WNV (MOI of 30) for 48 hours. NS5 and dsRNA levels were quantified by flow cytometry. Bars: mean ± SD of N = 3 biological replicates. Two-way ANOVA with Holm-Sidak test. f) Huh7.5 cells expressing HA.paRTP4 or a vector control were infected with WNV (MOI of 30) for 48 hours. NS5 and dsRNA levels were visualized by immunofluorescence microscopy. Representative image of N = 3 biological replicates. Scale bar: 30µm. g) Huh7.5 cells expressing HA.paRTP4 were infected with WNV (MOI of 30) for 48 hours. A proximity ligation assay was performed for HA and either NS5 or dsRNA. Representative image of N = 2 biological replicates. Scale bar: 30µm. Related data (PLA controls): 10E. h) Huh7.5 cells expressing the indicated paRTP4 constructs were infected with WNV (MOI of 30) for 48 hours. Quantification by plaque assay. Bars: mean ± SD of N = 3 biological replicates. One-way ANOVA with Dunnett's test performed on log-transformed data. i) Huh7.5 cells expressing the indicated paRTP4 constructs were infected with WNV (MOI of 30) for 48h. WNV NS5 was immunoprecipitated and quantitative western blotting was performed using a Li-COR imager. Representative blot of N = 3 biological replicates. j) Quantification of (I) showing the co-immunoprecipitation of NS3 by NS5, normalized to NS5 pulldown efficiency. Bars: mean ± SD of N = 3 biological replicates. One-way ANOVA with

Dunnett's test. k) Huh7.5 cells expressing HA.paRTP4 or a vector control were infected with WNV (MOI of 30) for 48h. CLIP-qPCR with limited nuclease digestion identified the binding profile of NS5 on viral genomic RNA. UV/Ctrl: cross-linked vector control cells, IP NS5. UV/RTP4: crosslinked paRTP4-expressing cells, IP NS5. UV/IgG: crosslinked control cells, IP IgG. NoUV: non-crosslinked vector control cells, IP NS5. Bars: mean ± SD of N = 3 biological replicates. Two-way ANOVA with Holm-Sidak test.

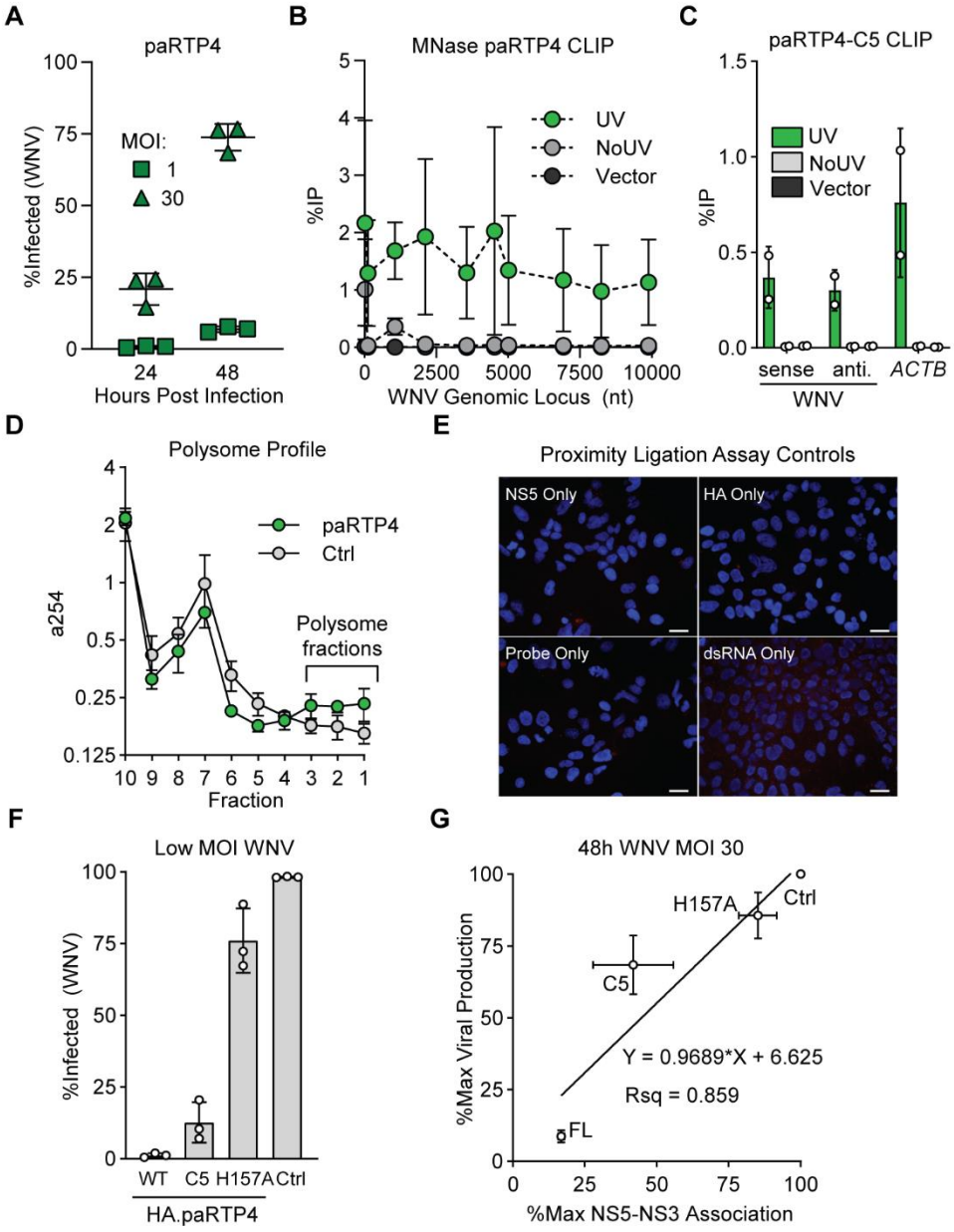

Figure 10. Supporting data for figure 9

a) Huh7.5 cells stably expressing paRTP4 were challenged with WNV at an MOI of 1 or 30 for 24 or 48h. Antibody staining for viral protein and flow cytometry were used to quantify infectivity. Points indicate the mean ± SD of N = 3 biological replicates. b) Huh7.5 cells expressing HA.paRTP4 or a vector control were infected with WNV at an MOI of 30 for 48h. UV: UV cross-

linked HA.RTP4 cells. NoUV: non-crosslinked HA.paRTP4 cells. Vector: UV cross-linked vector control cells. CLIP-qPCR with limited nuclease digestion was used to identify RNA bound by paRTP4. Bars indicate the mean ± SD of N = 3 biological replicates. c) Huh7.5 cells expressing HA.paRTP4-C5 or a vector control were infected with WNV at an MOI of 30 for 48h. UV: UV cross-linked HA.RTP4 cells. NoUV: non-crosslinked HA.paRTP4 cells. Vector: UV cross-linked vector control cells. CLIP-qPCR was used to identify RNA bound by paRTP4. Bars indicate the mean ± SD of N = 2 biological replicates. d) UV absorbance profiles for polysome profiles of WNV-infected cells. Points represent the mean ± SD of N = 3 biological replicates. Related to Figure 9D. e) Controls for proximity ligation assay. Huh7.5 cells stably expressing HA-tagged paRTP4 were infected with WNV at an MOI of 30 for 48 hours, after which they were fixed and assayed by the DuoLink proximity ligation assay system (Sigma). Representative images of N = 2 biological replicates. Scale bar: 30μm. f) Huh7.5 cells stably expressing the indicated constructs were challenged with WNV-GFP at an MOI 0.05 for 48h. Flow cytometry was used to quantify infectivity. Bars indicate the mean ± SD of N = 3 biological replicates. g) Comparison of WNV infectious particle production and NS3/NS5 association. Points indicate the mean ± SD of N = 3 biological replicates. Linear regression calculated in GraphPad Prism. Related to Figure 9H-J.

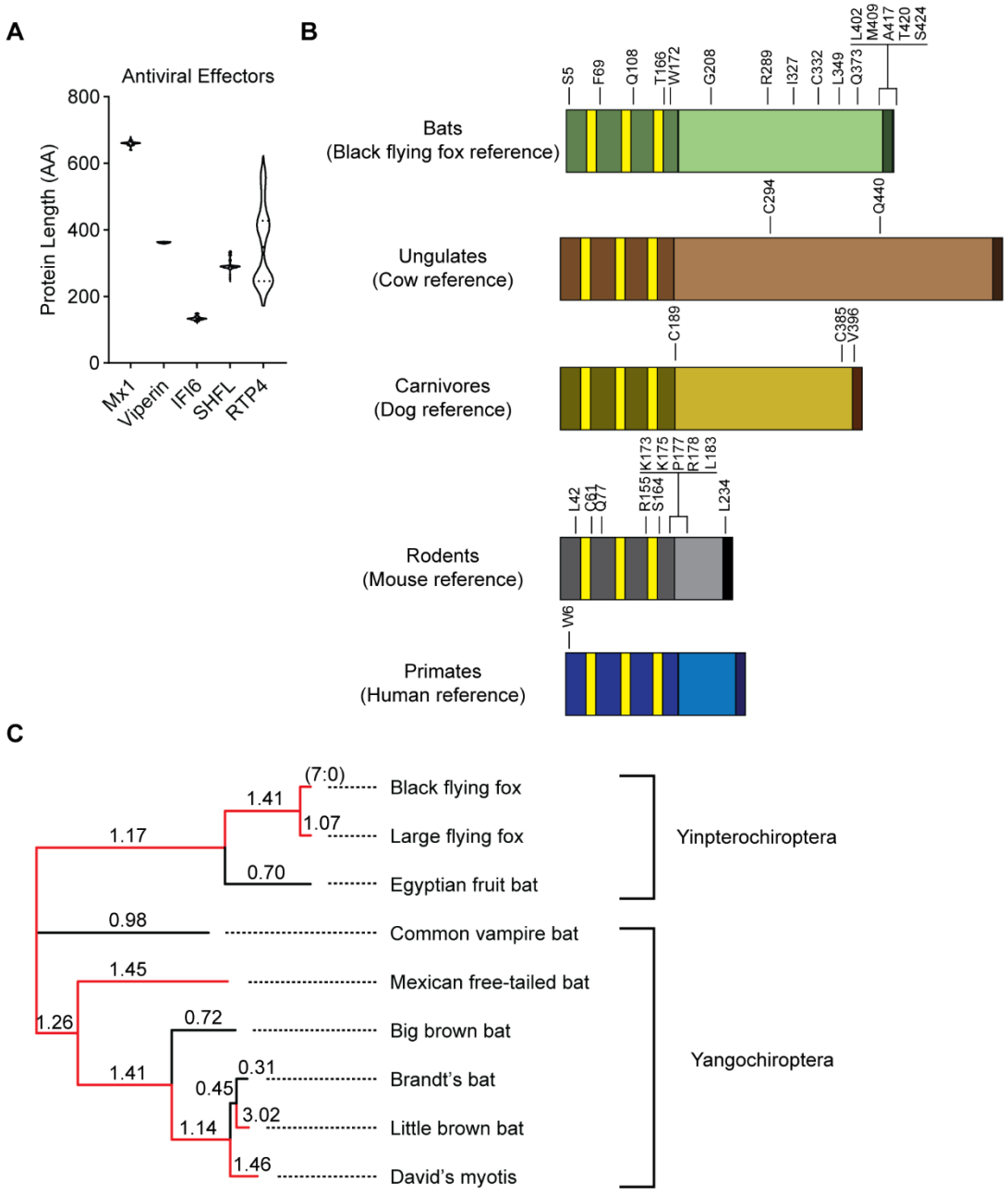

Figure 11. Evolutionary analysis of RTP4

a) RTP4 ortholog lengths were downloaded from the NCBI on 2/10/2020. Outliers were removed using the ROUT test with Q = 1. N = 72 (Mx1), 101 (Viperin), 85 (IFI6), 145 (SHFL), and 118 (RTP4). b) Cartoon depiction of RTP4 orthologs with positively-selected sites (M8 BEB P>95%).

c) Free-ratio analysis of bat RTP4. Annotated values indicate the dN/dS of each branch. Branches with dN/dS > 1 are marked in red.

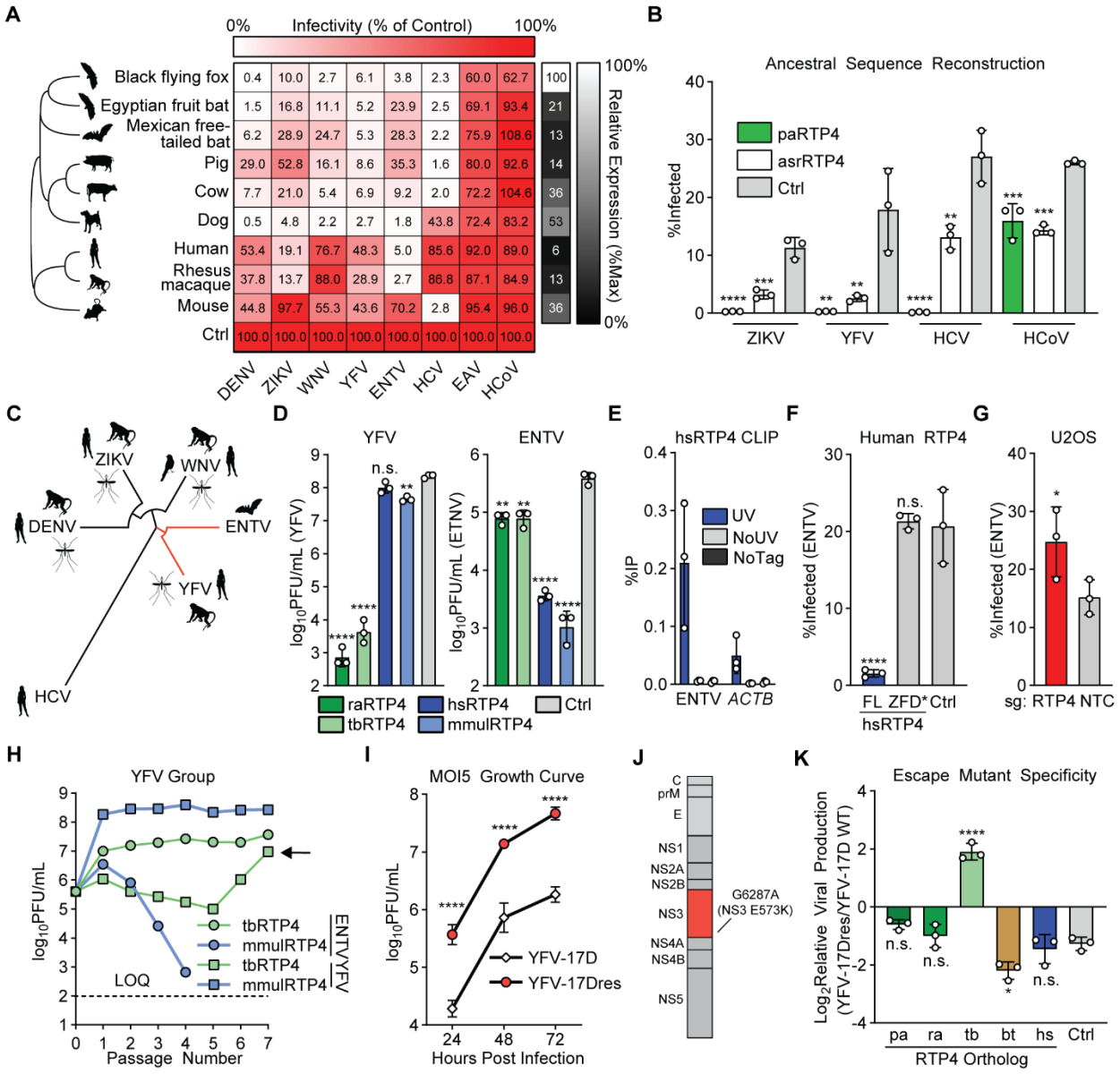

Figure 12. RTP4 is a species-specific mammalian restriction factor

a) Huh7.5 cells expressing HA-tagged RTP4 orthologs or a vector control were infected with the indicated viruses. Large heatmap: Cells represent the mean infectivity of N = 3 biological replicates, normalized to within-replicate control. Small heatmap: Cells represent the mean protein

expression of N = 3 biological replicates, relative to ACTB and normalized to within-replicate maximum expression. Raw infectivity data in Supplemental Table 2. b) Huh7.5 cells expressing paRTP4, asrRTP4 or a control were infected with the indicated viruses. Bars: mean ± SD of N = 3 biological replicates. One-way ANOVA with Dunnett's test. c) Maximum-likelihood phylogenetic tree for polyprotein of flaviviruses screened in 12A. Common amplifying hosts are indicated by silhouettes. d) Huh7.5 cells expressing the indicated constructs were infected with YFV-17D and ENTV (MOI of 0.05) for 24h (ENTV) or 48h (YFV). Quantification by plaque assay. Bars: mean ± SD of N = 3 biological replicates. One-way ANOVA with Dunnett's test performed on log-transformed data. e) Huh7.5 cells expressing either HA-tagged hsRTP4 or untagged hsRTP4 as a control were infected with ENTV (MOI of 5) for 24h. CLIP-qPCR identified RNA bound by RTP4. UV: UV-crosslinked HA.hsRTP4 cells. NoUV: non-crosslinked HA.hsRTP4 cells. NoTag: UV-crosslinked hsRTP4 cells. Bars: mean ± SD of N = 3 biological replicates. f) Huh7.5 cells expressing the indicated hsRTP4 constructs were infected with ENTV at an MOI of 0.5 for 16h. Bars: mean ± SD of N = 3 biological replicates. One-way ANOVA with Dunnett's test. g) CRISPR-targeted U2OS cells were infected with ENTV (MOI of 2.5) for 24 hours. Bars: mean ± SD of N = 3 biological replicates. Paired two-tailed t-test. h) Cells expressing rhesus macaque (mmul) or Mexican free-tailed bat (tb) RTP4 were infected with ENTV or YFV-17D (MOI of 5). Supernatant was collected at 24h (ENTV) or 48h (YFV) and transferred to naive cells for seven passages. Quantification by plaque assay. Points represent N = 1 plaque assay. i) Huh7.5 cells expressing tbRTP4 were infected with YFV-17D or YFV-17Dres$_p$ (MOI of 5) for 72h. Quantification by plaque assay. Points indicate the mean ± SD of N = 3 biological replicates. Two-way ANOVA on log-transformed data with Holm-Sidak test j) Cartoon representing the YFV

polyprotein. NS3 point mutation is indicated. k) Huh7.5 cells expressing the indicated RTP4 constructs or a vector control were infected with YFV-17D or YFV-17Dres$_c$ (MOI of 5) for 24h. Quantification by plaque assay. The ratio of viral production from wild-type YFV-17D and YFV-17Dres$_c$ is shown. Bars: mean ± SD of N = 3 biological replicates. One-way ANOVA with Dunnett's test. Related data: Figure13J-K.

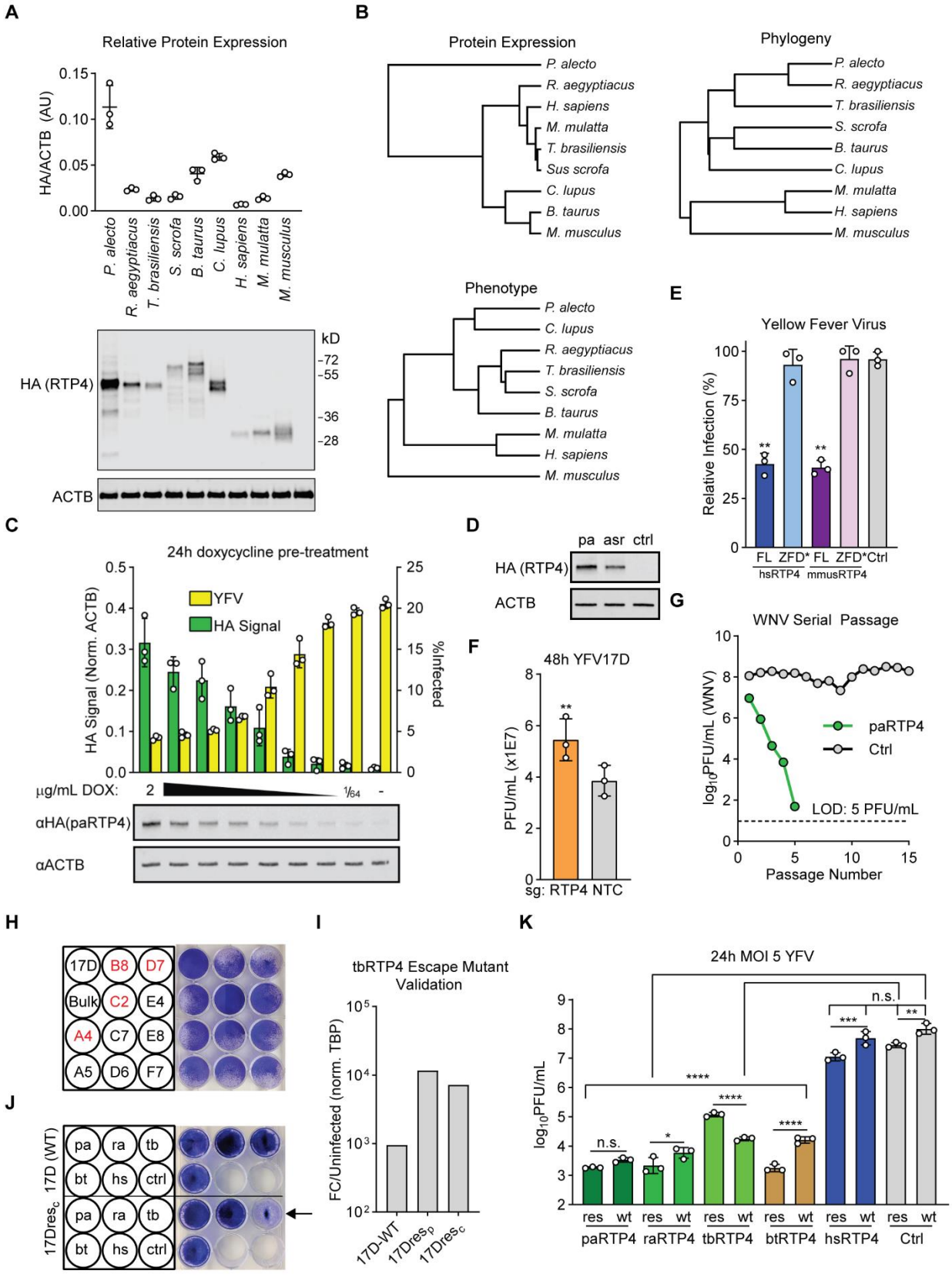
A
Relative Protein Expression
HA/ACTB (AU)
P. alecto
R. aegyptiacus
T. brasiliensis
S. scrofa
B. taurus
C. lupus
H. sapiens
M. mulatta
M. musculus
HA (RTP4)
ACTB
kD
B
Protein Expression
Phylogeny
Phenotype
C
24h doxycycline pre-treatment
YFV
HA Signal
HA Signal (Norm. ACTB)
%Infected
µg/mL DOX:
αHA(paRTP4)
αACTB
D
pa asr ctrl
HA (RTP4)
ACTB
E
Yellow Fever Virus
Relative Infection (%)
FL ZFD* FL ZFD* Ctrl
hsRTP4 mmusRTP4
F
48h YFV17D
PFU/mL (x1E7)
sg: RTP4 NTC
G
WNV Serial Passage
log10PFU/mL (WNV)
paRTP4
Ctrl
LOD: 5 PFU/mL
Passage Number
H
17D B8 D7
Bulk C2 E4
A4 C7 E8
A5 D6 F7
I
tbRTP4 Escape Mutant Validation
FC/Uninfected (norm. TBP)
17D-WT
17Dres
J
17D (WT)
17Dres
pa ra tb
bt hs ctrl
K
24h MOI 5 YFV
log10PFU/mL
n.s.
res wt
paRTP4 raRTP4 tbRTP4 btRTP4 hsRTP4 Ctrl

Figure 13: Supporting data for figure 12

a) Representative blot and quantification of protein expression for RTP4 orthologs. Replicate wells plated for ortholog screen (Figure 12A) were lysed in 1x SDS buffer and protein expression was assessed by western blotting. Quantitative western blotting was performed using a LI-COR imager. Points indicate the mean ± SD of N = 3 biological replicates. b) Dendrograms representing protein expression (generated in R based on 13A), phylogeny (TimeTree.org), and antiviral phenotype (generated in R based on Figure 12A). Dendrograms were used for calculation of Baker's gamma as reported in main text. c) Huh7.5 cells stably expressing doxycycline-inducible HA.paRTP4 were treated with doxycycline at the indicated concentrations for 24h hours, after which they were infected with YFV 24h. At the time of infection, replicate wells were harvested for quantitative immunoblotting. Quantification of infection by flow cytometry. Bars indicate the mean ± SD of N = 3 biological replicates. d) HA-tagged paRTP4, asrRTP4, and vector control cells. Representative western blot of N = 3 replicates. e) Huh7.5 cells expressing human RTP4, mouse RTP4, ZFD-targeted point mutants, or a vector control were infected with YFV at an MOI of 0.5 for 24h. Data generated by Elaine Xu. Infectivity was quantified by flow cytometry. Bars represent the mean ± SD of N = 3 biological replicates, normalized to max within each replicate. Ratio-paired t-tests were performed on raw data. (** $P < 0.01$). f) Bulk populations of CRISPR-targeted PK15 cells were infected with YFV at an MOI of 10 for 48 hours. Data generated with the assistance of Elaine Xu. Viral production was quantified by plaque assay. Bars indicate the mean ± SD of N = 3 biological replicates. Paired two-tailed t-test. (** $P < 0.01$). g) Huh7.5 cells expressing paRTP4 or a vector control were initially challenged with WNV at an MOI of 30. Every 48 hours, supernatant was transferred to naïve cells to propagate virus. Viral production was quantified by plaque assay.

h) Crystal violet stain of Huh7.5 cells stably expressing tbRTP4 infected with clonal escape mutants at an MOI of 10 for seven days. Parental YFV-17D and the bulk passaged escape mutant were included for comparison. Escape clones (A4, B8, D7) and non-escape clone (C4) that were selected for sequencing are indicated. Related to Table 3. i) N = 1 qPCR validation of engineered escape mutant. tbRTP4-expressing cells were challenged with WT YFV, YFV-17Dres$_p$, or engineered YFV-17Dres$_c$ virus at an MOI of 10 for 48h. One-step RT-qPCR was performed for YFV (bp3425) and normalized to TBP. j) Crystal violet stain of CPE validation of escape mutant related to Figure 12K. Representative image of N = 3 biological replicates. k) Raw data related to Figure 12K. Bars indicate the mean of N = 3 biological replicates. One-way ANOVA was performed on log-transformed data with Dunnett's test for multiple comparisons. (* $P < 0.05$, ** $P < 0.01$, *** $P < 0.001$, **** $P < 0.0001$).

CHAPTER FOUR
Results

FUNCTIONAL-GENOMIC ANALYSIS REVEALS INTRASPECIES DIVERSIFICATION OF ANTIVIRAL RECEPTOR TRANSPORTING PROTEINS IN XENOPUS LAEVIS

Introduction

Receptor Transporting Proteins (RTPs) were initially identified as regulators of chemosensory receptors (Saito et al., 2004). In mammals, there are four RTPs: RTP1s, RTP2, RTP3, and RTP4. Since their discovery, RTPs have been implicated in diverse cellular and physiological processes. Mammalian RTPs have been shown to regulate the localization of diverse G-coupled protein receptors (Behrens et al., 2006; Yu et al., 2017), and, in the case of RTP1 and RTP2, influence the development of the olfactory system (Sharma et al., 2017). Uniquely among mammalian RTPs, recent work has uncovered roles for RTP4 in the interferon (IFN) response, a key component of antiviral immunity. RTP4 is both an antiviral effector that restricts infection by RNA viruses of the family *Flaviviridae* (Chapter 3 above) (Boys et al., 2020) and a negative regulator of TBK1-mediated signaling pathways (He et al., 2020). We recently found evidence of a genetic arms race between mammalian RTP4 and flaviviruses, in which viruses have driven unique adaptations in RTP4 in diverse mammals (Table 2, Figures 11 and 12). This finding prompted us to ask whether similar RTP-virus evolutionary conflicts have arisen in other vertebrates.

The RTP family is ancient, dating back to the origin of jawed vertebrates; however, little is known about the function of these evolutionarily distant vertebrate RTPs. Interestingly, RTP

homologs from several species of fish are induced by IFN (Dehler et al., 2019; Liu et al., 2016; Xu et al., 2015) and one homolog has been implicated as a resistance allele to viral disease in Asian sea bass (Liu et al., 2017). This is suggestive of a role for non-mammalian RTPs in the innate immune response to viruses. Here, we take an evolution-guided approach to identify non-mammalian RTPs with antiviral properties by characterizing the evolutionary trajectories of multiple RTP clades. Unexpectedly, we encountered a remarkable expansion of RTPs within the African clawed frog, *Xenopus laevis*. We used RNA sequencing to identify pathogen-associated molecular pattern (PAMP)-induced *X. laevis* RTPs and screened for their ability to inhibit viral infection relative to representative RTPs from other species. Using this functional-genomic approach, we identified multiple antiviral *X. laevis* RTPs with unique viral specificities, indicating that antiviral innovation is a common property of vertebrate RTPs.

Results

Non-mammalian RTPs, such as fish "*RTP3*", have been previously described as orthologs – not homologs – of mammalian RTPs. A maximum-likelihood tree generated from an alignment of 303 vertebrate RTPs shows that non-mammalian RTPs generally form distinct clades among related species, consistent with a model in which intragenomic RTP expansions have typically resulted from more recent duplication events rather than ancient duplications (Figure 14A). Anamniote (fish and amphibian) RTPs form a phylogenetically-distinct cluster, yet there is some ambiguity regarding the relationships between sauropsid (reptile and bird) and mammalian RTPs. While mammalian RTPs distinctly cluster in pairs (*RTP1* with *RTP2* and *RTP3* with *RTP4*), bird RTPs cluster with the RTP3/4 clade, whereas reptile RTPs cluster variably with the RTP1/2 clade

and the RTP3/4 clade, and one from the bearded dragon clusters weakly with anamniote RTPs (Figure 14A). It is unclear whether this is indicative of a divergence of the progenitor RTPs of mammalian RTP1/2 and RTP3/4 before or after the divergence of sauropsids and mammals.

Jawed fish have between one and three RTPs, some of which cluster most closely within species. For example, the two Atlantic herring RTPs are more-closely related to each other than to those found in other fish, suggestive of repeat gene duplications over evolutionary time (Figure 14B). Concerted evolution, a phenomenon in which homologous recombination events and other processes result in increased similarity between paralogous genes within one species than between orthologs from related species, could partially underly this observation. However, we found only limited evidence of recombination in fish RTPs. An analysis of fish RTPs using a Genetic Algorithm for Recombination Detection (GARD) (Kosakovsky Pond et al., 2006) indicated one likely recombination breakpoint ($\Delta AIC_c = 14.96$) at nucleotide 383 in our alignment of fish RTPs. Maximum-likelihood trees for gene fragments on either side of the recombination breakpoint produced a similar topology (Figure 15A), consistent with a model in which recent duplications, not gene conversion events, have resulted in the topology observed in Figure 14B. Further supporting this conclusion, using GENECONV (Sawyer, 1989), we found among fish RTPs evidence of only one possible partial gene conversion (Milkfish RTP 1 outer $p = 0.0160$), which corresponded to an indel-rich region in fish RTPs (position 73-90 in fish alignment). Additional support for recent duplication events was found within the Euteleostei, where salmoniforme (an order which contains salmon and trout) genomes contain three RTPs, and the closely-related Northern pike has only one, indicative of two duplication events following their divergence.

Despite these recurrent duplications, RTPs are generally syntenic (Figure 16A). There are two examples of non-syntenic RTPs in the genomes of species we analyzed: one in salmon and one in the house mouse (Figure 16A). Our analysis revealed a curious discrepancy in domain architecture between representative anamniote (fish and amphibian) and amniote (reptile, bird, and mammals) RTPs. All amniote RTPs contain transmembrane (TM) domains, RTPs from fish lack a TM domain, and RTPs from amphibians are variable (Figure 16A). Importantly, studies have found that the TM domain of mammalian RTPs is dispensable for their receptor trafficking (Wu et al., 2012) and antiviral (Figure 8) roles. Thus, the lack of a TM domain in many anamniote RTPs does not exclude them from serving either a receptor trafficking or antiviral function.

We also noted that the RTP family is remarkably expanded in the African clawed frog, *Xenopus laevis*; its tetraploid genome contains eleven RTPs, more than any other species for which genomic information is available (Figure 16A). The evolutionary history of *X. laevis* is unique among known vertebrates. Approximately 34 million years ago, an ancestral species diverged, forming two *X. laevis* progenitors. Around 17 million years later, the divergent diploid ancestors hybridized and both subgenomes were maintained in their tetraploid descendants, which over the next 17 million years evolved to become the *X. laevis* of the present day (Session et al., 2016). Previous work has identified disproportionate pseudogenization on the smaller of the two *X. laevis* genomes (S) when compared to the larger (L) genome (Elurbe et al., 2017; Furman et al., 2018), which is likely a result of an energy-saving adaptation to limit genetic redundancy. We found no evidence of pseudogenization of *X. laevis* RTPs, and a "free-ratio" analysis using Phylogenetic Analysis by Maximum Likelihood (PAML) (Yang, 2007) found evidence of positive selection (ratio of nonsynonymous to synonymous codon substitutions, or dN/dS, > 1) in multiple branches

of *X. laevis* RTPs (Figure 16B). We further used adaptive Branch-Site Random Effects Likelihood (aBSREL) (Smith et al., 2015), a more-stringent test, to assess selection in the most-expanded syntenic family of *X. laevis* RTPs, here termed the "epsilon" family. This analysis detected evidence of episodic positive selection for two out of three genes (εL1 $p = 0.0018$, εL2 $p = 0.0017$), supporting our PAML results and highlighting the continued adaptation of *X. laevis* RTPs over evolutionary time. Together, these results are consistent with continued functional relevance despite the potential genetic redundancy that results from tetraploidy. Since more *X. laevis* RTPs exist than can be described by allotetraploidy, we next assessed whether any duplications occurred during the separation of the S and L genomes or following their rehybridization. We used a set of mammalian RTP4s to calibrate a time tree and estimate the divergence times of *X. laevis* RTPs (Figure 16C). Some nodes are ambiguous, such as that between the S genome "delta" RTP and the L genome "epsilon" RTPs. Conversely, the "beta", "gamma", and "alpha" gene families all had S and L paralog divergence times that roughly overlapped with the known divergence time between the S and L genomes (34 million years ago). Interestingly, we observed that the two L genome "alpha" RTPs, which have undergone episodic diversification (Figure 16B), diverged post-hybridization, further suggesting that RTP family expansion has been selected for in *X. laevis*.

Positive selection is a hallmark of genes which are involved in host defense against pathogens (Daugherty and Malik, 2012). We previously found that mammalian *RTP4* is a rapidly evolving antiviral effector which inhibits infection by RNA viruses from the family *Flaviviridae* (Chapter 3). We used Fast, Unconstrained Bayesian AppRoximation for Inferring Selection (FUBAR) (Murrell et al., 2013), Branch-site Unrestricted Statistical Test for Episodic Diversification (BUSTED) (Murrell et al., 2015), and PAML to assess whether other RTPs are

evolving under positive selection. Using gene-level models (PAML M7 vs M8 and M8 vs M8a in addition to BUSTED), we found evidence of positive selection in several non-mammalian RTP clades. At least two of the three models found evidence of positive selection in the bird RTP, as well as in two of the three salmon RTPs (Table4). Similar to *RTP4*, mammalian *RTP3* exhibits signatures of positive selection in bats, rodents, and primates. The third salmon RTP, as well as mammalian *RTP1* and *RTP2*, did not exhibit robust or consistent signatures of positive selection. Complementing these analyses, site-specific (PAML M8 Bayes Empirical Bayes and FUBAR) tests identified positively-selected residues in many of the same genes which displayed a gene-wide signature of selection.

Since we observed signatures of positive selection for mammalian *RTP3* (Table 4) which could be consistent with a role in host defense, we assessed the antiviral potential of mammalian RTP paralogs in mice, humans, and the black flying fox, by ectopic expression in a human hepatoma cell line (Huh7.5) that is permissive to infection by diverse viruses. Black flying fox RTP3 (paRTP3) was the only RTP other than the RTP4 homologs that inhibited viral infection (Figure 17A). paRTP3, which expressed at high levels (Figure 17B) was broadly antiviral, inhibiting the diverse RNA viruses yellow fever virus (YFV, a flavivirus), hepatitis C virus (HCV, a hepacivirus), Venezuelan equine encephalitis virus (VEEV, an alphavirus), and coxsackievirus B3 (CVB, a picornavirus). This contrasts with antiviral mammalian RTP4s, which primarily inhibit closely related flaviviruses and hepaciviruses (compare Figure 17A with Figure 5A, 12A). This lack of viral specificity was paired with qualitative alterations in cellular morphology such as swelling and increased granularity (Figure 17C) as well as differences in cellular metabolism, as assayed by WST-1 conversion (Figure 17D). Broad antiviral phenotypes and altered cellular

properties are consistent with viral inhibition via an indirect, host-dependent process, suggesting, albeit not concluding, that paRTP3 is not a bona fide antiviral effector.

The gene family expansions noted in Figures 14 and 16, as well as evidence of recurrent positive selection (Table 4) in non-mammalian RTPs, led us to hypothesize that some non-mammalian RTPs may have antiviral functions. Antiviral genes are often upregulated during infection, either directly as a result of the host cell sensing pathogen-associated molecular patterns (PAMPs), or as a result of IFN signaling (Schneider et al., 2014). Indeed, antiviral mammalian RTP4 is induced by IFN, as are several fish RTPs (Dehler et al., 2019; Liu et al., 2016; Xu et al., 2015). Additionally, one RTP from the Eastern newt, *Notophthalmus viridescens*, is upregulated during fungal infection, suggesting an immune role in amphibians (McDonald et al., 2020). The inducibility of *X. laevis* RTPs, however, has not been explored. *X. laevis* A6 kidney cells are IFN-competent and respond to a variety of immune agonists, including poly(I:C), a viral PAMP mimic (Sang et al., 2016). We confirmed that Mx-family GTPases, a canonical family of interferon-stimulated genes (ISGs), were induced following transfection of A6 cells with poly(I:C) (Figure 18A). We next performed RNA-sequencing on poly(I:C)-transfected A6 cells over a time course. We identified n = 614, n = 859, and n = 647 upregulated ($p < 0.05$, fold-change > 4) genes 6, 12, and 24 hours post-transfection, respectively (Figure 18B). Temporal subcluster analysis of gene expression kinetics revealed ten clusters (Figure 18C), including two distinct clusters (SC4 and SC5) which were characterized by rapid and sustained induction following poly(I:C) transfection (Figure 18D). While poly(I:C) is less specific than IFN at inducing ISGs, these subclusters were rich in canonical ISGs, such as *IFIT*s, *RSAD2*, *CH25H*, and *MX2*, but also contained many RTPs

(Figure 18E). Indeed, ten of the eleven *X. laevis* RTPs (all except for εL3) were significantly-induced at one or more time points (Figure 18F).

Unexpectedly, we also observed that two transcripts in SC5 are endogenized adintovirus polymerase genes (Supplemental Table 2). *Adintoviridae* is a recently-proposed (Starrett et al., 2020) viral family that was identified in metagenomic data. Adintoviruses are characterized by adenovirus-like virion proteins that are associated with a retrovirus-like integrase. Endogenized gene fragments of adintoviruses are found in a variety of animal genomes. While endogenized viral DNA polymerases from the unrelated *Hepadnaviridae* have been described in birds (Cui and Holmes, 2012; Gilbert and Feschotte, 2010), this is to our knowledge the first description of an immune agonist-responsive endogenized viral polymerase. Such regulation raises the prospect that amphibian species may have co-opted such proteins for a role in antiviral immunity.

While many genes with no known direct effector function are upregulated upon pathogen sensing, the inducibility of multiple *X. laevis* RTPs (Figure 18F), coupled with their robust signatures of positive selection (Figure 16B), led us to hypothesize that *X. laevis* RTPs may represent an expanded antiviral protein family with similarities to the IFN-inducible, antiviral mammalian RTP4. To explore the antiviral potential of *X. laevis* RTPs and other non-mammalian RTPs, we expressed in Huh7.5 cells HA-epitope tagged, codon-optimized RTP homologs from two birds (great tit and golden-collared manakin), an IFN-induced RTP (Xu et al., 2015) from the Atlantic salmon (salmoniform RTP 2), and all eleven homologs from *X. laevis*. We included black flying fox RTP4 (*Pteropus alecto* RTP4, paRTP4), a potent inhibitor of most flaviviruses, as a positive control for antiviral activity (Figure 12). We performed a screen with a panel of representative positive-sense single-stranded RNA viruses, including yellow fever virus (YFV, a

flavivirus), human coronavirus OC43 (HCoV-OC43), coxsackievirus B3 (CVB, a picornavirus), and Venezuelan equine encephalitis virus (VEEV, an alphavirus), as well as the negative-sense single-stranded RNA virus vesicular stomatitis virus (VSV, a rhabdovirus). Expression levels were variable, as epitope-tagged RTPα homologs, RTPδS, Great tit RTP, and the Atlantic salmon RTP were undetectable by western blot (Figure 20A) while some RTPs such as RTPε and RTPγ homologs were expressed at moderate levels compared to higher-expressing RTPs such as RTPβL and paRTP4. This discrepancy across RTPs suggests that a lack of antiviral activity for any orthologs may be linked to a lack of efficient protein expression. Despite this limitation, we found that two homologs from *X. laevis* reduced infection by at least 50% relative to a vector control: *X. laevis* RTPγS restricted the flavivirus YFV, and *X. laevis* RTPαL1 restricted the picornavirus CVB (Figure 19A, Supplemental Figure 20B).

Mammalian RTP4 orthologs exhibit distinct, mosaic antiviral specificities towards members of the *Flaviviridae* (Figure 12). We therefore screened the YFV-inhibiting RTPγS and its counterpart on the L genome, RTPγL, for their ability to inhibit other members of the *Flaviviridae* when ectopically expressed. We found that, in addition to YFV, RTPγS modestly inhibited the flaviviruses dengue virus (DENV) and Entebbe bat virus (ENTV) but did not inhibit other viruses (Figures 19B-C). Unexpectedly, while RTPγL did not inhibit any flaviviruses, it restricted the related hepacivirus Hepatitis C virus (HCV), which was not inhibited by RTPγS (Figure 19B-C).

We next sought to determine which phase of the flavivirus replication cycle is targeted by RTPγS. After viral entry, the replication cycle can broadly be divided into three phases: initial translation of the incoming viral genome, genome replication, and virion assembly/egress. Mammalian RTP4 binds viral RNA and inhibits flavivirus genome amplification, a later step in

the replication cycle (Figures 5 and 9). To assess which step is affected by RTPγS, we used a minimal, replication-competent, Renilla luciferase (RLuc)-expressing YFV RNA referred to as a 'subgenomic replicon' which bypasses viral entry and differentiates early (translation) and late (replication) steps. We found that RTPγS inhibits replication but does not inhibit primary translation (Figure 19D), consistent with what is known for mammalian RTP4 (Figure 5).

We next assessed whether RTPαL1, which inhibited the picornavirus CVB, or the related RTPαL2 or RTPαS, inhibited other picornaviruses when ectopically expressed. We found that, in addition to CVB, RTPαL1 inhibited Mengovirus (MenV, also called EMCV), and to a lesser degree poliovirus (PV), but did not significantly inhibit echovirus E11 (Figures 19E-F). RTPαL2 and RTPαS, however, did not significantly inhibit any of the viruses tested.

We previously determined that the 3CXXC zinc finger domain (ZFD) of RTP4 is its core antiviral domain, and we identified conserved cysteine residues that, when mutated to alanine, led to a loss of antiviral function (Figure 8). We used site-directed mutagenesis to disrupt one of these motifs in RTPαL1 and RTPγS (Figure 20C) and found that RTPs bearing these ZFD-disrupting mutations (*ZFD) no longer inhibited MenV and YFV, respectively (Figures 19G-H). Importantly, RTPγS*ZFD expressed to higher levels than WT RTPγS, suggesting that the loss of function was not the result of protein instability (Figure 20D). Our inability to detect RTPαL1 by western blot (Figure 20A), however, precluded our ability to assess whether the loss of antiviral function of RTPαL1*ZFD is independent of protein expression. Finally, we used cross-linking immunoprecipitation (CLIP) paired with qPCR to assess whether antiviral *X. laevis* RTPs bind viral RNA during infection. Perhaps because of low expression levels of RTPαL1, we only observed modest yet insignificant enhancement of MenV RNA bound to RTPαL1 compared to a

vector control (Figure 20E). RTPγS, however, robustly bound YFV RNA, as well as host RNA, during infection (Figure 19I). Paired with the replication-specific phenotype (Figure 19D), the robust association of RTPγS with viral RNA indicates that antiviral *Xenopus* RTPs may share a similar antiviral mechanism of action with mammalian RTP4.

Discussion

In the present study, we extend functional and genetic characterization of Receptor Transporting Proteins beyond Mammalia. It has previously been shown that RTP4 in mammals is an IFN-induced antiviral effector (Chapter 3), and that several RTPs in fish are likewise upregulated by IFN (Liu et al., 2016; Xu et al., 2015). However, mechanistic studies have thus far not been performed to assess the antiviral potential of non-mammalian RTPs. We identify signatures of positive selection in many vertebrate RTP clades, and characterize multiple, independent expansions of the RTP family outside of what was previously described in mammals. We identify a marked expansion of RTPs in the tetraploid African clawed frog, *X. laevis*, and find that these RTPs have continued to adapt and diversify following expansion. By performing what is to our knowledge the first deep sequencing-based analysis of PAMP-induced genes in *Xenopus laevis*, we additionally find that 10 of these *Xenopus* RTPs are induced by the innate immune response to a mimic of viral infection. Critically, we functionally characterize these *Xenopus* RTPs and find that several inhibit viral infection. Like mammalian RTP4 orthologs, these antiviral *X. laevis* RTPs exhibit distinct antiviral specificity, inhibiting only certain viruses from certain viral families. One *X. laevis* RTP, RTPγS, inhibits viral replication and directly binds viral RNA during infection which is a similar antiviral mechanism as mammalian RTP4. Mammalian RTP4 is

engaged in a host-pathogen molecular "arms race" (Figure 12), and if RTPs in non-mammalian species are bona-fide antiviral effectors, they may have influenced RNA virus evolution over the course of nearly half a billion years.

A key limitation of the present study is its reliance upon artificial combinations of non-mammalian RTPs with viruses that are known to predominantly infect mammals. While this allowed us to identify RTPs with antiviral activity, we predict that these RTPs may be evolutionarily honed to inhibit viruses that they are more likely to encounter in nature. Indeed, in our studies regarding mammalian RTP4, we encountered orthologs, such as human RTP4 and mouse Rtp4, which seem to have narrow antiviral specificity towards distinct subsets of pathogenic mammalian viruses (Figure 12). The identification and phenotypic screening of amphibian RNA viruses that are relatives of those in the present work may provide better models for the study of antiviral *Xenopus* RTPs, which may yield candidate genes for knockout studies to investigate their physiological relevance in innate immunity. Indeed, a novel family of picornaviruses has recently been characterized in amphibians (Pankovics et al., 2017; Reuter et al., 2015), and metagenomic studies have found that amphibians are unappreciated hosts to RNA viruses that are related to those which infect mammals (Shi et al., 2018). In addition to identifying RNA viruses that naturally infect amphibians and could therefore serve as models for RTP knockout studies, an important focus of future work will be the development of tissue culture-based models that permit the study of *Xenopus* RTPs and other antiviral effectors in a native cellular background. Of note, ectopic gene expression in A6 cells is inefficient (Ramirez-Gordillo et al., 2011), so it would be helpful to test other *Xenopus* cell lines as possible models.

A next step after our expression profiling of *Xenopus* RTPs in cell culture would be to assess *in vivo* expression patterns of RTPs following viral infection or immune stimulation. The expression of *X. laevis* RTPs at steady state (Fortriede et al., 2020; Karimi et al., 2018) may however provide hints of their potential immune function as well as those outside of cell-intrinsic immunity. Many RTPs (RTPγL, RTPγS, RTPαL2, RTPβL) are expressed at low to intermediate levels in most tissues, which is perhaps expected for genes that are involved in antiviral immunity. By contrast, some RTPs are expressed highly in some tissues but not in others, which could be indicative of either tissue-specific antiviral roles, or tissue-specific developmental or housekeeping functions. RTPαS is highly expressed in the ovaries and during embryonic development, and RTPaL1 is expressed highly in the heart and lung. All three members of the RTPε family and RTPδS are predominantly expressed in the intestine, and RTPβS is expressed at the highest levels in the brain and lung. While we limited the scope of our mechanistic studies to the identification of antiviral roles for *Xenopus* RTPs, such expression patterns may warrant their study in other contexts. For instance, mammalian RTPs have been extensively studied in the context of olfaction, and *X. laevis* is an important model organism for the study of the olfactory system, particularly from a developmental perspective (Manzini and Schild, 2010). It is thus possible that *Xenopus laevis* may provide an attractive model for studying the impact of RTP evolution on the olfactory system.

Table 4. Evolutionary analysis of select vertebrate RTP families.

	n sequences	*P* (M7 vs M8)	*P* (M8 vs M8a)	*P BUSTED*	NS BEB ω > 1	*FUBAR* (n positive)	*FUBAR* (n purifying)	dN/dS (gene)
Bird	18	*0.007962	*0.033198	0.354	1	0	30	0.364
Salmoniform 1	7	*3.45E-04	*6.98E-05	0.221	3	8	6	0.852
Salmoniform 2	5	*7.22E-01	*4.23E-01	0.500	0	1	6	0.684
Salmoniform 3	6	0.56841	0.29089	*0.031	0	2	9	0.255
X. laevis	11	*0.019284	*0.00691	0.500	1	1	17	0.436
Primate 1	25	0.999725	0.3054	0.500	0	0	38	0.096
Primate 2	26	*0.036599	0.1958	0.500	0	2	33	0.148
Primate 3	27	*4.28E-05	*1.21E-05	0.147	4	9	11	0.704
Primate 4	28	*0.000482	*0.000371	0.136	3	4	17	0.630
Rodent 1	23	*5.26E-05	0.3585	0.500	0	0	152	0.040
Rodent 2	24	0.366	*0.03493	0.497	0	4	108	0.067
Rodent 3	22	*0.000163	*0.000265	*0.001	1	1	57	0.504
Rodent 4	16	*1.42E-09	*5.05E-07	*0.000	9	7	13	0.630
Bat 1	9	0.9995	0.4176	0.500	0	0	58	0.065
Bat 2	11	0.9997	0.113	0.500	0	0	54	0.081
Bat 3	11	*1.97E-05	*8.17E-06	*0.000	6	11	17	0.698
Bat 4	9	*6.19E-12	*1.36E-12	*0.000	16	26	6	1.114

For PAML analyses: Positively-selected sites are those with an M8 BEB >95%. Both M7 vs M8 and M8a vs M8 tests compare site models which allow positive selection (M8) and those that do not (M7, M8a). Test results which indicate gene-wide signatures of positive selection are denoted with an asterisk.

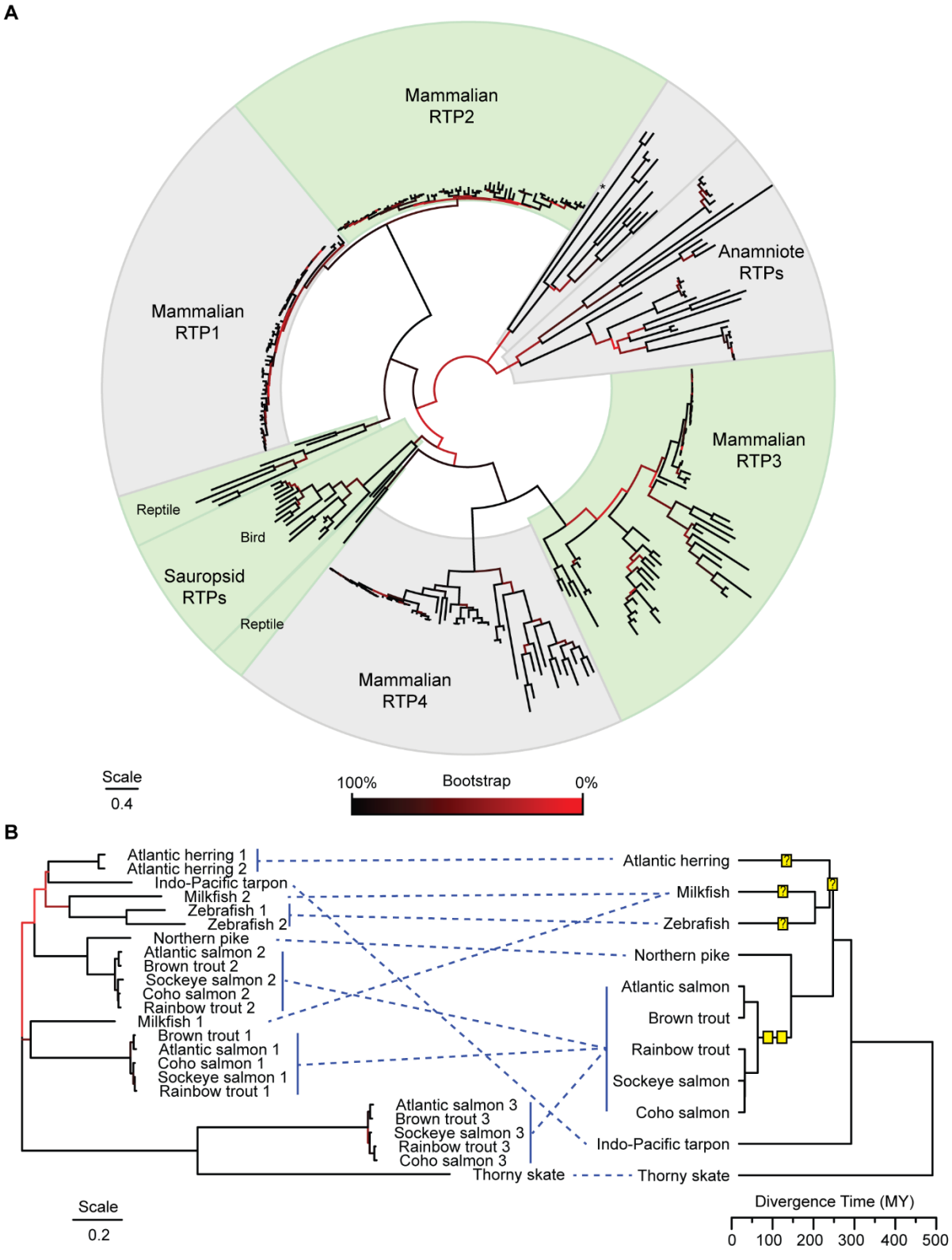
A
Mammalian RTP2
Anamniote RTPs
Mammalian RTP1
Mammalian RTP3
Reptile
Bird
Sauropsid RTPs
Reptile
Mammalian RTP4
Scale
0.4
100%
Bootstrap
0%
B
Atlantic herring 1
Atlantic herring 2
Indo-Pacific tarpon
Milkfish 2
Zebrafish 1
Zebrafish 2
Northern pike
Atlantic salmon 2
Brown trout 2
Sockeye salmon 2
Coho salmon 2
Rainbow trout 2
Milkfish 1
Brown trout 1
Atlantic salmon 1
Coho salmon 1
Sockeye salmon 1
Rainbow trout 1
Atlantic salmon 3
Brown trout 3
Sockeye salmon 3
Rainbow trout 3
Coho salmon 3
Thorny skate
Atlantic herring
Milkfish
Zebrafish
Northern pike
Atlantic salmon
Brown trout
Rainbow trout
Sockeye salmon
Coho salmon
Indo-Pacific tarpon
Thorny skate
Scale
0.2
Divergence Time (MY)
0
100
200
300
400
500

Figure 14. Evolutionary survey of vertebrate RTPs

a) Maximum Likelihood tree for 303 vertebrate RTPs was inferred by using the Maximum Likelihood method and Tamura-Nei model. The tree with the highest log likelihood (-99002.44) is shown. 500 bootstrap replicates were performed to test robustness of the ML tree, and branches are colored by percentage of bootstrap replicates which reflect this topology. A discrete Gamma distribution was used to model evolutionary rate differences among sites (5 categories (+G, parameter = 0.8741)). The tree is drawn to scale, with branch lengths measured in the number of substitutions per site. Asterix marks the bearded dragon RTP that clustered with anamniote RTPs. b) Left: A Maximum Likelihood tree for 24 representative fish RTPs was inferred by using the Maximum Likelihood method and Tamura-Nei model. The tree with the highest log likelihood (-6168.52) is shown. 500 bootstrap replicates were performed to test robustness of the ML tree, and branches are colored by percentage of bootstrap replicates which reflect this topology. A discrete Gamma distribution was used to model evolutionary rate differences among sites (5 categories (+G, parameter = 2.2558)). The tree is drawn to scale, with branch lengths measured in the number of substitutions per site. Right: A TimeTree describing the evolutionary relationships between the different fish species. Yellow squares denote inferred duplication events. Question marks denote ambiguous duplication events.

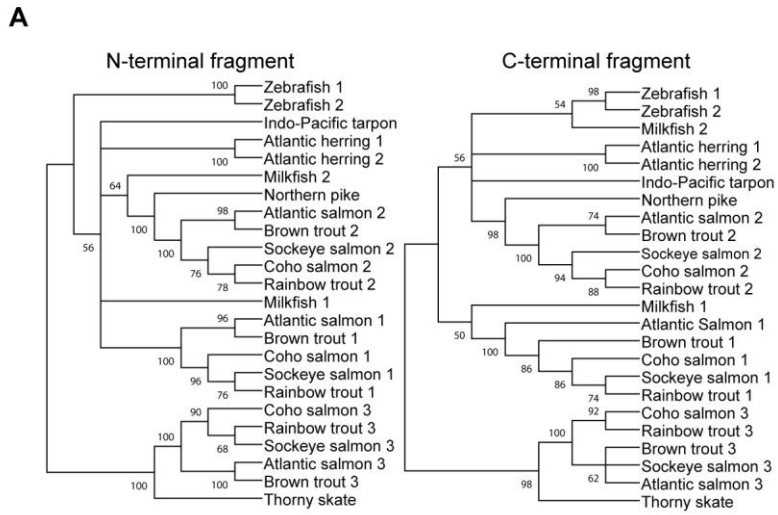

Figure 15. Comparison of possible fish RTP phylogenies

a) Collapsed maximum-likelihood trees for N-terminal and C-terminal fish RTP gene fragments, relative to a predicted recombination breakpoint (nt383). Numbers indicate the percentage of 50 bootstrap replicates for which the associated taxa clustered together. Nodes with <50% bootstrap confidence were collapsed. Trees were generated as in Figure 14B.

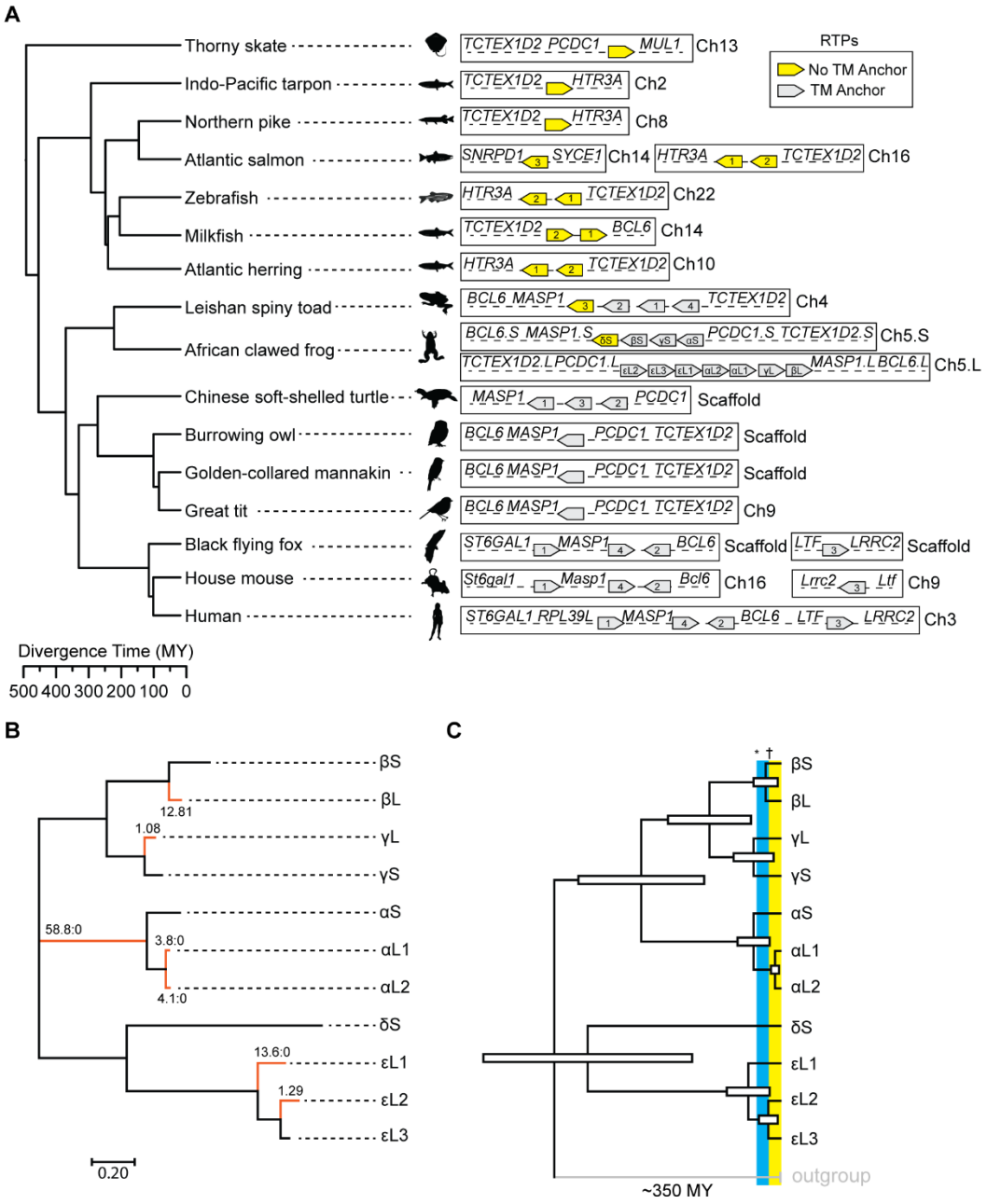

Figure 16. RTP locus synteny and evolutionary analysis of *Xenopus laevis* RTPs

a) Left: A TimeTree (Kumar et al., 2017) of representative RTP-containing vertebrate species. Right: chromosomal arrangement of RTPs. Common proximal genes and chromosome numbers, when available, are indicated. b) Free-ratio analysis of *X. laevis* RTPs. Annotated values indicate

the dN/dS of each branch. Branches with dN/dS > 1 are marked in red. c) A TimeTree for *X. laevis* RTPs inferred using the Reltime method (Tamura et al., 2012) (Tamura et al., 2018) and the Tamura-Nei model (Tamura and Nei, 1993). Divergence times were estimated by calibration by designating mammalian RTP4 sequences as an outgroup. The estimated log likelihood value is -9335.49. A discrete Gamma distribution was used to model evolutionary rate differences among sites (5 categories (+G, parameter = 2.9731)). The rate variation model allowed for some sites to be evolutionarily invariable ([+I], 6.22% sites). White rectangles denote 95% CI of divergence times. Asterix (*) indicates estimated L and S genome divergence time. Dagger (†) indicates estimated L and S genome hybridization time.

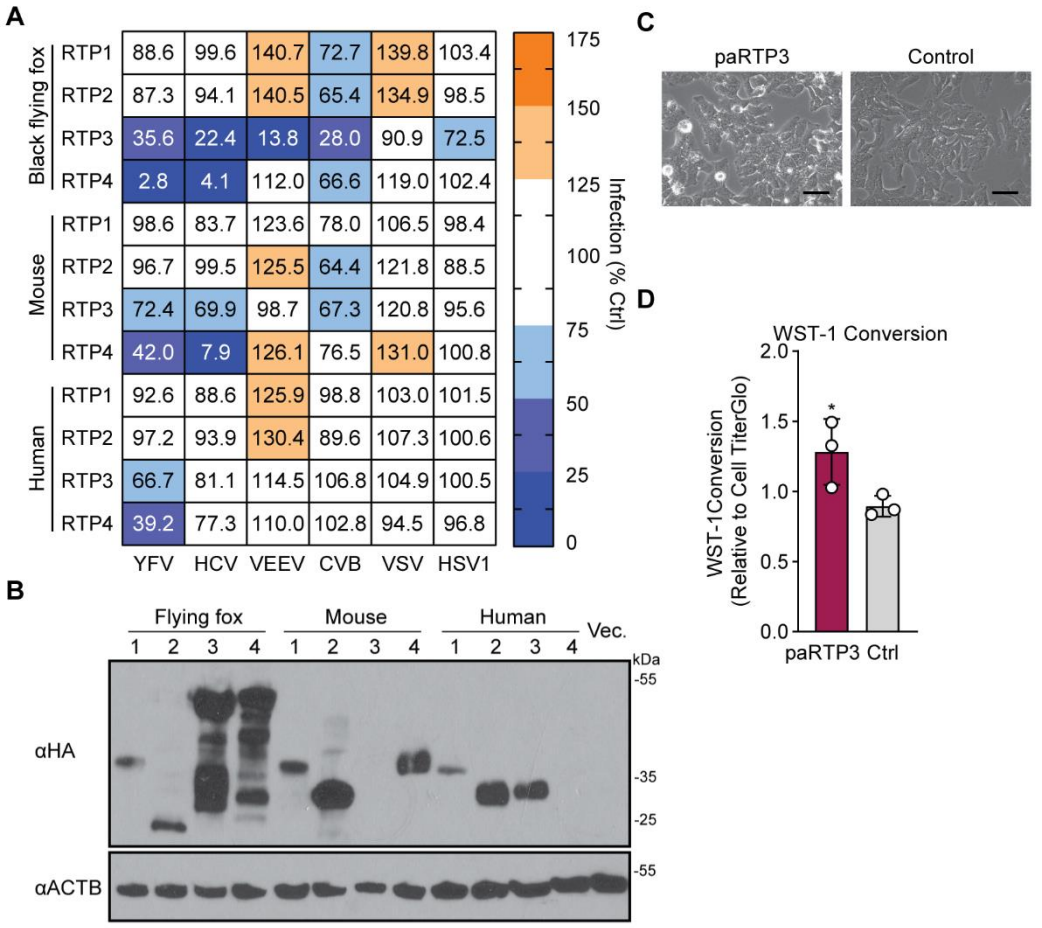

Figure 17. Functional survey of mammalian RTP paralogs

a) Huh7.5 cells ectopically expressing the indicate RTPs or a vector control were infected with a panel of viruses at an MOI of 0.5 to 1. Cells were harvested after the completion of approximately one replication cycle and percent infection was assessed by flow cytometry. Cells represent the mean of n = 2 (HCV) or n = 3 (all other viruses) biological replicates, normalized to control. b) Western blot of ectopically-expressed RTPs. For each screen replicate, an additional well of cells was harvested alongside infections for protein expression analysis. Blot is representative of n = 3 replicates. c) Representative micrograph of paRTP3-expressing Huh7.5 cells and vector control cells. Scale bar: 20μm. d) Huh7.5 cells expressing the indicated construct were seeded at 10,000

cells per well on a 96-well plate one day prior to assay. The day of WST assay, WST reagent (Takara) was added (10uL in 100uL media) and cells were incubated for two hours, after which visual absorbance was assayed. In parallel, cell density was measured using Cell Titer-Glo (Promega) and luminometry.

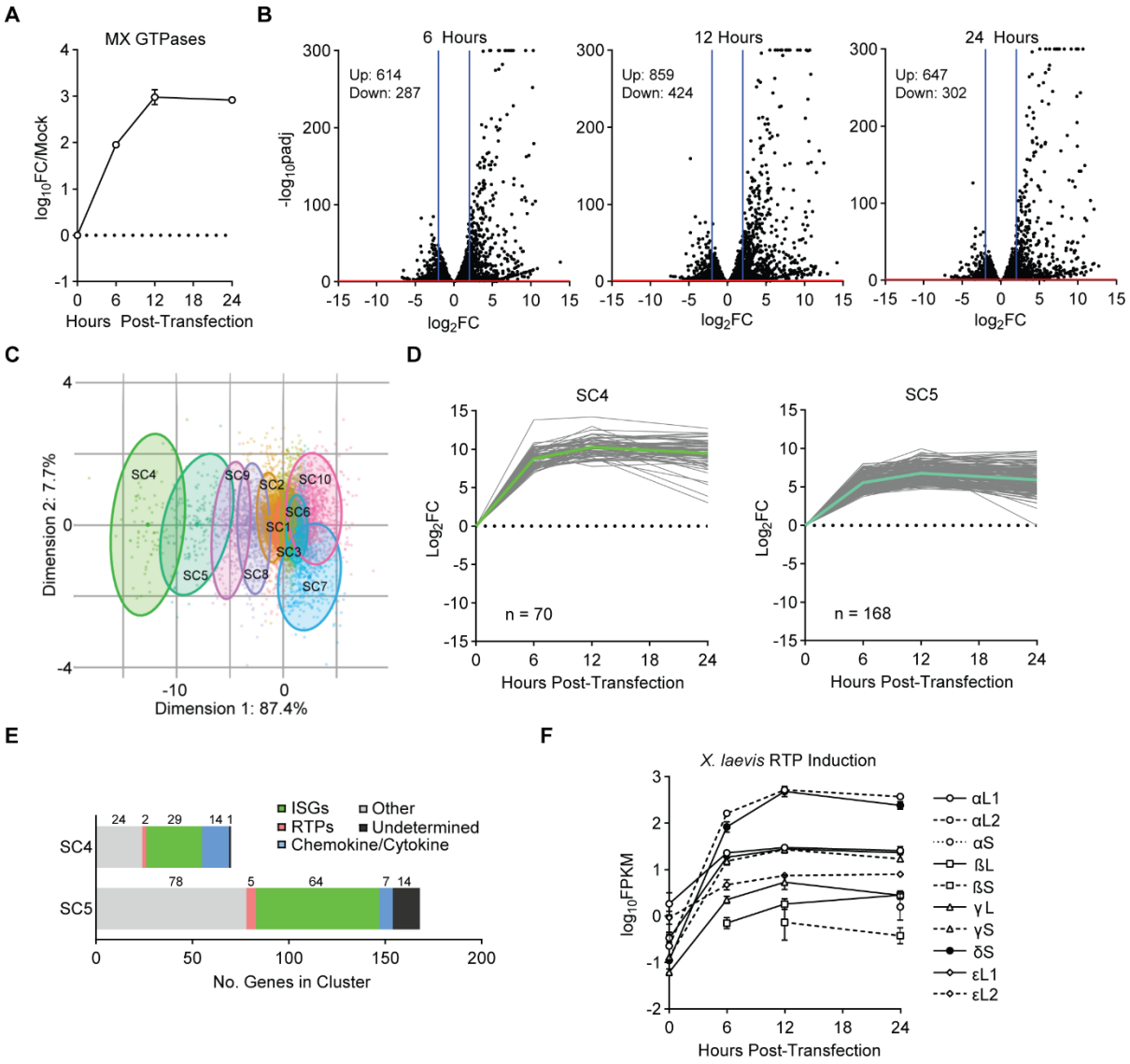

Figure 18. Identification of poly(I:C)-induced *Xenopus laevis* RTPs

a) qPCR was used to assess MX-family GTPase induction following transfection of A6 cells with poly(I:C) over a time course. As designed, primers are capable of detecting all *X. laevis* MX-family transcripts. Points represent the mean ± SD of n = 3 biological replicates. b) Volcano plots for A6 cells treated with poly(I:C) for 6, 12, or 24 hours, relative to mock transfection. Differentially-expressed genes (padj < 0.05, fold change > 4) are indicated. Data are derived from three biological

replicates. c) PCA analysis of gene expression kinetics. Ten subclusters were identified. d) Kinetic profiles of top-induced, ISG-rich clusters (SC4 and SC5). Lines represent individual genes. Colored/bolded line indicates mean profile for the cluster. e) Annotation of genes in SC4 and SC5. ISGs annotated per inducibility in other datasets, as detailed in methods. Other: non-ISGs with clear annotation. Undetermined: insufficient homology to determine identify of transcript. f) Induction of RTP family members following poly(I:C) transfection. Plotted points indicate when significant enrichment over background was observed.

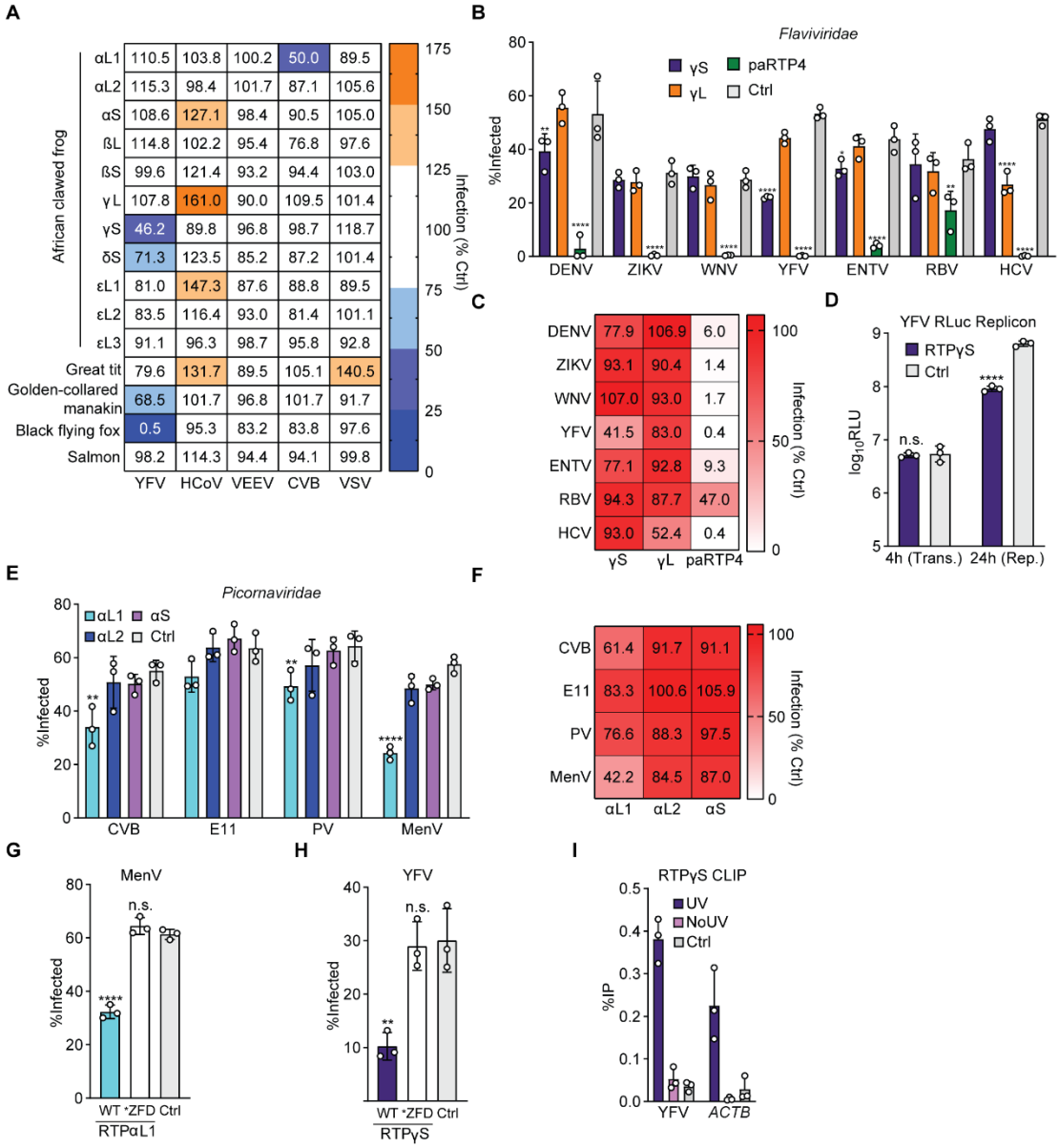

Figure 19. Identification of antiviral *Xenopus laevis* RTPs

a) Huh7.5 cells ectopically expressing the indicated RTPs or a vector control were infected with a panel of RNA viruses at an MOI of 0.5 to 1. Cells were harvested after the completion of approximately one replication cycle and percent infection was assessed by flow cytometry. Cells represent the mean of n = 2 biological replicates, normalized to control. Raw data: Supplemental

Figure 2B. b) Huh7.5 cells ectopically expressing the indicated RTPs or a vector control were infected with a panel of flaviviruses at an MOI of 0.5 to 1. Cells were harvested after the completion of approximately one replication cycle and percent infection was assessed by flow cytometry. Bars represent the mean ± SD of n = 3 biological replicates. c) Data from (B), represented as percent of control. d) Huh7.5 cells ectopically expressing either RTPγS or a vector control were transfected with a YFV-RLuc replicon and protein production was assessed by luminometry. Bars represent the mean ± SD of n = 3 biological replicates. e) Huh7.5 cells ectopically expressing the indicated RTPs or a vector control were infected with a panel of picornaviruses at an MOI of 0.5 to 1. Cells were harvested after the completion of approximately one replication cycle and percent infection was assessed by flow cytometry. Bars represent the mean ± SD of n = 3 biological replicates. f) Data from (E), represented as percent of control. g) Huh7.5 cells expressing HA.RTPγS, HA.RTPγS.C151A, or a vector control were infected with YFV-17D for 24 hours. Cells were harvested after the completion of approximately one replication cycle and percent infection was assessed by flow cytometry. Bars represent the mean ± SD of n = 3 biological replicates. h) Huh7.5 cells expressing HA.RTPαL1, HA.RTP αL1.C154A, or a vector control were infected with MenV for 6 hours. Cells were harvested after the completion of approximately one replication cycle and percent infection was assessed by flow cytometry. Bars represent the mean ± SD of n = 3 biological replicates. i) Huh7.5 cells expressing HA.RTPγS or a vector control were infected with WNV (MOI of 2) for 24h. CLIP-qPCR identified RNA bound by HA.RTPγS. UV: UV crosslinked HA.RTPγS cells. NoUV: non-crosslinked HA.RTPγS cells. Vector: UV crosslinked vector control cells. Bars: mean ± SD of n = 3 biological replicates.

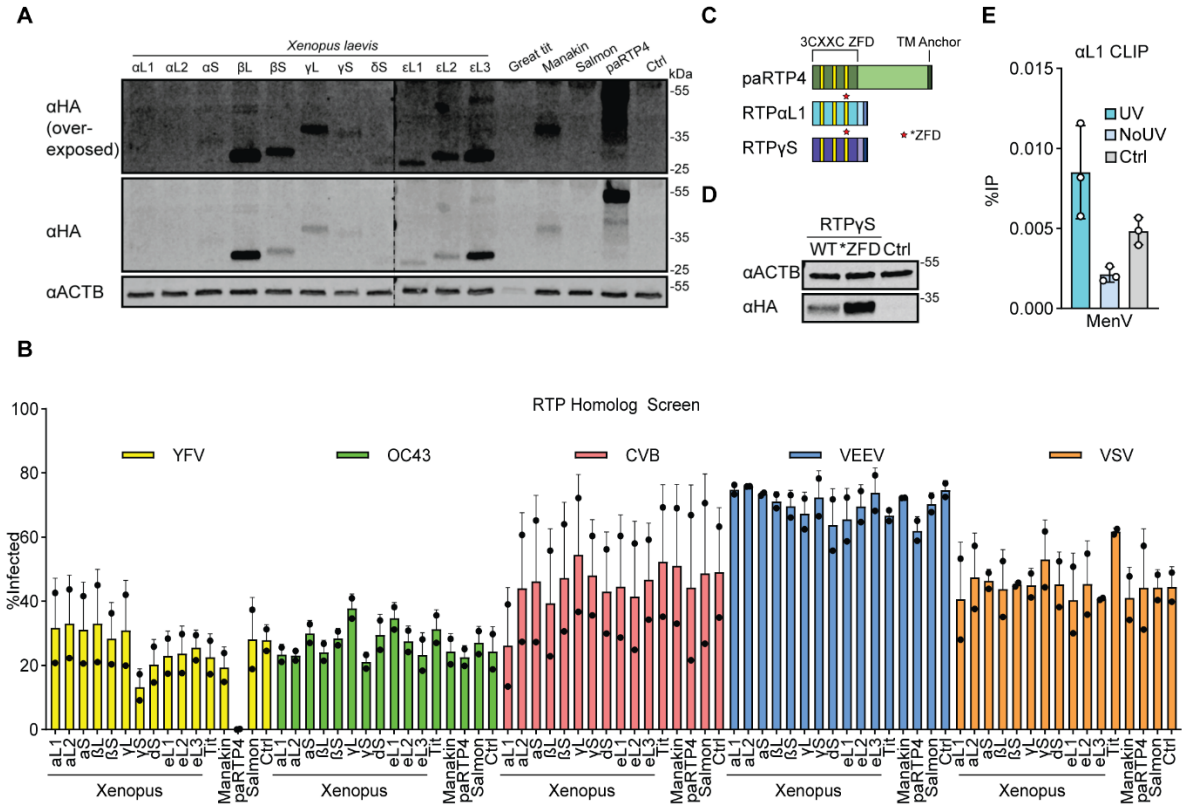

Figure 20. Supporting data for figure 19

a) Western blot of ectopically-expressed RTPs. Vertical dotted line indicates splice site for two independently-run gels. For each screen replicate, an additional well of cells was harvested alongside infections for protein expression analysis. Blot is representative of n = 2 replicates. b) Raw data related to Figure 19A. Huh7.5 cells ectopically expressing the indicate RTPs or a vector control were infected with a panel of RNA viruses at an MOI of 0.5 to 1. Cells were harvested after the completion of approximately one viral life cycle and percent infection was assessed by flow cytometry. Bars represent the mean ± SD of n = 2 biological replicates. c) Cartoon representation of *X. laevis* RTPαL1 and RTPγS with paRTP4 as a reference. Yellow boxes denote N-terminal CXXC motifs, the third of which was targeted for disruption by site-directed

mutagenesis to generate *ZFD RTPs. d) Western blot of ectopically-expressed RTPγS and RTPγS*ZFD. Blot is representative of n = 2 replicates. e) Huh7.5 cells expressing HA.RTPαL1 or a vector control were infected with MenV (MOI of 2) for 6h. CLIP-qPCR identified RNA bound by HA.RTPαL1. UV: UV crosslinked HA.RTPαL1 cells. NoUV: non-crosslinked HA.RTPαL1 cells. Vector: UV crosslinked vector control cells. Bars: mean ± SD of n = 3 biological replicates.

CHAPTER FIVE
Conclusions and Recommendations

CONCLUSIONS

Some vertebrate RTPs are antiviral effectors

This work describes a previously unknown mechanism by which IFN inhibits viral infection in vertebrates. First, I performed a screen for antiviral effectors in bats and identified RTP4 from the black flying fox, *Pteropus alecto* as a potent inhibitor of flaviviruses. Through comparative studies, I found that diverse RTP4 orthologs have adapted to restrict different members of the *Flaviviridae*. Some RTP4 orthologs are broadly antiviral, while others seem to have narrower patterns of specificity. Unique among the RTP4 orthologs I screened, *P. alecto* RTP4 modestly inhibits the nidoviruses EAV and HCoV-OC43, suggesting that RTP4 in some lineages may have broader activity than appreciated in my screens with flaviviruses. Indeed, when I expanded my study to RTP homologs from the African clawed frog, *Xenopus laevis*, I found RTPs that inhibit members of the *Flaviviridae* and also found an RTP that inhibits picornaviruses.

The ability of separate RTPs to inhibit flaviviruses, nidoviruses, and picornaviruses raises the question of whether other RTPs have adapted to inhibit other positive-sense RNA viruses. While only correlative, a study linked an RTP to nodavirus susceptibility in the Asian seabass, perhaps suggesting that this may be the case (Liu et al., 2017). A separate study also found that human RTP4, when ectopically expressed, can suppress the replication of a human norovirus (HNoV) replicon (Dang et al., 2018). We assessed whether RTP4 orthologs from several species were able to inhibit the related murine norovirus (MNoV) and did not observe a reduction in viral production in cells expressing any ortholog (Figure 21). This does not exclude the possibility that

RTPs may inhibit noroviruses such as HNoV, and additional follow-up experiments to assess whether this is the case are merited.

Biochemical and cellular properties of RTPs

The present work additionally provides insight into the basic biology of RTPs. Localization studies provided evidence that RTP4 is ER-localized, as suggested by a recent study of murine Rtp4 (Fujita et al., 2019). I also found that the N-terminal zinc finger domain (ZFD) of RTP4 is an RNA-binding domain and that this property is shared by antiviral *Xenopus* RTPs. Whether RNA binding is involved in other roles of RTPs is an area for future investigation.

RTP4 inhibits flavivirus replication

Reporter virus and replicon data suggest that antiviral RTPs (RTP4 in mammals and antiviral *Xenopus* RTPs) inhibit the replication stage of the viral life cycle. My mechanistic studies of RTP4 localize it to flavivirus replication machinery and demonstrate that interactions between NS5 and NS3, as well as between NS5 and its genomic RNA substrate, are altered in the presence of RTP4. This supports a model in which RTP4 interferes with NS5-NS3 replicase function, decreasing its efficiency. My data do not distinguish between a model in which RTP4 specifically disrupts interactions between NS5 and NS3, or one in which it indirectly promotes a state in which such interactions are less frequent. However, my observations that RTP4 binds evenly across the flavivirus genome (Figure 10B) and that NS5 polymerase appears to accumulate across the genome in the presence of RTP4 (Figure 9K) is consistent with a mechanism in which RTP4 sterically

hinders NS5 polymerase as it replicates viral RNA. It may be possible to test this hypothesis through a combination of *in vitro* and cell-culture based reporter assays, as detailed below.

Recurrent expansions of the RTP family

By performing detailed evolutionary analyses, I found that the RTP gene family has undergone multiple, independent expansions in several vertebrate lineages. I found that many of these RTPs are rapidly evolving, suggestive of roles in immunity outside of mammals. Mechanistic studies revealed that these duplicated antiviral RTPs can functionally diversify within the same species, as was the case for the "gamma" family of *Xenopus* RTPs.

FUTURE DIRECTIONS

Determinants of antiviral activity

While I found that RTP4 orthologs exhibit differential antiviral specificity and potency, the determinants of this specificity are unclear. Some antiviral effectors such as MX1 (Mitchell et al., 2012) and TRIM5α (Sawyer et al., 2005) have specific residues that determine the viral specificity of orthologs. In these and other cases, evolutionary analyses identified these rapidly-evolving regions as probable hotspots in a host-pathogen genetic arms race, and mechanistic studies confirmed this assessment. We, however, found no overlap in signatures of rapid evolution in separate mammalian lineages (Figure 11A), suggesting that this may not be the case for RTP4.

In an attempt to determine which domain of RTP4 determines its antiviral specificity, I generated chimeric RTP4 constructs comprised of either the human or black flying fox ZFD and c-terminal domains (paNhsC: flying fox ZFD and human CTD, hsNpaC: human ZFD and flying

fox CTD). I assessed the ability of these chimeric constructs to inhibit a flavivirus (YFV), a hepacivirus (HCV), and a coronavirus (HCoV-OC43) when ectopically expressed (Figure 22A). To my surprise, both chimeric proteins potently inhibited YFV, hsNpaC, like paRTP4, potently inhibited HCV, and neither inhibited OC43. These results suggest that both N- and C-terminal attributes of RTP4 underlie its antiviral activity. Notably, as observed for RTP4 orthologs, expression levels do not correlate with antiviral activity; hsNpaC, despite expressing at low levels (Figure 22B), inhibits HCV whereas paNhsC, which expresses at high levels, does not.

The exact contribution of these regions, as assessed by these chimeras, is difficult to discern. The ZFD of hsRTP4, when joined to the expanded CTD of paRTP4, gains antiviral activity against HCV, yet curiously the ZFD of paRTP4, which when expressed without a C terminus can inhibit HCV (Figures 7E, 8G, and 22A), loses this ability when joined to the CTD of hsRTP4. Additionally, hsRTP4 loses antiviral activity when truncated (Figure 22A). Thus, it seems that the C terminus of paRTP4 uniquely "enhances" any core antiviral RTP4 ZFD, while the C terminus of hsRTP4 modestly enhances the ZFD of hsRTP4 but conversely inhibits the ZFD of paRTP4 in the context of OC43 and HCV. These patterns of specificity are perhaps more complex than those of different RTP4 orthologs themselves, suggesting that ortholog and virus-specific properties may influence the contribution of N and C-terminal regions of RTP4.

I would suggest that the study of the minimal antiviral domain (ZFD) of RTP4 be a first step towards assessing determinants of antiviral specificity. The apparent accessory role of the CTD could subsequently be assessed after more is known about the properties of the ZFD. Likewise, it would perhaps be most prudent to consider phenotypes for different viruses separately, since different trends were observed for YFV, HCV, and OC43 with the ZFD/CTD chimeras (Figure

22A). It is possible that a "block chimera" strategy could be used – either by exchanging portions of the ZFDs of paRTP4 and another RTP4 (perhaps hsRTP4), or even by swapping portions of RTP4 with another RTP, such as RTP1, which is not antiviral (Figure 17). Indeed, a study of the role of RTP1 in odorant receptor trafficking (Wu et al., 2012) successfully used chimeras of human RTP1 and RTP4 to pinpoint functional regions of the ZFD of RTP1, suggesting that intra-RTP chimeras can retain function.

Deep mutational scanning of the ZFD of RTP4, or perhaps more limited saturating mutagenesis of positively-selected residues of different RTP4 orthologs, is an alternative approach that could provide insight into the contribution of different regions of RTP4 to its antiviral properties. While such strategies may pinpoint residues which when mutagenized result in gains or losses of function, it may be difficult to capture true "determinants" of antiviral specificity if multiple regions or residues of the protein are responsible for these properties. Nevertheless, I would propose two experiments if a library of paRTP4 mutants were generated. First, since paRTP4 was initially identified in a cell-death based assay with DENV and ZIKV, these viruses could be used to comprehensively identify loss-of-function mutations using a bulk drop-out screen. Loss-of-function RTPs would fail to protect cells from flavivirus-induced cell death, and RTPs which phenocopy WT paRTP4 would be retained. Second, the ability of WNV to overwhelm paRTP4 could be used to identify "super-restrictor" RTP4 variants using a similar strategy. WNV eventually overwhelms paRTP4, leading to cell death, so RTP-expressing cells that survive a CPE-based screen would be candidate gain-of-function variants.

It is also possible that localization could underlie the ability of RTP4 orthologs to inhibit different viruses. Does the CTD of hsRTP4 prevent an RTP4 ZFD from associating with the HCV

replicase? Does the longer, intrinsically-disordered CTD of paRTP4 augment the ability of a ZFD to access viral replication machinery? Proximity ligation assays between dsRNA and these chimeras, as in Figure 9G, could be informative. I would however suggest that FRET, perhaps implemented in a flow-cytometry-based assay, be explored if this hypothesis is pursued since it is less expensive and higher-throughput than PLA.

RNA-binding properties

While I determined that RTP4 binds viral and cellular RNA, I did not determine 1) whether RTP4 favors specific RNA sequences or structures or 2) what portion of the ZFD is responsible for its RNA-binding properties.

Nuclease digestion of RTP4-bound West Nile virus genomic RNA (Figure 10B) paired with qPCR did not reveal a gross skew of RTP4 towards any specific genomic location, though this does not conclude that RTP4 binds RNA in a nonspecific manner. Two complementary approaches could address this question. First, CLIP-seq of RTP4 is a logical next step, following my successful CLIP-qPCR experiments which had a high signal-to-noise ratio. CLIP-seq would provide nucleotide-level resolution of RTP4 binding profiles along viral and host substrates and may reveal conserved motifs which are preferentially enriched in RTP4-bound RNA. Second, *in vitro* assays with model RNA substrates could reveal the specific RNA-binding properties of RTP4. Unfortunately, while I found that the N terminal ZFD of RTP4 is soluble when expressed in bacteria, recombinant RTP4 co-purifies with bacterial nucleic acids and forms aggregates, complicating downstream work. Future work to better purify RTP4, possibly by purification under denaturing conditions with a subsequent refolding step, may enable *in vitro* binding assays such

as EMSAs. Importantly, recombinant NS5 and NS3 retain function in *in vitro* assays; if purification of functional RTP4 is successful this would allow the direct testing of whether RTP4 interferes with polymerase or helicase activity.

While I identified the N-terminal ZFD of RTP4 as an RNA-binding domain, I did not characterize the mechanism by which this domain binds RNA. Since RTP4 cross-links to cellular mRNAs, oligo(dT) capture represents an opportunity to characterize RTP4-RNA interactions. I would recommend a strategy similar to that employed by Castello et al, in which oligo(dT)-captured RNA-binding proteins are digested with proteinases so that peptides which interact with RNAs can be identified by mass spectrometry (Castello et al., 2016). RNA-binding zinc finger motifs are relatively uncommon (Font and Mackay, 2010), so it is possible that the zinc finger motifs of the ZFD domain of RTPs serve a separate function and the RNA-binding properties result from some other motif. A relatively unbiased approach, as outlined above, may help elucidate whether this is the case. Finally, structural data for RTP4 or any RTP would be an invaluable tool for the prediction of potential RNA interaction surfaces.

Antiviral mechanism

The precise mechanism by which antiviral RTPs inhibit viral infection remains elusive. It is likely that additional biochemical or structural data, as discussed above, would be of utility. In lieu of this, functional assays with the model antiviral RTP RTP4 may provide insight into the antiviral activity of RTPs.

First, if the anti-flavivirus activity of RTP4 is specific to the NS5-NS3 replicase, assessing whether RTP4 inhibits a virus with a similar replicase may be informative. Jingmenviruses are a

recently-identified family of segmented, positive-sense RNA viruses that contain an NS5-NS3 replicase which originates from flaviviruses (Ladner et al., 2016). This similarity between flaviviruses and jingmenviruses, despite their otherwise divergent replication strategies and genome architectures, makes these viruses an attractive tool to test the theory that RTP4 interferes with the coordinated activities of NS5 and NS3.

Further interrogation of the mechanism of escape of RTP4-mediated suppression by YFV NS3.E573K may provide hints of a mechanism. Indeed, this mutation maps to a region of NS3 which, at least in the case of dengue virus, has been suggested to mediate its interaction with NS5 (Tay et al., 2015). Assessing whether the interactions of NS5-NS3 or NS5-NS3.E573K are in some way altered could be informative. Does, for example, this mutation increase the affinity of NS3 for NS5, preventing species-specific RTP4-mediated replicase disruption while also incurring a fitness cost? Co-immunoprecipitations in a reduced component system could address this and other questions. Subgenomic reporters which assess polymerase activity in the absence of other nonstructural proteins have been designed and successfully utilized for cell culture drug screens (Lee et al., 2015). Such tools could be repurposed for use alongside ectopically-expressed proteins, including RTP4 and perhaps NS3, to assess whether RTP4 activity is specific to NS5 and NS3. As with the *in vitro* assays discussed above, these reporters could be used in combination with the NS3.E573K escape mutation to assess the specific mechanism of escape.

In vivo relevance

An attractive future direction would be to confirm the status of RTP4 as an antiviral effector *in vivo*. A mouse model of Rtp4 deficiency would provide the framework for such assessment, and

Rtp4 knockout mice are readily available (He et al., 2020). Importantly, however, *Rtp4* knockout mice were used to assess the *in vivo* regulatory function of Rtp4. In a mouse model of West Nile virus infection, a flavivirus that is not effectively restricted by murine Rtp4 (Figure 12A), Rtp4 ablation promoted increased IFN signaling and thus conferred a survival advantage relative to Rtp4-suficient wild-type mice (He et al., 2020). This regulatory phenotype may be dominant in the context of infection by viruses for which murine Rtp4 is not evolutionarily "honed" as a restriction factor. A critical first step would be to screen viruses, perhaps those that naturally infect other rodents and/or for which a mouse infection model exists, for sensitivity to Rtp4 in cell culture. If murine Rtp4 potently restricts candidate viruses in cell culture, the importance of Rtp4 as a restriction factor could then be assessed *in vivo*.

Survey of other RTP functions

My functional research has focused on a subset of mammalian RTP4s and *Xenopus laevis* RTPs. This only scratches the surface of the diversity that is found in vertebrate RTPs (Figure 14A). Likewise, I only investigated the antiviral activity of RTPs – not their other functions – and then only for a miniscule fraction of the positive-sense RNA viruses that are known to infect vertebrates. My work could therefore be a starting point for several exploratory projects, detailed below.

The trafficking of odorant receptors is an important function of mammalian RTPs. Recently, it was shown that murine Rtp2 can interact with and traffic the drosophila odorant receptor Orco to the cell surface (Halty-deLeon et al., 2016). This conservation of function suggests that Orco could be used as a tool to identify functional homologs of mammalian RTP2 among other

vertebrate RTPs. A co-transfection screen of *Xenopus* RTPs and Orco would be a simple first step to see if this function is conserved in amphibians and other species.

A recent study (He et al., 2020) found that RTP4 is a negative regulator of the IFN response in humans and mice. Many of the assays used by He and colleagues could be readily be adapted to other experimental systems. Does ectopically expressed RTP4 dampen TBK1-mediated signaling in *P. alecto* cells? Does genetic ablation of RTP4 in cells from diverse species lead to enhanced ISG induction and IFN production upon poly(I:C) stimulation? Do both the ZFD and CTD of RTP4 contribute to this regulatory role? If RTP4 serves an important regulatory role in humans and mice, comparative studies in other vertebrates may provide insight into immunological differences that could contribute to observed differences in immunopathology in certain species, such as bats. One could hypothesize that there is a balance between antiviral breadth and other biological functions of RTP4; characterizing this additional function of RTP4 in other species would provide insight into the evolutionary constraints of a rapidly-evolving multifunctional protein.

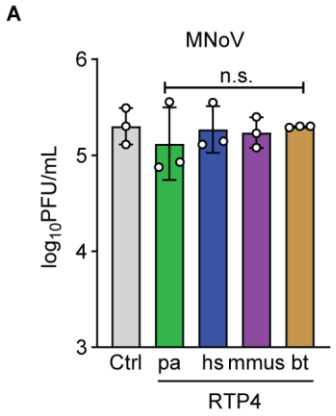

Figure 21. Murine norovirus plaque assay

a) *STAT1*$^{-/-}$ fibroblasts stably expressing CD300lf, the MNoV receptor, were transduced with lentivirus encoding the indicated RTP orthologs or a FLuc control and challenged with MNoV (strain CW3) at an MOI of 10 for 18 hours, after which supernatant was collected and viral production was assessed by plaque assay on BV2 cells. One way ANOVA on log-transformed data. n = 3 biological replicates.

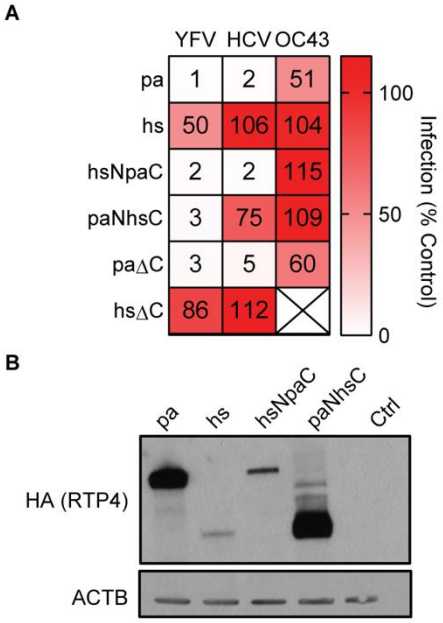

Figure 22. Chimeric RTP4 phenotypes

a) Huh7.5 cells stably-expressing the indicated constructs were infected with YFV, HCV, or HCoV-OC43 at an MOI of 0.5 for one viral replication cycle. Percent infection was assessed by flow cytometry. Cells represent the mean of n = 3 biological replicates, normalized to a vector control. The cell that is marked by an X represents an infection that was not performed. b) Representative western blot (n = 3) of Huh7.5 cells stably expressing WT *P. alecto*, *H. sapiens*, or chimeric RTP4.

APPENDIX A
Primers

Use	Name	Sequence (5'-3')	Notes
qPCR	entv_qPCR_3768_L	GGTTTCGTCACGGGCTATTA	ENTV qPCR
	entv_qpcr_3768_R	CAGACAGTACCACTTGGGATATG	ENTV qPCR
	WNV_qPCR_12_F	TGTGTGAGCTGACAAACTTAGTA	WNV qPCR
	WNV_qPCR_12_r	CCTCCTGGTTTCTTAGACATCG	WNV qPCR
	WNV_qPCR_2111_F	CATACATAGTGGTGGGCAGAG	WNV qPCR
	WNV_qPCR_2111_r	CTCCTTTGAGGGTGGTTGTAA	WNV qPCR
	WNV_qPCR_3560_F	GCCTTCTGGTCGTGTTCTT	WNV qPCR
	WNV_qPCR_3560_r	GGACTAGCAGAGCAATCAGTATAG	WNV qPCR
	WNV_qPCR_6918_F	CGAGATGGGTTGGCTAGATAAG	WNV qPCR
	WNV_qPCR_6918_r	GGCCTCAAGTCCAGAAGAAA	WNV qPCR
	WNV_qPCR_10933_F	CACCTGGGATAGACTAGGAGAT	WNV qPCR
	WNV_qPCR_10933_r	GTGTTCTCGCACCACCA	WNV qPCR
	WNV_qpcr_anti_2673_F	GAAGCTCGACTCACCCAATAC	WNV qPCR
	WNV_qpcr_anti_2673_R	CCCTACATGCCGAAAGTCATAG	WNV qPCR
	WNV_qpcr_anti_5906_F	CATCCTTTCACCCTGCACTATC	WNV qPCR
	WNV_qpcr_anti_5906_R	GGAACATCAGGCTCACCAATAG	WNV qPCR
	WNV_qpcr_anti_9499_F	CCACTGTCACCTCTCCATATTC	WNV qPCR
	WNV_qpcr_anti_9499_R	CACGGAAACTACTCCACACA	WNV qPCR
	WNV_NS3_5007_fwd	GGAACATCAGGCTCACCAATAG	WNV qPCR
	WNV_NS3_5007_rev	CATCCTTTCACCCTGCACTATC	WNV qPCR
	WNV_qPCR_177_fwd	GATTGGACTGAAGAGGGCTATG	WNV qPCR
	WNV_qPCR_177_rev	AACCTGAAGAACGCCAAGAG	WNV qPCR
	WNV_qPCR_1065_fwd	CATGTCTAAGGACAAGCCTACC	WNV qPCR
	WNV_qPCR_1065_rev	TGACGGTAGCCAAATAGCAATA	WNV qPCR

	WNV_qPCR_4520_fwd	GAATGGTCTGTCTCGCGATTAG	WNV qPCR
	WNV_qPCR_4520_rev	CGCCTCCTCTCTTTGTGTATTG	WNV qPCR
	WNV_qPCR_8236_fwd	CCCTACATGCCGAAAGTCATAG	WNV qPCR
	WNV_qPCR_8236_rev	GAAGCTCGACTCACCCAATAC	WNV qPCR
	WNV_qPCR_9880_fwd	CGAGGACAGGATGAATTGGTAG	WNV qPCR
	WNV_qPCR_9880_rev	CAGCCACATCTGGGCATAA	WNV qPCR
	YFV qpcr_878_fwd	GTGACGGCTCTGACCAT	YFV qPCR
	YFV qpcr_878_rev	ATGCAGTGAGCTGAGTA	YFV qPCR
	YFV qpcr_3425_fwd	GGTAGTGATGGGTGTTGGTATC	YFV qPCR
	YFV qpcr_3425_rev	GGGACAGCATGTATTTCTCCA	YFV qPCR
	YFV qpcr_6657_fwd	CTCCCAAAGGCATCAGTAGAA	YFV qPCR
	YFV qpcr_6657_rev	ATAGGAGATGTGAGTGGGTTTG	YFV qPCR
	YFV qpcr_10226_fwd	GCCTCCCACATCCATTTAGT	YFV qPCR
	YFV qpcr_10226_rev	CAGGTCAGCATCCACAGAATA	YFV qPCR
	YFV_qpcr_as4084_fwd	ATAGGAGATGTGAGTGGGTTTG	YFV qPCR
	YFV_qpcr_as4084_rev	CTCCCAAAGGCATCAGTAGAA	YFV qPCR
	YFV_qpcr_as7313_fwd	GGGACAGCATGTATTTCTCCA	YFV qPCR
	YFV_qpcr_as7313_rev	GGTAGTGATGGGTGTTGGTATC	YFV qPCR
	paRTP4_qPCR_l1	CTACAGCCCACACAGAAGGA	black flying fox RTP4 qPCR
	paRTP4_qPCR_r1	TGATTGAAGGAAGAGCGTCCA	black flying fox RTP4 qPCR
	Beta Actin qRT-PCR FWD (human)	GCACAGAGCCTCGCCTTT	human ACTB qPCR
	Beta Actin qRT-PCR REV (Human)	TATCATCATCCATGGTGAGCTGG	human ACTB qPCR

	RPS11 (P. alecto) RT-PCR FWD	ATCCGCCGAGACTATCTCCA	black flying fox RPS11 qPCR
	RSP11 (P. alecto) RT-PCR REV	GGACATCTCTGAAGCAGGGT	black flying fox RPS11 qPCR
	MX1 (P. alecto) RT-PCR Fwd	ATGTATGGCATGGAGACGCC	black flying fox MX1 qPCR
	MX1 (P. alecto) RT-PCR Rev	AGCCGAGTGTTGCTCTTCTC	black flying fox MX1 qPCR
	AAV_ITR_qPCR_F	GGAACCCCTAGTGATGGAGTT	Used to titer AAV by qPCR
	AAV_ITR_qPCR_R	CGGCCTCAGTGAGCGA	Used to titer AAV by qPCR
	Alecto_ACTB_fwd	CAGAGCAAGAGAGGCATCC	black flying fox ACTB qPCR
	Alecto_ACTB_rev	CCAGATCTTCTCCATGTCATCC	black flying fox ACTB qPCR
Cloning	paRTP4 FWD	GGGGACAAGTTTGTACAAAAAAGCAGGCTTCACCATGGACTCTCAGTCTC	clone P. alecto RTP4 from cDNA library
	paRTP4 Rev	GGGGACCACTTTGTACAAGAAAGCTGGGTTCTAATTAAAGTACTTAGACATC	clone P. alecto RTP4 from cDNA library
	tbRTP4_FWD	ATGTACCCATACGATGTTCCAGATTACGCTTCTGCCATGAACTCCAAG	clone T.brasiliensis RTP4 from cDNA
	tbRTP4_REV	GGGGACCACTTTGTACAAGAAAGCTGGGTTTTATAAGTATTTGCCTAC	clone T.brasiliensis RTP4 from cDNA
	mmRTP4_HA_fwd	*ATGTACCCATACGATG*TTCCAGATTACGCTTCTGCCATGCTGTTCCCCGATGAC	add HA tag to M. musculus RTP4
	mmRTP4_rev_ATTB2	GGGGACCACTTTGTACAAGAAAGCTGGGTTTTATCTAGTGAAAAGACTAAAAAGG	add HA tag to M. musculus RTP4
	asrRTP4_HA_f	ATGTACCCATACGATGTTCCAGATTACGCTTCTGCCATGGACTCCCAGCCTCAGAGGAAG	Add HA tag to asrRTP4
	asrRTP4_R	GGGGACCACTTTGTACAAGAAAGCTGGGTTCTACAATAAAGACAAACAGAAC	Add HA tag to asrRTP4
	raRTP4_fwd	GGGGACAAGTTTGTACAAAAAAGCAGGCTTCACCATGGACTCTCAGTCTC	clone R. aegyptiacus RTP4 from cDNA
	raRTP4_rev	GGGGACCACTTTGTACAAGAAAGCTGGGTTctacttaaagagcTTAGATATCAAAACG	clone R. aegyptiacus RTP4 from cDNA
	btRTP4_fwd	GGGGACAAGTTTGTACAAAAAAGCAGGCTTCACCATGGACGCCAAGCC	move B. taurus RTP4 from cDNA clone to gateway vector

	btRTP4_rev	GGGGACCACTTTGTACAAGAAAGCTGGGTTTCATAAGTATTTAGACACCAG	move B. taurus RTP4 from cDNA clone to gateway vector
	clHA.rtp4_fwd	ATGTACCCATACGATGTTCCAGATTACGCTTCTGCCATGGCTTCCCAG	clone C. lupus RTP4 from cDNA. Includes N terminal HA tag
	clHA.rtp4_rev	GGGGACCACTTTGTACAAGAAAGCTGGGTTTTATTTTGATCTTTCTG	clone C. lupus RTP4 from cDNA
	ssHA.RTP4_fwd	ATGTACCCATACGATGTTCCAGATTACGCTTCTGCCATGGATTCCAAAGC	clone S scrofa RTP4 from cDNA. Includes N terminal HA tag
	ssHA.RTP4_rev	GGGGACCACTTTGTACAAGAAAGCTGGGTTTTATAAGTATTTAGATACAAGAAAGG	clone S scrofa RTP4 from cDNA.
	paSHFL_FWD	GGGGACAAGTTTGTACAAAAAAGCAGGCTTCACCATGTCGCAGGAAGGTG	clone P. alecto SHFL from cDNA library
	paSHFL_REV	GGGGACCACTTTGTACAAGAAAGCTGGGTTTCACTCCCCGTGCC	clone P. alecto SHFL from cDNA library
	HA_universal_FWD_ATTB	GGGGACAAGTTTGTACAAAAAAGCAGGCTTCACCATGTACCCATACGATG	Forward primer used for generation of truncations.
	Alecto_c4	GGGGACCACTTTGTACAAGAAAGCTGGGTTctaGGAATACCCACTCC	Generate C-terminal P. alecto truncation (dC206)
	Alecto_c3	GGGGACCACTTTGTACAAGAAAGCTGGGTTctaTTGGATGGGCTGCA	Generate C-terminal P. alecto truncation (dC156)
	Alecto_c2	GGGGACCACTTTGTACAAGAAAGCTGGGTTctaTGAACACCTTAGAACCTG	Generate C-terminal P. alecto truncation (dC106)
	Alecto_c1	GGGGACCACTTTGTACAAGAAAGCTGGGTTctaCTGGGCATCTTGAGT	Generate C-terminal P. alecto truncation (dC56)
	Alecto_dTM	GGGGACCACTTTGTACAAGAAAGCTGGGTTCTAGTTATCCTGGTTAAGG	Generate C-terminal P. alecto truncation (dC22)
	Alecto_c5	GGGGACCACTTTGTACAAGAAAGCTGGGTTctaGTTTGTTATGCAGTT	Generate C-terminal P. alecto truncation (dC245)
	HA oligo FWD	catgTACCCATACGATGTTCCAGATTACGCTtctgc	Addition of HA oligo by digest and ligation
	HA oligo REV	CATGgcagaAGCGTAATCTGGAACATCGTATGGGTA	Addition of HA oligo by digest and ligation
	YFV17DE2057K-F	GGTGTTTTGAAGGCCCTGAGAAACATGAGATCTTGAATGACAGC	freetail bat RTP4 escape mutant cloning

	YFV17DE2057K-R	GCTGTCATTCAAGATCTCATGTTTCTCAGGGCCTTCAAAACACC	freetail bat RTP4 escape mutant cloning
	TRIPZoE.HA_f	agaccggtCGCCACCATGTACCCATACG	Inducible RTP4 cloning
	TRIPZoE.HA_r	CGGATACGCGTCTAATTAAAGTACTTAGACATC	Inducible RTP4 cloning
Sequencing	paRTP4_edit_fwd	GAGCTGACATCAGGGCACG	CRISPR: PCR to sequence-validate genomic edits
	paRTP4_edit_rev	GGTATTGCTTCCACCCTTGGG	CRISPR: PCR to sequence-validate genomic edits
	pAAV_gateway_f	cgttgcctgacaacgg	Sequence inserts in pAAV gateway
	pAAV_gateway_r	TCGAGGTCGACGGTATC	Sequence inserts in pAAV gateway
	paRTP4_internal_seq	CCATCCAGTAGAAGGATC	Internal sequencing primer for paRTP4
LentiCRISPRv2 oligos	paRTP4_guide1_A	CACCGGGAGAAAATTGTTTCCAATG	Genomic editing of RTP4 in P. alecto cells
	paRTP4_guide1_B	AAACCATTGGAAACAATTTTCTCCC	Genomic editing of RTP4 in P. alecto cells
	paSTAT1_guide_A	CACCGTGATCAAGGCAAGCGTTGGG	Genomic editing of STAT1 in P. alecto cells
	paSTAT1_guide_B	AAACCCCAACGCTTGCCTTGATCAC	Genomic editing of STAT1 in P. alecto cells
	sscrof_rtp4_A_oligo1	caccgAGCCAAACTCCGTGGCTCTA	Genomic editing of RTP4 in PK-15 cells
	sscrof_rtp4_A_oligo2	aaacTAGAGCCACGGAGTTTGGCTc	Genomic editing of RTP4 in PK-15 cells
	sscrof_rtp4_B_oligo1	caccgCATCACGGATGTTGAGACAT	Genomic editing of RTP4 in PK-15 cells
	sscrof_rtp4_B_oligo2	aaacATGTCTCAACATCCGTGATGc	Genomic editing of RTP4 in PK-15 cells
	RTP4 sgRNA-1 For (BrLiv47387)	caccgAATACTATGGAAATGGCACG	Genomic editing of RTP4 in human U2-OS cells
	RTP4 sgRNA-1 Rev (BrLiv47387)	aaacCGTGCCATTTCCATAGTATTc	Genomic editing of RTP4 in human U2-OS cells
	RTP4 sgRNA-3 For (BrLiv47389)	caccgATTTCAAGAACTAATCCAAG	Genomic editing of RTP4 in human U2-OS cells

	RTP4 sgRNA-3 Rev (BrLiv47389)	aaacCTTGGATTAGTTCTTGAAATc	Genomic editing of RTP4 in human U2-OS cells
YFV Tiling PCR	YFVwalk_1f	AATCCTGTGTGCTAATTGAGGT	5
	YFVwalk_1r	CCAACAGCCAAGACCAGTAG	941
	YFVwalk_2f	GGCAACTGCACAACAAACA	563
	YFVwalk_2r	CCTGACAGGGCATCAAACT	1452
	YFVwalk_3f	TGGACATCTCACTAGAGACAGTAG	1095
	YFVwalk_3r	TCACCTCAATCAGCACTTCATC	2054
	YFVwalk_4f	GGACACAAATGACAACAACCTTTA	1771
	YFVwalk_4r	CTTCTCCACATCTCATGCTCAA	2640
	YFVwalk_5f	GGTTGGCATCAACACAAGAAAC	2362
	YFVwalk_5r	CGTGGTGGATCTGGTTGATTT	3338
	YFVwalk_6f	ACCATAGACTGCGATGGATCT	2978
	YFVwalk_6r	GCAAGATGGTATTTGATGCTTTCC	3933
	YFVwalk_7f	AGACAGGGACCAAAGCAAAT	3578
	YFVwalk_7r	CCTAGCTCTCCTGACATGAAAC	4546
	YFVwalk_8f	GCATATTTGGGCGAAGGAGTA	4164
	YFVwalk_8r	TTAGCATTGTCGGGATCTCTTG	5114
	YFVwalk_9f	GATTCCATCTTGGGCTTCAGTA	4771
	YFVwalk_9r	CAGGACCACCACACTCTTTC	5721
	YFVwalk_10f	CCATGCCACCCTAACTTACA	5368
	YFVwalk_10r	CTTGCCACGAAAGCCAAAC	6212
	YFVwalk_11f	CCACTTCGTATCTCCGCATC	5918
	YFVwalk_11r	TTGTCTTGGATGGACCTTTGT	6811
	YFVwalk_12f	CCACTCTGAGGAAGGCTCTA	6531
	YFVwalk_12r	GGCTGGTGTTTCCCTCTATG	7507
	YFVwalk_13f	GGTCAGTGGCTGGAATTCAATA	7177
	YFVwalk_13r	CAAGAACTCTCACGGTCCTTTC	8111
	YFVwalk_14f	TGTGGAGGTGGATCGTGATA	7732
	YFVwalk_14r	GTTGTGTCAGTCATTGCCATTC	8658
	YFVwalk_15f	AGAATGAGGCGTCCAACTG	8363
	YFVwalk_15r	GTGATGTGGGCTCATGTAGTT	9302
	YFVwalk_16f	CTGTCCAAGACCCAAAGTTCT	8913
	YFVwalk_16r	CAATGAGCTCGTCCTGTTCT	9835
	YFVwalk_17f	GCAGAAGCAGAGATGGTGATAC	9509

	YFVwalk_17r	CCGTGGTTTATATCCCGGTTTC	10420
	YFVwalk_18f	CAACATGTGGTCACTGATGTATTT	9925
	YFVwalk_18r	TTGTGTTTGTCATCCAAAGGTC	10834
Ch. 5 primers	MENV-qPCR-fwd	GCCGAAAGCCACGTGTGTAA	
	MENV-qPCR-rev	AGATCCCAGCCAGTGGGGTA	
	XlaeMx_qpcr-fwd	AGAGAAGCTCACCAACGAGC	
	XlaeMx_qpcr-rev	GGTGCCCAGGTTTCTCAGTT	
	XlaeACTB_qpcr-fwd	AGACCTTTAACACTCCAGCTATG	

BIBLIOGRAPHY

Ahn, M., Anderson, D.E., Zhang, Q., Tan, C.W., Lim, B.L., Luko, K., Wen, M., Chia, W.N., Mani, S., Wang, L.C., *et al.* (2019). Dampened NLRP3-mediated inflammation in bats and implications for a special viral reservoir host. Nat Microbiol *4*, 789-799.

Anisimova, M., Bielawski, J.P., and Yang, Z. (2001). Accuracy and power of the likelihood ratio test in detecting adaptive molecular evolution. Mol Biol Evol *18*, 1585-1592.

Ashkenazy, H., Penn, O., Doron-Faigenboim, A., Cohen, O., Cannarozzi, G., Zomer, O., and Pupko, T. (2012). FastML: a web server for probabilistic reconstruction of ancestral sequences. Nucleic Acids Res *40*, W580-584.

Baker, F.B. (1974). Stability of Two Hierarchical Grouping Techniques Case I: Sensitivity to Data Errors. Journal of the American Statistical Association *69*, 440-445.

Balinsky, C.A., Schmeisser, H., Wells, A.I., Ganesan, S., Jin, T., Singh, K., and Zoon, K.C. (2017). IRAV (FLJ11286), an Interferon-Stimulated Gene with Antiviral Activity against Dengue Virus, Interacts with MOV10. J Virol *91*.

Banerjee, A., Zhang, X., Yip, A., Schulz, K.S., Irving, A.T., Bowdish, D., Golding, B., Wang, L.F., and Mossman, K. (2020). Positive Selection of a Serine Residue in Bat IRF3 Confers Enhanced Antiviral Protection. iScience *23*, 100958.

Barrows, N.J., Campos, R.K., Liao, K.C., Prasanth, K.R., Soto-Acosta, R., Yeh, S.C., Schott-Lerner, G., Pompon, J., Sessions, O.M., Bradrick, S.S., *et al.* (2018). Biochemistry and Molecular Biology of Flaviviruses. Chem Rev *118*, 4448-4482.

Behrens, M., Bartelt, J., Reichling, C., Winnig, M., Kuhn, C., and Meyerhof, W. (2006). Members of RTP and REEP gene families influence functional bitter taste receptor expression. J Biol Chem *281*, 20650-20659.

Benfield, C.T., MacKenzie, F., Ritzefeld, M., Mazzon, M., Weston, S., Tate, E., Teo, B.H., Smith, S.E., Kellam, P., Holmes, E.C., *et al.* (2020). Bat IFITM3 restriction depends on S-palmitoylation and a polymorphic site within the CD225 domain. Life Sci Alliance *3*.

Bernheim, A., Millman, A., Ofir, G., Meitav, G., Avraham, C., Shomar, H., Rosenberg, M.M., Tal, N., Melamed, S., Amitai, G., *et al.* (2021). Prokaryotic viperins produce diverse antiviral molecules. Nature *589*, 120-124.

Boys, I.N., Xu, E., Mar, K.B., De La Cruz-Rivera, P.C., Eitson, J.L., Moon, B., and Schoggins, J.W. (2020). RTP4 Is a Potent IFN-Inducible Anti-flavivirus Effector Engaged in a Host-Virus Arms Race in Bats and Other Mammals. Cell Host Microbe *28*, 712-723 e719.

Brand, C., Bisaillon, M., and Geiss, B.J. (2017). Organization of the Flavivirus RNA replicase complex. Wiley Interdiscip Rev RNA *8*.

Calisher, C.H., Childs, J.E., Field, H.E., Holmes, K.V., and Schountz, T. (2006). Bats: important reservoir hosts of emerging viruses. Clin Microbiol Rev *19*, 531-545.

Castello, A., Horos, R., Strein, C., Fischer, B., Eichelbaum, K., Steinmetz, L.M., Krijgsveld, J., and Hentze, M.W. (2016). Comprehensive Identification of RNA-Binding Proteins by RNA Interactome Capture. Methods Mol Biol *1358*, 131-139.

Castresana, J. (2000). Selection of conserved blocks from multiple alignments for their use in phylogenetic analysis. Mol Biol Evol *17*, 540-552.

Charlesworth, A., Yamamoto, T.M., Cook, J.M., Silva, K.D., Kotter, C.V., Carter, G.S., Holt, J.W., Lavender, H.F., MacNicol, A.M., Ying Wang, Y., *et al.* (2012). Xenopus laevis zygote arrest 2 (zar2) encodes a zinc finger RNA-binding protein that binds to the translational control sequence in the maternal Wee1 mRNA and regulates translation. Dev Biol *369*, 177-190.

Chen, Q., Sun, L., and Chen, Z.J. (2016). Regulation and function of the cGAS-STING pathway of cytosolic DNA sensing. Nat Immunol *17*, 1142-1149.

Christofi, T., and Zaravinos, A. (2019). RNA editing in the forefront of epitranscriptomics and human health. J Transl Med *17*, 319.

Colon-Thillet, R., Hsieh, E., Graf, L., McLaughlin, R.N., Jr., Young, J.M., Kochs, G., Emerman, M., and Malik, H.S. (2019). Combinatorial mutagenesis of rapidly evolving residues yields super-restrictor antiviral proteins. PLoS Biol *17*, e3000181.

Conrad, N.K. (2008). Chapter 15. Co-immunoprecipitation techniques for assessing RNA-protein interactions in vivo. Methods Enzymol *449*, 317-342.

Conticello, S.G. (2008). The AID/APOBEC family of nucleic acid mutators. Genome Biol *9*, 229.

Conticello, S.G., Thomas, C.J., Petersen-Mahrt, S.K., and Neuberger, M.S. (2005). Evolution of the AID/APOBEC family of polynucleotide (deoxy)cytidine deaminases. Mol Biol Evol *22*, 367-377.

Crameri, G., Todd, S., Grimley, S., McEachern, J.A., Marsh, G.A., Smith, C., Tachedjian, M., De Jong, C., Virtue, E.R., Yu, M., *et al.* (2009). Establishment, immortalisation and characterisation of pteropid bat cell lines. PLoS One *4*, e8266.

Cui, J., and Holmes, E.C. (2012). Endogenous hepadnaviruses in the genome of the budgerigar (Melopsittacus undulatus) and the evolution of avian hepadnaviruses. J Virol *86*, 7688-7691.

Dang, W., Xu, L., Yin, Y., Chen, S., Wang, W., Hakim, M.S., Chang, K.O., Peppelenbosch, M.P., and Pan, Q. (2018). IRF-1, RIG-I and MDA5 display potent antiviral activities against norovirus coordinately induced by different types of interferons. Antiviral Res *155*, 48-59.

Daszak, P., Cunningham, A.A., and Hyatt, A.D. (2001). Anthropogenic environmental change and the emergence of infectious diseases in wildlife. Acta Trop *78*, 103-116.

Daugherty, M.D., and Malik, H.S. (2012). Rules of engagement: molecular insights from host-virus arms races. Annu Rev Genet *46*, 677-700.

De La Cruz-Rivera, P.C., Kanchwala, M., Liang, H., Kumar, A., Wang, L.F., Xing, C., and Schoggins, J.W. (2018). The IFN Response in Bats Displays Distinctive IFN-Stimulated Gene Expression Kinetics with Atypical RNASEL Induction. J Immunol *200*, 209-217.

Decaillot, F.M., Rozenfeld, R., Gupta, A., and Devi, L.A. (2008). Cell surface targeting of mu-delta opioid receptor heterodimers by RTP4. Proc Natl Acad Sci U S A *105*, 16045-16050.

Dehler, C.E., Lester, K., Della Pelle, G., Jouneau, L., Houel, A., Collins, C., Dovgan, T., Machat, R., Zou, J., Boudinot, P., *et al.* (2019). Viral Resistance and IFN Signaling in STAT2 Knockout Fish Cells. J Immunol *203*, 465-475.

den Boon, J.A., Diaz, A., and Ahlquist, P. (2010). Cytoplasmic viral replication complexes. Cell Host Microbe *8*, 77-85.

Dobin, A., Davis, C.A., Schlesinger, F., Drenkow, J., Zaleski, C., Jha, S., Batut, P., Chaisson, M., and Gingeras, T.R. (2013). STAR: ultrafast universal RNA-seq aligner. Bioinformatics *29*, 15-21.

Domingo, E. (1992). Genetic variation and quasi-species. Curr Opin Genet Dev *2*, 61-63.

Domingo, E., Sheldon, J., and Perales, C. (2012). Viral quasispecies evolution. Microbiol Mol Biol Rev *76*, 159-216.

Duggal, N.K., and Emerman, M. (2012). Evolutionary conflicts between viruses and restriction factors shape immunity. Nat Rev Immunol *12*, 687-695.

Dukhovny, A., Lamkiewicz, K., Chen, Q., Fricke, M., Jabrane-Ferrat, N., Marz, M., Jung, J.U., and Sklan, E.H. (2019). A CRISPR Activation Screen Identifies Genes That Protect against Zika Virus Infection. J Virol *93*.

Dupuis, S., Jouanguy, E., Al-Hajjar, S., Fieschi, C., Al-Mohsen, I.Z., Al-Jumaah, S., Yang, K., Chapgier, A., Eidenschenk, C., Eid, P., *et al.* (2003). Impaired response to interferon-alpha/beta and lethal viral disease in human STAT1 deficiency. Nat Genet *33*, 388-391.

Elurbe, D.M., Paranjpe, S.S., Georgiou, G., van Kruijsbergen, I., Bogdanovic, O., Gibeaux, R., Heald, R., Lister, R., Huynen, M.A., van Heeringen, S.J., *et al.* (2017). Regulatory remodeling in the allo-tetraploid frog Xenopus laevis. Genome Biol *18*, 198.

Enard, D., Cai, L., Gwennap, C., and Petrov, D.A. (2016). Viruses are a dominant driver of protein adaptation in mammals. Elife *5*.

Fajardo, T., Sanford, T.J., Mears, H.V., Jasper, A., Storrie, S., Mansur, D.S., and Sweeney, T.R. (2020). The flavivirus polymerase NS5 regulates translation of viral genomic RNA. Nucleic Acids Res *48*, 5081-5093.

Farnham, G., and Baulcombe, D.C. (2006). Artificial evolution extends the spectrum of viruses that are targeted by a disease-resistance gene from potato. Proc Natl Acad Sci U S A *103*, 18828-18833.

Font, J., and Mackay, J.P. (2010). Beyond DNA: zinc finger domains as RNA-binding modules. Methods Mol Biol *649*, 479-491.

Fortriede, J.D., Pells, T.J., Chu, S., Chaturvedi, P., Wang, D., Fisher, M.E., James-Zorn, C., Wang, Y., Nenni, M.J., Burns, K.A., *et al.* (2020). Xenbase: deep integration of GEO & SRA RNA-seq and ChIP-seq data in a model organism database. Nucleic Acids Res *48*, D776-D782.

Fuchs, J., Holzer, M., Schilling, M., Patzina, C., Schoen, A., Hoenen, T., Zimmer, G., Marz, M., Weber, F., Muller, M.A., *et al.* (2017). Evolution and Antiviral Specificities of Interferon-Induced Mx Proteins of Bats against Ebola, Influenza, and Other RNA Viruses. J Virol *91*.

Fujita, W., Yokote, M., Gomes, I., Gupta, A., Ueda, H., and Devi, L.A. (2019). Regulation of an Opioid Receptor Chaperone Protein, RTP4, by Morphine. Mol Pharmacol *95*, 11-19.

Fukutani, Y., Tamaki, R., Inoue, R., Koshizawa, T., Sakashita, S., Ikegami, K., Ohsawa, I., Matsunami, H., and Yohda, M. (2019). The N-terminal region of RTP1S plays important roles in dimer formation and odorant receptor-trafficking. J Biol Chem *294*, 14661-14673.

Furman, B.L.S., Dang, U.J., Evans, B.J., and Golding, G.B. (2018). Divergent subgenome evolution after allopolyploidization in African clawed frogs (Xenopus). J Evol Biol *31*, 1945-1958.

Galili, T. (2015). dendextend: an R package for visualizing, adjusting and comparing trees of hierarchical clustering. Bioinformatics *31*, 3718-3720.

Garcia-Blanco, M.A., Vasudevan, S.G., Bradrick, S.S., and Nicchitta, C. (2016). Flavivirus RNA transactions from viral entry to genome replication. Antiviral Res *134*, 244-249.

Gifford, C.A., Assiri, A.M., Satterfield, M.C., Spencer, T.E., and Ott, T.L. (2008). Receptor transporter protein 4 (RTP4) in endometrium, ovary, and peripheral blood leukocytes of pregnant and cyclic ewes. Biol Reprod *79*, 518-524.

Gilbert, C., and Feschotte, C. (2010). Genomic fossils calibrate the long-term evolution of hepadnaviruses. PLoS Biol *8*.

Gillespie, L.K., Hoenen, A., Morgan, G., and Mackenzie, J.M. (2010). The endoplasmic reticulum provides the membrane platform for biogenesis of the flavivirus replication complex. J Virol *84*, 10438-10447.

Gizzi, A.S., Grove, T.L., Arnold, J.J., Jose, J., Jangra, R.K., Garforth, S.J., Du, Q., Cahill, S.M., Dulyaninova, N.G., Love, J.D., *et al.* (2018). A naturally occurring antiviral ribonucleotide encoded by the human genome. Nature *558*, 610-614.

Glez-Pena, D., Gomez-Blanco, D., Reboiro-Jato, M., Fdez-Riverola, F., and Posada, D. (2010). ALTER: program-oriented conversion of DNA and protein alignments. Nucleic Acids Res *38*, W14-18.

Halpin, K., Young, P.L., Field, H.E., and Mackenzie, J.S. (2000). Isolation of Hendra virus from pteropid bats: a natural reservoir of Hendra virus. J Gen Virol *81*, 1927-1932.

Halty-deLeon, L., Miazzi, F., Kaltofen, S., Hansson, B.S., and Wicher, D. (2016). The mouse receptor transporting protein RTP1S and the fly SNMP1 support the functional expression of the Drosophila odorant coreceptor Orco in mammalian culture cells. J Neurosci Methods *271*, 149-153.

Hanners, N.W., Eitson, J.L., Usui, N., Richardson, R.B., Wexler, E.M., Konopka, G., and Schoggins, J.W. (2016). Western Zika Virus in Human Fetal Neural Progenitors Persists Long Term with Partial Cytopathic and Limited Immunogenic Effects. Cell Rep *15*, 2315-2322.

Hawkins, J.A., Kaczmarek, M.E., Muller, M.A., Drosten, C., Press, W.H., and Sawyer, S.L. (2019). A metaanalysis of bat phylogenetics and positive selection based on genomes and transcriptomes from 18 species. Proc Natl Acad Sci U S A *116*, 11351-11360.

He, X., Ashbrook, A.W., Du, Y., Wu, J., Hoffmann, H.H., Zhang, C., Xia, L., Peng, Y.C., Tumas, K.C., Singh, B.K., *et al.* (2020b). RTP4 inhibits IFN-I response and enhances experimental cerebral malaria and neuropathology. Proc Natl Acad Sci U S A *117*, 19465-19474.

Hou, F., Sun, L., Zheng, H., Skaug, B., Jiang, Q.X., and Chen, Z.J. (2011). MAVS forms functional prion-like aggregates to activate and propagate antiviral innate immune response. Cell *146*, 448-461.

Irving, A.T., Rozario, P., Kong, P.S., Luko, K., Gorman, J.J., Hastie, M.L., Chia, W.N., Mani, S., Lee, B.P., Smith, G.J.D., *et al.* (2019). Robust dengue virus infection in bat cells and limited innate immune responses coupled with positive serology from bats in IndoMalaya and Australasia. Cell Mol Life Sci.

Irving, A.T., Zhang, Q., Kong, P.S., Luko, K., Rozario, P., Wen, M., Zhu, F., Zhou, P., Ng, J.H.J., Sobota, R.M., *et al.* (2020). Interferon Regulatory Factors IRF1 and IRF7 Directly Regulate Gene Expression in Bats in Response to Viral Infection. Cell Rep *33*, 108345.

Johnson, A.G., Grosely, R., Petrov, A.N., and Puglisi, J.D. (2017). Dynamics of IRES-mediated translation. Philos Trans R Soc Lond B Biol Sci *372*.

Johnson, W.E., and Sawyer, S.L. (2009). Molecular evolution of the antiretroviral TRIM5 gene. Immunogenetics *61*, 163-176.

Jones, C.T., Patkar, C.G., and Kuhn, R.J. (2005). Construction and applications of yellow fever virus replicons. Virology *331*, 247-259.

Kamp, W., Berk, M.B., Visser, C.J., and Nottet, H.S. (2000). Mechanisms of HIV-1 to escape from the host immune surveillance. Eur J Clin Invest *30*, 740-746.

Kane, M., Zang, T.M., Rihn, S.J., Zhang, F., Kueck, T., Alim, M., Schoggins, J., Rice, C.M., Wilson, S.J., and Bieniasz, P.D. (2016). Identification of Interferon-Stimulated Genes with Antiretroviral Activity. Cell Host Microbe *20*, 392-405.

Karimi, K., Fortriede, J.D., Lotay, V.S., Burns, K.A., Wang, D.Z., Fisher, M.E., Pells, T.J., James-Zorn, C., Wang, Y., Ponferrada, V.G., *et al.* (2018). Xenbase: a genomic, epigenomic and transcriptomic model organism database. Nucleic Acids Res *46*, D861-D868.

Knoops, K., Kikkert, M., Worm, S.H., Zevenhoven-Dobbe, J.C., van der Meer, Y., Koster, A.J., Mommaas, A.M., and Snijder, E.J. (2008). SARS-coronavirus replication is supported by a reticulovesicular network of modified endoplasmic reticulum. PLoS Biol *6*, e226.

Koonin, E.V., and Dolja, V.V. (2013). A virocentric perspective on the evolution of life. Curr Opin Virol *3*, 546-557.

Koonin, E.V., Dolja, V.V., and Krupovic, M. (2015). Origins and evolution of viruses of eukaryotes: The ultimate modularity. Virology *479-480*, 2-25.

Kosakovsky Pond, S.L., Posada, D., Gravenor, M.B., Woelk, C.H., and Frost, S.D. (2006). GARD: a genetic algorithm for recombination detection. Bioinformatics *22*, 3096-3098.

Kumar, S., Stecher, G., Li, M., Knyaz, C., and Tamura, K. (2018). MEGA X: Molecular Evolutionary Genetics Analysis across Computing Platforms. Mol Biol Evol *35*, 1547-1549.

Kumar, S., Stecher, G., Suleski, M., and Hedges, S.B. (2017). TimeTree: A Resource for Timelines, Timetrees, and Divergence Times. Mol Biol Evol *34*, 1812-1819.

Ladner, J.T., Wiley, M.R., Beitzel, B., Auguste, A.J., Dupuis, A.P., 2nd, Lindquist, M.E., Sibley, S.D., Kota, K.P., Fetterer, D., Eastwood, G., *et al.* (2016). A Multicomponent Animal Virus Isolated from Mosquitoes. Cell Host Microbe *20*, 357-367.

Lazear, H.M., Schoggins, J.W., and Diamond, M.S. (2019). Shared and Distinct Functions of Type I and Type III Interferons. Immunity *50*, 907-923.

Lee, J.C., Tseng, C.K., Wu, Y.H., Kaushik-Basu, N., Lin, C.K., Chen, W.C., and Wu, H.N. (2015). Characterization of the activity of 2'-C-methylcytidine against dengue virus replication. Antiviral Res *116*, 1-9.

Li, J., Ding, S.C., Cho, H., Chung, B.C., Gale, M., Jr., Chanda, S.K., and Diamond, M.S. (2013). A short hairpin RNA screen of interferon-stimulated genes identifies a novel negative regulator of the cellular antiviral response. mBio *4*, e00385-00313.

Lindenbach, B.D., and Rice, C.M. (1997). trans-Complementation of yellow fever virus NS1 reveals a role in early RNA replication. J Virol *71*, 9608-9617.

Lindenbach, B.D., and Rice, C.M. (2003). Molecular biology of flaviviruses. Adv Virus Res *59*, 23-61.

Liu, P., Wang, L., Kwang, J., Yue, G.H., and Wong, S.M. (2016). Transcriptome analysis of genes responding to NNV infection in Asian seabass epithelial cells. Fish Shellfish Immunol *54*, 342-352.

Liu, P., Wang, L., Ye, B.Q., Huang, S., Wong, S.M., and Yue, G.H. (2017). Characterization of a novel disease resistance gene rtp3 and its association with VNN disease resistance in Asian seabass. Fish Shellfish Immunol *61*, 61-67.

Love, M.I., Huber, W., and Anders, S. (2014). Moderated estimation of fold change and dispersion for RNA-seq data with DESeq2. Genome Biol *15*, 550.

Luis, A.D., Hayman, D.T., O'Shea, T.J., Cryan, P.M., Gilbert, A.T., Pulliam, J.R., Mills, J.N., Timonin, M.E., Willis, C.K., Cunningham, A.A., *et al.* (2013). A comparison of bats and rodents as reservoirs of zoonotic viruses: are bats special? Proc Biol Sci *280*, 20122753.

Manz, B., Dornfeld, D., Gotz, V., Zell, R., Zimmermann, P., Haller, O., Kochs, G., and Schwemmle, M. (2013). Pandemic influenza A viruses escape from restriction by human MxA through adaptive mutations in the nucleoprotein. PLoS Pathog *9*, e1003279.

Manzini, I., and Schild, D. (2010). Olfactory Coding in Larvae of the African Clawed Frog Xenopus laevis. In The Neurobiology of Olfaction, A. Menini, ed. (Boca Raton (FL)).

Marukian, S., Jones, C.T., Andrus, L., Evans, M.J., Ritola, K.D., Charles, E.D., Rice, C.M., and Dustin, L.B. (2008). Cell culture-produced hepatitis C virus does not infect peripheral blood mononuclear cells. Hepatology *48*, 1843-1850.

McDonald, C.A., Longo, A.V., Lips, K.R., and Zamudio, K.R. (2020). Incapacitating effects of fungal coinfection in a novel pathogen system. Mol Ecol *29*, 3173-3186.

ME, J.W., Adair, K., and Brierley, L. (2013). RNA Viruses: A Case Study of the Biology of Emerging Infectious Diseases. Microbiol Spectr *1*.

Mitchell, P.S., Patzina, C., Emerman, M., Haller, O., Malik, H.S., and Kochs, G. (2012). Evolution-guided identification of antiviral specificity determinants in the broadly acting interferon-induced innate immunity factor MxA. Cell Host Microbe *12*, 598-604.

Murrell, B., Moola, S., Mabona, A., Weighill, T., Sheward, D., Kosakovsky Pond, S.L., and Scheffler, K. (2013). FUBAR: a fast, unconstrained bayesian approximation for inferring selection. Mol Biol Evol *30*, 1196-1205.

Murrell, B., Weaver, S., Smith, M.D., Wertheim, J.O., Murrell, S., Aylward, A., Eren, K., Pollner, T., Martin, D.P., Smith, D.M., *et al.* (2015). Gene-wide identification of episodic selection. Mol Biol Evol *32*, 1365-1371.

Naito, Y., Hino, K., Bono, H., and Ui-Tei, K. (2015). CRISPRdirect: software for designing CRISPR/Cas guide RNA with reduced off-target sites. Bioinformatics *31*, 1120-1123.

Olival, K.J., and Hayman, D.T. (2014). Filoviruses in bats: current knowledge and future directions. Viruses *6*, 1759-1788.

Olival, K.J., Hosseini, P.R., Zambrana-Torrelio, C., Ross, N., Bogich, T.L., and Daszak, P. (2017). Host and viral traits predict zoonotic spillover from mammals. Nature *546*, 646-650.

Pankovics, P., Boros, A., Toth, Z., Phan, T.G., Delwart, E., and Reuter, G. (2017). Genetic characterization of a second novel picornavirus from an amphibian host, smooth newt (Lissotriton vulgaris). Arch Virol *162*, 1043-1050.

Paul, D., and Bartenschlager, R. (2015). Flaviviridae Replication Organelles: Oh, What a Tangled Web We Weave. Annu Rev Virol *2*, 289-310.

Pavlovich, S.S., Lovett, S.P., Koroleva, G., Guito, J.C., Arnold, C.E., Nagle, E.R., Kulcsar, K., Lee, A., Thibaud-Nissen, F., Hume, A.J., *et al.* (2018). The Egyptian Rousette Genome Reveals Unexpected Features of Bat Antiviral Immunity. Cell *173*, 1098-1110 e1018.

Perera-Lecoin, M., Meertens, L., Carnec, X., and Amara, A. (2013). Flavivirus entry receptors: an update. Viruses *6*, 69-88.

Pflug, A., Guilligay, D., Reich, S., and Cusack, S. (2014). Structure of influenza A polymerase bound to the viral RNA promoter. Nature *516*, 355-360.

Pierson, T.C., and Diamond, M.S. (2020). The continued threat of emerging flaviviruses. Nat Microbiol *5*, 796-812.

Platanias, L.C. (2005). Mechanisms of type-I- and type-II-interferon-mediated signalling. Nat Rev Immunol *5*, 375-386.

Ramirez-Gordillo, D., Trujillo-Provencio, C., Knight, V.B., and Serrano, E.E. (2011). Optimization of gene delivery methods in Xenopus laevis kidney (A6) and Chinese hamster ovary (CHO) cell lines for heterologous expression of Xenopus inner ear genes. In Vitro Cell Dev Biol Anim *47*, 640-652.

Reikine, S., Nguyen, J.B., and Modis, Y. (2014). Pattern Recognition and Signaling Mechanisms of RIG-I and MDA5. Front Immunol *5*, 342.

Reuter, G., Boros, A., Toth, Z., Gia Phan, T., Delwart, E., and Pankovics, P. (2015). A highly divergent picornavirus in an amphibian, the smooth newt (Lissotriton vulgaris). J Gen Virol *96*, 2607-2613.

Richardson, R.B., Ohlson, M.B., Eitson, J.L., Kumar, A., McDougal, M.B., Boys, I.N., Mar, K.B., De La Cruz-Rivera, P.C., Douglas, C., Konopka, G., *et al.* (2018). A CRISPR screen identifies IFI6 as an ER-resident interferon effector that blocks flavivirus replication. Nat Microbiol *3*, 1214-1223.

Riera Romo, M., Perez-Martinez, D., and Castillo Ferrer, C. (2016). Innate immunity in vertebrates: an overview. Immunology *148*, 125-139.

Robinson, M.D., McCarthy, D.J., and Smyth, G.K. (2010). edgeR: a Bioconductor package for differential expression analysis of digital gene expression data. Bioinformatics *26*, 139-140.

Robson, F., Khan, K.S., Le, T.K., Paris, C., Demirbag, S., Barfuss, P., Rocchi, P., and Ng, W.L. (2020). Coronavirus RNA Proofreading: Molecular Basis and Therapeutic Targeting. Mol Cell *79*, 710-727.

Romero-Lopez, C., Barroso-Deljesus, A., Garcia-Sacristan, A., Briones, C., and Berzal-Herranz, A. (2014). End-to-end crosstalk within the hepatitis C virus genome mediates the conformational switch of the 3'X-tail region. Nucleic Acids Res *42*, 567-582.

Saeedi, B.J., and Geiss, B.J. (2013). Regulation of flavivirus RNA synthesis and capping. Wiley Interdiscip Rev RNA *4*, 723-735.

Saito, H., Kubota, M., Roberts, R.W., Chi, Q., and Matsunami, H. (2004). RTP family members induce functional expression of mammalian odorant receptors. Cell *119*, 679-691.

Sang, Y., Liu, Q., Lee, J., Ma, W., McVey, D.S., and Blecha, F. (2016). Expansion of amphibian intronless interferons revises the paradigm for interferon evolution and functional diversity. Sci Rep *6*, 29072.

Sanjana, N.E., Shalem, O., and Zhang, F. (2014). Improved vectors and genome-wide libraries for CRISPR screening. Nat Methods *11*, 783-784.

Sawicki, S.G., Sawicki, D.L., and Siddell, S.G. (2007). A contemporary view of coronavirus transcription. J Virol *81*, 20-29.

Sawyer, S. (1989). Statistical tests for detecting gene conversion. Mol Biol Evol *6*, 526-538.

Sawyer, S.L., Emerman, M., and Malik, H.S. (2007). Discordant evolution of the adjacent antiretroviral genes TRIM22 and TRIM5 in mammals. PLoS Pathog *3*, e197.

Sawyer, S.L., Wu, L.I., Emerman, M., and Malik, H.S. (2005). Positive selection of primate TRIM5alpha identifies a critical species-specific retroviral restriction domain. Proc Natl Acad Sci U S A *102*, 2832-2837.

Sayah, D.M., Sokolskaja, E., Berthoux, L., and Luban, J. (2004). Cyclophilin A retrotransposition into TRIM5 explains owl monkey resistance to HIV-1. Nature *430*, 569-573.

Schlee, M., and Hartmann, G. (2016). Discriminating self from non-self in nucleic acid sensing. Nat Rev Immunol *16*, 566-580.

Schneider, W.M., Chevillotte, M.D., and Rice, C.M. (2014). Interferon-stimulated genes: a complex web of host defenses. Annu Rev Immunol *32*, 513-545.

Schoggins, J.W., Dorner, M., Feulner, M., Imanaka, N., Murphy, M.Y., Ploss, A., and Rice, C.M. (2012). Dengue reporter viruses reveal viral dynamics in interferon receptor-deficient mice and sensitivity to interferon effectors in vitro. Proc Natl Acad Sci U S A *109*, 14610-14615.

Schoggins, J.W., MacDuff, D.A., Imanaka, N., Gainey, M.D., Shrestha, B., Eitson, J.L., Mar, K.B., Richardson, R.B., Ratushny, A.V., Litvak, V., *et al.* (2014). Pan-viral specificity of IFN-induced genes reveals new roles for cGAS in innate immunity. Nature *505*, 691-695.

Schoggins, J.W., Wilson, S.J., Panis, M., Murphy, M.Y., Jones, C.T., Bieniasz, P., and Rice, C.M. (2011). A diverse range of gene products are effectors of the type I interferon antiviral response. Nature *472*, 481-485.

Schwarz, M.C., Sourisseau, M., Espino, M.M., Gray, E.S., Chambers, M.T., Tortorella, D., and Evans, M.J. (2016). Rescue of the 1947 Zika Virus Prototype Strain with a Cytomegalovirus Promoter-Driven cDNA Clone. mSphere *1*.

Secombes, C.J., and Zou, J. (2017). Evolution of Interferons and Interferon Receptors. Front Immunol *8*, 209.

Session, A.M., Uno, Y., Kwon, T., Chapman, J.A., Toyoda, A., Takahashi, S., Fukui, A., Hikosaka, A., Suzuki, A., Kondo, M., *et al.* (2016). Genome evolution in the allotetraploid frog Xenopus laevis. Nature *538*, 336-343.

Sette, A., and Crotty, S. (2020). Pre-existing immunity to SARS-CoV-2: the knowns and unknowns. Nat Rev Immunol *20*, 457-458.

Sharma, R., Ishimaru, Y., Davison, I., Ikegami, K., Chien, M.S., You, H., Chi, Q., Kubota, M., Yohda, M., Ehlers, M., *et al.* (2017). Olfactory receptor accessory proteins play crucial roles in receptor function and gene choice. Elife *6*.

Shaw, A.E., Hughes, J., Gu, Q., Behdenna, A., Singer, J.B., Dennis, T., Orton, R.J., Varela, M., Gifford, R.J., Wilson, S.J., *et al.* (2017). Fundamental properties of the mammalian innate immune system revealed by multispecies comparison of type I interferon responses. PLoS Biol *15*, e2004086.

Shi, M., Lin, X.D., Chen, X., Tian, J.H., Chen, L.J., Li, K., Wang, W., Eden, J.S., Shen, J.J., Liu, L., *et al.* (2018). The evolutionary history of vertebrate RNA viruses. Nature *556*, 197-202.

Shi, Z., and Hu, Z. (2008). A review of studies on animal reservoirs of the SARS coronavirus. Virus Res *133*, 74-87.

Siegrist, F., Ebeling, M., and Certa, U. (2011). The small interferon-induced transmembrane genes and proteins. J Interferon Cytokine Res *31*, 183-197.

Simmonds, P., Becher, P., Bukh, J., Gould, E.A., Meyers, G., Monath, T., Muerhoff, S., Pletnev, A., Rico-Hesse, R., Smith, D.B., *et al.* (2017). ICTV Virus Taxonomy Profile: Flaviviridae. J Gen Virol *98*, 2-3.

Smith, M.D., Wertheim, J.O., Weaver, S., Murrell, B., Scheffler, K., and Kosakovsky Pond, S.L. (2015). Less is more: an adaptive branch-site random effects model for efficient detection of episodic diversifying selection. Mol Biol Evol *32*, 1342-1353.

Sniegowski, P.D., Gerrish, P.J., Johnson, T., and Shaver, A. (2000). The evolution of mutation rates: separating causes from consequences. Bioessays *22*, 1057-1066.

Starrett, G.J., Tisza, M.J., Welch, N.L., Belford, A.K., Peretti, A., Pastrana, D.V., and Buck, C.B. (2020). Adintoviruses: A Proposed Animal-Tropic Family of Midsize Eukaryotic Linear dsDNA (MELD) Viruses. Virus Evolution.

Stremlau, M., Owens, C.M., Perron, M.J., Kiessling, M., Autissier, P., and Sodroski, J. (2004). The cytoplasmic body component TRIM5alpha restricts HIV-1 infection in Old World monkeys. Nature *427*, 848-853.

Suzuki, Y., Chin, W.X., Han, Q., Ichiyama, K., Lee, C.H., Eyo, Z.W., Ebina, H., Takahashi, H., Takahashi, C., Tan, B.H., *et al.* (2016). Characterization of RyDEN (C19orf66) as

an Interferon-Stimulated Cellular Inhibitor against Dengue Virus Replication. PLoS Pathog *12*, e1005357.

Szretter, K.J., Balish, A.L., and Katz, J.M. (2006). Influenza: propagation, quantification, and storage. Curr Protoc Microbiol *Chapter 15*, Unit 15G 11.

Tabula Muris, C., Overall, c., Logistical, c., Organ, c., processing, Library, p., sequencing, Computational data, a., Cell type, a., Writing, g., *et al.* (2018). Single-cell transcriptomics of 20 mouse organs creates a Tabula Muris. Nature *562*, 367-372.

Tamura, K., Battistuzzi, F.U., Billing-Ross, P., Murillo, O., Filipski, A., and Kumar, S. (2012). Estimating divergence times in large molecular phylogenies. Proc Natl Acad Sci U S A *109*, 19333-19338.

Tamura, K., and Nei, M. (1993). Estimation of the number of nucleotide substitutions in the control region of mitochondrial DNA in humans and chimpanzees. Mol Biol Evol *10*, 512-526.

Tamura, K., Tao, Q., and Kumar, S. (2018). Theoretical Foundation of the RelTime Method for Estimating Divergence Times from Variable Evolutionary Rates. Mol Biol Evol *35*, 1770-1782.

Tay, M.Y., Saw, W.G., Zhao, Y., Chan, K.W., Singh, D., Chong, Y., Forwood, J.K., Ooi, E.E., Gruber, G., Lescar, J., *et al.* (2015). The C-terminal 50 amino acid residues of dengue NS3 protein are important for NS3-NS5 interaction and viral replication. J Biol Chem *290*, 2379-2394.

tenOever, B.R. (2016). The Evolution of Antiviral Defense Systems. Cell Host Microbe *19*, 142-149.

van den Hurk, A.F., Smith, C.S., Field, H.E., Smith, I.L., Northill, J.A., Taylor, C.T., Jansen, C.C., Smith, G.A., and Mackenzie, J.S. (2009). Transmission of Japanese Encephalitis virus from the black flying fox, Pteropus alecto, to Culex annulirostris mosquitoes, despite the absence of detectable viremia. Am J Trop Med Hyg *81*, 457-462.

Van Valen, L. (1973). A new evolutionary law. Evolutionary Theory *1*, 1-30.

Venkatesan, S., Rosenthal, R., Kanu, N., McGranahan, N., Bartek, J., Quezada, S.A., Hare, J., Harris, R.S., and Swanton, C. (2018). Perspective: APOBEC mutagenesis in drug resistance and immune escape in HIV and cancer evolution. Ann Oncol *29*, 563-572.

Wang, X., Xuan, Y., Han, Y., Ding, X., Ye, K., Yang, F., Gao, P., Goff, S.P., and Gao, G. (2019). Regulation of HIV-1 Gag-Pol Expression by Shiftless, an Inhibitor of Programmed -1 Ribosomal Frameshifting. Cell *176*, 625-635 e614.

Ward, J.H. (1963). Hierarchical Grouping to Optimize an Objective Function. Journal of the American Statistical Association *58*, 236-244.

Warren, C.J., and Sawyer, S.L. (2019). How host genetics dictates successful viral zoonosis. PLoS Biol *17*, e3000217.

Weaver, S., Shank, S.D., Spielman, S.J., Li, M., Muse, S.V., and Kosakovsky Pond, S.L. (2018). Datamonkey 2.0: A Modern Web Application for Characterizing Selective and Other Evolutionary Processes. Mol Biol Evol *35*, 773-777.

Westra, E.R., van Houte, S., Gandon, S., and Whitaker, R. (2019). The ecology and evolution of microbial CRISPR-Cas adaptive immune systems. Philos Trans R Soc Lond B Biol Sci *374*, 20190101.

White, J.M., and Whittaker, G.R. (2016). Fusion of Enveloped Viruses in Endosomes. Traffic *17*, 593-614.

White, M.D., Milne, R.V., and Nolan, M.F. (2011). A Molecular Toolbox for Rapid Generation of Viral Vectors to Up- or Down-Regulate Neuronal Gene Expression in vivo. Front Mol Neurosci *4*, 8.

Wolf, Y.I., Kazlauskas, D., Iranzo, J., Lucia-Sanz, A., Kuhn, J.H., Krupovic, M., Dolja, V.V., and Koonin, E.V. (2018). Origins and Evolution of the Global RNA Virome. mBio *9*.

Wolf, Y.I., Silas, S., Wang, Y., Wu, S., Bocek, M., Kazlauskas, D., Krupovic, M., Fire, A., Dolja, V.V., and Koonin, E.V. (2020). Doubling of the known set of RNA viruses by metagenomic analysis of an aquatic virome. Nat Microbiol *5*, 1262-1270.

Wroblewska, A., Dhainaut, M., Ben-Zvi, B., Rose, S.A., Park, E.S., Amir, E.D., Bektesevic, A., Baccarini, A., Merad, M., Rahman, A.H., *et al.* (2018). Protein Barcodes Enable High-Dimensional Single-Cell CRISPR Screens. Cell *175*, 1141-1155 e1116.

Wu, L., Pan, Y., Chen, G.Q., Matsunami, H., and Zhuang, H. (2012). Receptor-transporting protein 1 short (RTP1S) mediates translocation and activation of odorant receptors by acting through multiple steps. J Biol Chem *287*, 22287-22294.

Xie, J., Li, Y., Shen, X., Goh, G., Zhu, Y., Cui, J., Wang, L.F., Shi, Z.L., and Zhou, P. (2018). Dampened STING-Dependent Interferon Activation in Bats. Cell Host Microbe *23*, 297-301 e294.

Xu, C., Evensen, O., and Munang'andu, H.M. (2015). De novo assembly and transcriptome analysis of Atlantic salmon macrophage/dendritic-like TO cells following type I IFN treatment and Salmonid alphavirus subtype-3 infection. BMC Genomics *16*, 96.

Yang, Z. (1993). Maximum-likelihood estimation of phylogeny from DNA sequences when substitution rates differ over sites. Mol Biol Evol *10*, 1396-1401.

Yang, Z. (2007). PAML 4: phylogenetic analysis by maximum likelihood. Mol Biol Evol *24*, 1586-1591.

Yu, T., Su, X., Pan, Y., and Zhuang, H. (2017). Receptor-transporting protein (RTP) family members play divergent roles in the functional expression of odorant receptors. PLoS One *12*, e0179067.

Zhang, G., Cowled, C., Shi, Z., Huang, Z., Bishop-Lilly, K.A., Fang, X., Wynne, J.W., Xiong, Z., Baker, M.L., Zhao, W., *et al.* (2013). Comparative analysis of bat genomes provides insight into the evolution of flight and immunity. Science *339*, 456-460.

Zhou, P., Tachedjian, M., Wynne, J.W., Boyd, V., Cui, J., Smith, I., Cowled, C., Ng, J.H., Mok, L., Michalski, W.P., *et al.* (2016). Contraction of the type I IFN locus and unusual constitutive expression of IFN-alpha in bats. Proc Natl Acad Sci U S A *113*, 2696-2701.

Zhou, P., Yang, X.L., Wang, X.G., Hu, B., Zhang, L., Zhang, W., Si, H.R., Zhu, Y., Li, B., Huang, C.L., *et al.* (2020). A pneumonia outbreak associated with a new coronavirus of probable bat origin. Nature *579*, 270-273.

Zou, J., Tafalla, C., Truckle, J., and Secombes, C.J. (2007). Identification of a second group of type I IFNs in fish sheds light on IFN evolution in vertebrates. J Immunol *179*, 3859-3871.